UCLouvain

AGRO LOUVAIN

Faculté des bioingénieurs

What is the impact of reforestation on evapotranspiration?

How can we better assess evapotranspiration in the Atlantic Brazilian Forest?

A case study in Brazil's Atlantic Forest, in São Francisco Xavier, São Paulo State

Autor: Lola Parmentier
Promoter(s): Mathieu Javaux (UCL), Laura Borma (INPE)
Reader(s): Charles Bielders (UCL), Caroline Vincke (UCL)
Academic year 2023-2024
Final dissertation submitted with a view to obtaining the Bioengineering diploma: Master [120]: Bioingénieur en sciences et technologies de l'environnement, à finalité spécialisée, orientation Sustainability engineering.

ACKNOWLEDGMENTS

I would like to thank all those who contributed to the successful completion of this master thesis, whether through their support in everyday life or their valuable knowledge.

First, I would like to express my gratitude to Mathieu Javaux, the main promoter of this thesis, for having presented me with this project and convinced me to invest myself in it and to embark on this subject. I thank him for his help and advice during all our weekly meetings that allowed me to complete this thesis.

I would also like to thank Laura Borma, co-promoter of this thesis, for her help and valuable information on the study area of this thesis, which allowed me to better understand the region even without having had the chance to go there.

I would also like to thank Basile Delvoie, PhD student at UCLouvain, for his support, help and confidence over the past few months. His valuable advice and explanations allowed me to acquire new skills and enrich myself intellectually.

I thank Charlotte Dermauw for the mutual support she gave me throughout this year. Sharing the same subject from memory, her help and her presence were very useful to me.

I would also like to thank François Toussaint and Louis Delval for their help with coding during my debut, as well as Maxime Troiani and Pierre Houdmond for the time they gave to SEN-ET.

I would also like to thank Caroline Vincke and Charles Bielders for agreeing to be readers of this thesis and for their interest in it.

I wanted to thank all my relatives for their unconditional support daily, in easy and difficult times, my parents, family and friends.

Finally, I wanted to thank Dimitry Stoquart, translator-interpreter, for proofreading the spelling and grammar of my thesis.

TABLE OF CONTENT

LIST OF FIGURES

LIST OF TABLES

LIST OF ABBREVIATIONS

CA	Cleared area, was a forest before it has been deforested.
h	Water potential
EES-SFX	São Francisco Xavier Ecohydrological Experimental Station
ET	Evapotranspiration
ET_a	Actual evapotranspiration
ET_0	Reference evapotranspiration
ET_P	Potential evapotranspiration
IMNET	National Institute of Meteorology in Portuguese
INPE	Instituto Nacional de Pesquisas Espaciais, National Institute for Space Research
K_c	Cultural coefficient
Ksat	Hydraulic conductivity at saturation
P	Pasture
R10	Young Forest of 10 years of regeneration
R40	Mature Forest with over 40 years of regeneration
SEN-ET	Sentinels for Evapotranspiration
θ	Water content
WB	Water Balance

1. Introduction : Atlantic Brazilian Forest

1.1 Geographic situation

The Atlantic Forest, also known as the Mata Atlântica, is the second largest forest in Brazil, after the Amazon. Historically, it was the size of a quarter of the Amazon with 1.2 million square kilometers. It is a tropical rainforest that is located mainly in Brazil, extending through 13 of the 26 states, but is also present in Argentina, Paraguay, and Uruguay. Two of the largest cities in the world, Sao Paulo and Rio de Janeiro, were built on the Mata Atlântica region, thus inducing quite significant anthropic pressure on the forest. Figure 1 represents the Atlantic Forest with the study area, which will be explained in more details in Materials and methods section. The study area is located nearly São José dos Campos, in São Francisco Xavier in the state of São Paulo in Brazil. (Brazil's Atlantic Forest (Mata Atlântica), s. d.)

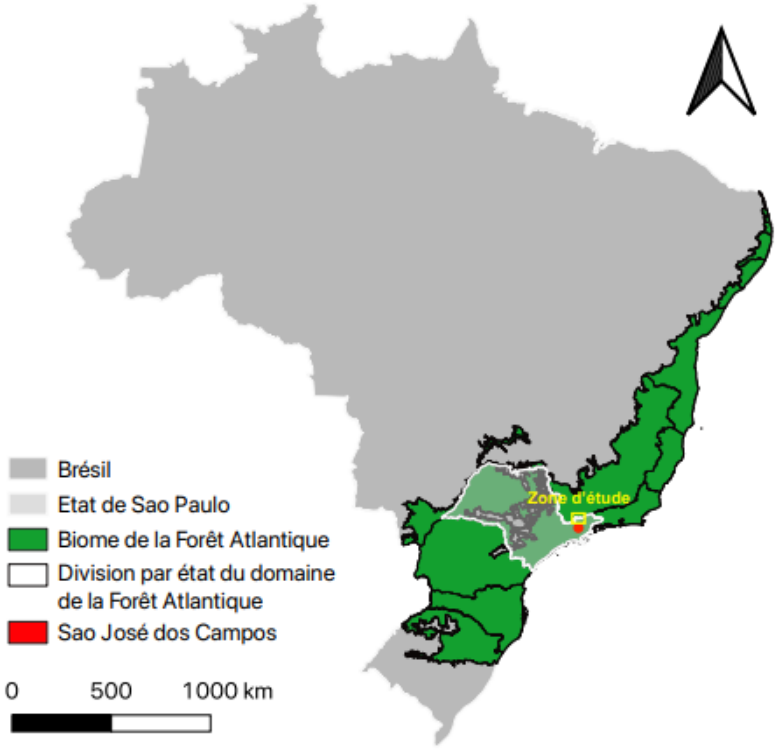

Figure 1: Map of Brazil showing the extent of the Atlantic Forest (green), the state of São Paulo (light grey), the city of São José dos Campos (red) and the São Francisco Xavier study area (yellow) (Delvoie B., 2023).

1.2 Climate

The Atlantic Forest is characterized by a subtropical humid climate with one dry and one wet period each year. The dry period is during winter from May to September while the wet period is in summer from October to April. According to the National Meteorological Institute (INMET), the annual mean temperature in the state of São Paulo is 20.4 [°C] (1991-2020). Temperatures are higher during the wet season.

Mean precipitations are 1658 mm/year in São Paulo and the average annual potential evapotranspiration is 1450 mm/year. (INMET: Météo, s. d.).

1.3 Ecology and vegetation

Although Mata Atlântica is nearly bordered by the Amazon rainforest, it has always been isolated from its larger, better-known neighbor. This isolation has allowed it to develop unique ecosystems, which are home to many species that are not found anywhere else on Earth. The Atlantic Forest is home to approximately 1.000 bird species, 456 amphibian species, 350 freshwater fish species, 300 reptile species and 264 mammal species. In total, 31% of these species cannot be found elsewhere. Some taxa are more endemic than others: for example, 61% of Mata Atlântica's amphibians are found only there. The flora includes 23.000 species of plants, 40% of which are endemic to Mata Atlântica. New species are constantly being discovered in Mata Atlântica. Between 1990 and 2006 more than a thousand new flowering plants were discovered. (Brazil's Atlantic Forest (Mata Atlântica), s. d.)

The different forest types in Mata Atlântica include:

- Mangroves: tropical forests adapted to coastal salt marshes. According to WWF, Mata Atlântica has four distinct mangrove areas. Mangroves are considered important buffer zones for tropical storms and breeding grounds for fish farming. They also contain many endemic species.
- Montane moist forests: high altitude wet forests across the mountains and plateaus of southern Brazil.
- Coastal Resingas: low forests growing on coastal dunes.
- Atlantic rainforests: also known as "coastal forests", they are four-layered evergreen rainforests.
- Semi-deciduous forests: inland forests where trees lose their leaves during the dry season.
- Atlantic Dry forests: this forest is one of the most remote inland forests and forms the border between the Cerrado and Caatinga scrub. Tropical climate with five months of drought.
- Campo rupestre: high altitude shrub meadows.

(Brazil's Atlantic Forest (Mata Atlântica), s. d.; What Is the Atlantic Forest and Why Do We Need to Save It?, s. d.)

1.4 Deforestation of the Mata Atlântica

Globally, temperate forests are recovering from previous deforestation, while tropical forests are being cut at an alarming rate (Foley et al., 2005; Hougthon, 1994). Deforestation and forest degradation began 20.000 years ago and continue today (Brown & Brown, 1992). The situation in Brazil is no exception, where intense forest degradation started more than 500 years ago (Dean, 1997). The Atlantic Forest was the first biome to be affected, and by the end of the last century it had virtually disappeared. Between 2001 and 2004, Brazil accounted for more deforestation annually due to commodities than in the rest of the world. From 2005, this annual deforestation began to decrease in Brazil and increased in the rest of the world, particularly in South Asia.

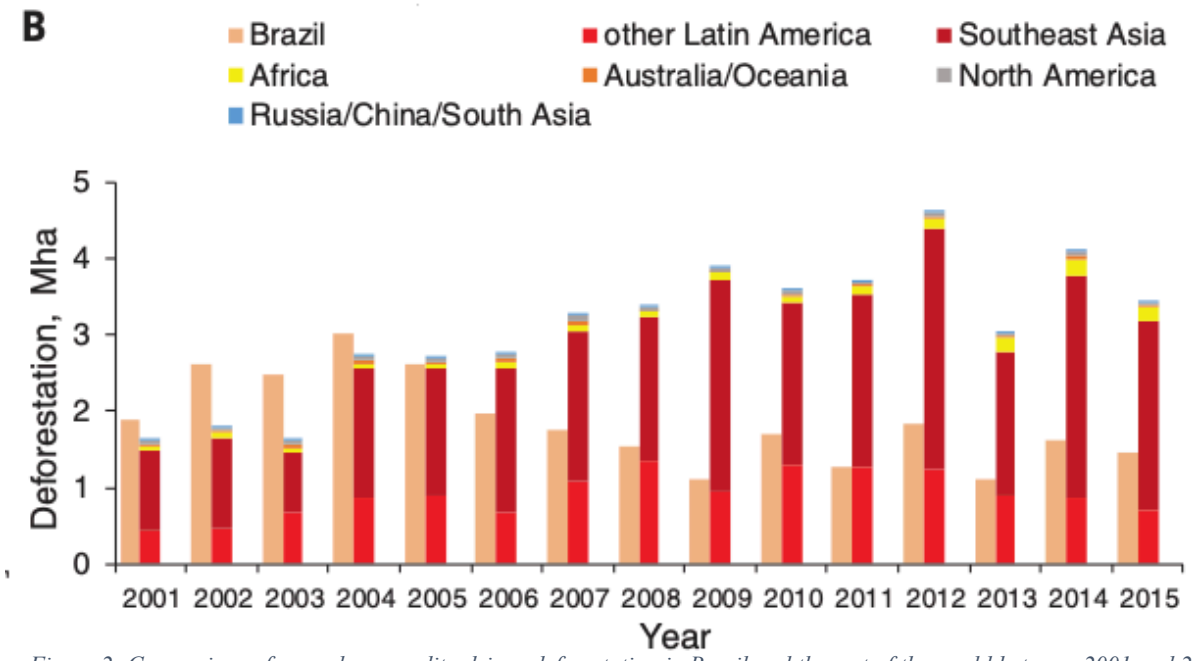

Figure 2: Comparison of annual commodity-driven deforestation in Brazil and the rest of the world between 2001 and 2015 .RESEARCH|REPORT (Classifying Drivers of Global Forest Loss, s. d.)

No large rainforest ecosystem has suffered as much damage as Mata Atlântica, which currently exists mainly in small, degraded patches and protected areas. After centuries of deforestation for wood, sugar cane, coffee, livestock and urban expansion, Mata Atlântica has lost more than 90% of its cover: today, the size of the Mata Atlântica is less than 100.000 square kilometers. 80% of the remaining ecosystem consists of fragments of less than half a square kilometer. Between 2000 and 2008, 277.763 hectares (2.777 square kilometers) of forest were lost. An average of 34.720 hectares (347 square kilometers) per year, an annual loss of 0.35 percent. Figure 3 shows the annual loss of tropical primary forests (intact, mature, and natural tropical forests that have not been significantly disturbed by human activity) in dark green and the loss of forest cover (referring to the loss of any type of forest) in light green of the Mata Atlântica between 2002 and 2019. Overall, we can see that these loss rates gradually increase until reaching a maximum peak in 2016 of approximately two losses of 18 million hectares. After 2016, annual loss rates are expected to decrease due to conservation measures, which are discussed in more detail in the next section. The loss of primary tropical forests has increased over time, meaning that previously intact ecosystems and biodiversity have now been impacted.

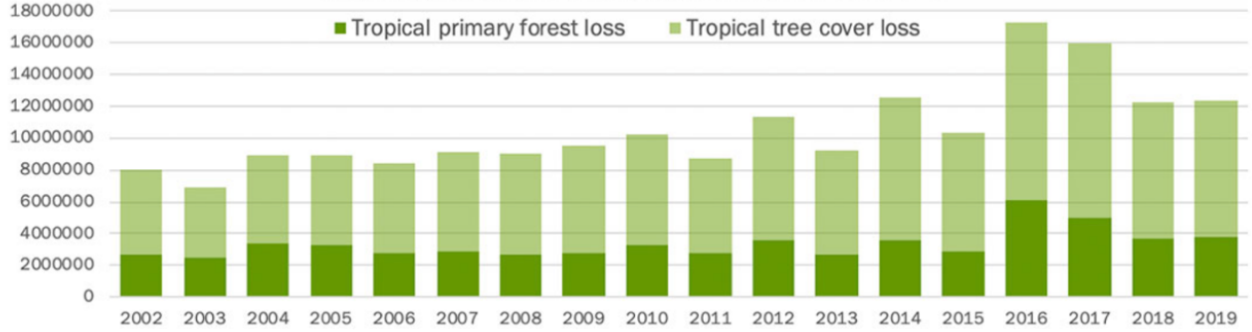

Figure 3 : Graph showing the Tropical primary forest loss in dark green and the tree cover loss in light green of the Mata Atlântica for the 2002-2019 period. Source: (Brazil's Atlantic Forest (Mata Atlântica), s. d.)

Current threats to the Mata Atlântica

Only 3 percent of the Mata Atlântica that once bordered the entire Brazilian coast survives (10% is the percentage remaining in all the countries on which the Mata Atlântica is). The largest losses occurred in the Brazilian states of Minas Gerais, Santa Catarina, and Bahia where only 9.7, 22.4 and 8.4% of the original surface remain (Figure 4). 13.6% of the original Mata Atlântica remains in Sao Paulo state. (Destruction of Brazil's Most Imperiled Rainforest Continues, 2009)

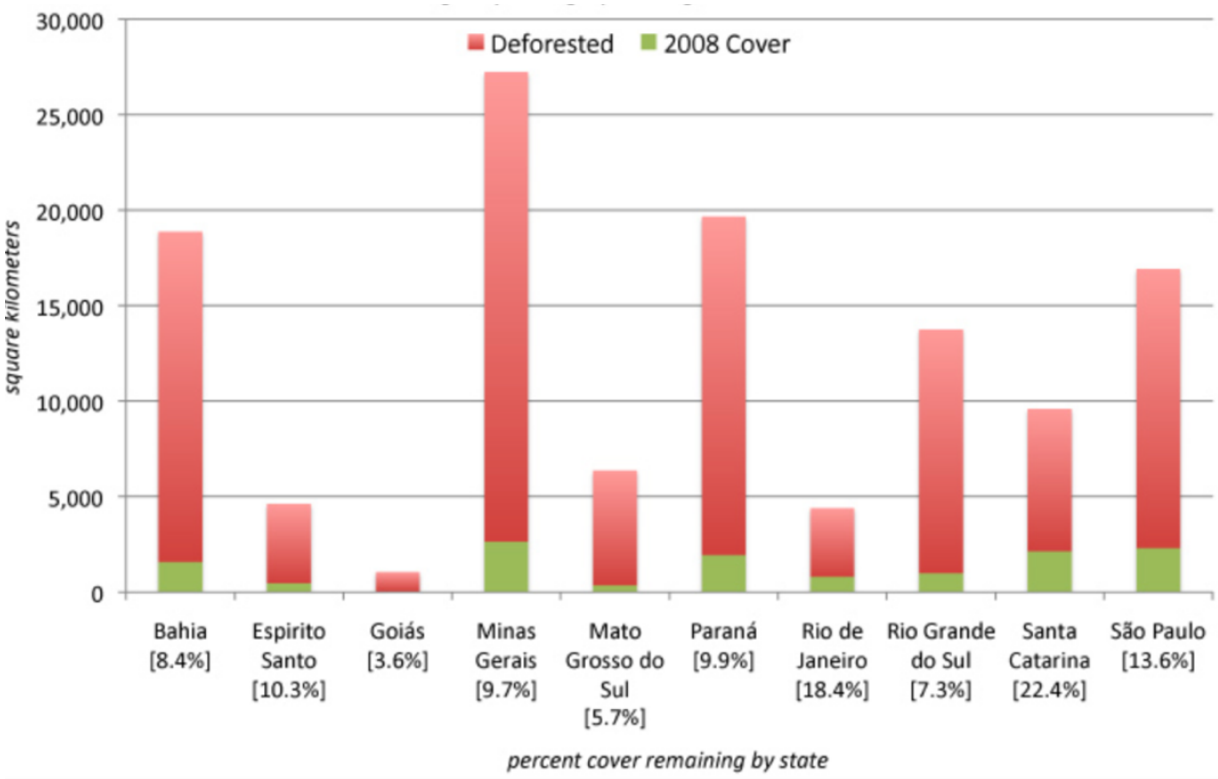

Figure 4: Extent of Mata Atlântica in Brazil in 2008 based in data from INPE. Deforested surface is represented in red in square kilometers while 2008 surface cover remaining is in green. (Destruction of Brazil's Most Imperiled Rainforest Continues, 2009)

The destruction of the Mata Atlântica began in the 1500s when the Portuguese arrived on the Brazilian seacoast. The export of wood began immediately, as did deforestation for livestock and sugar plantations. The region became the economic heart of Brazil in the 19th century by producing wood, coffee, beef, sugar, charcoal, and firewood. In the 20th century, eucalyptus plantations invaded vast forest areas, making Brazil the leading producer of wood pulp. Although very few remain, Mata Atlântica is no less threatened. As the forest spans four countries and encompasses a wide variety of forest types, different areas have very different threats. Forest clearing for agriculture, both industrial and small-scale, remains one of the main causes of deforestation. In some areas, forests are still cut for wood. (Figure 5)

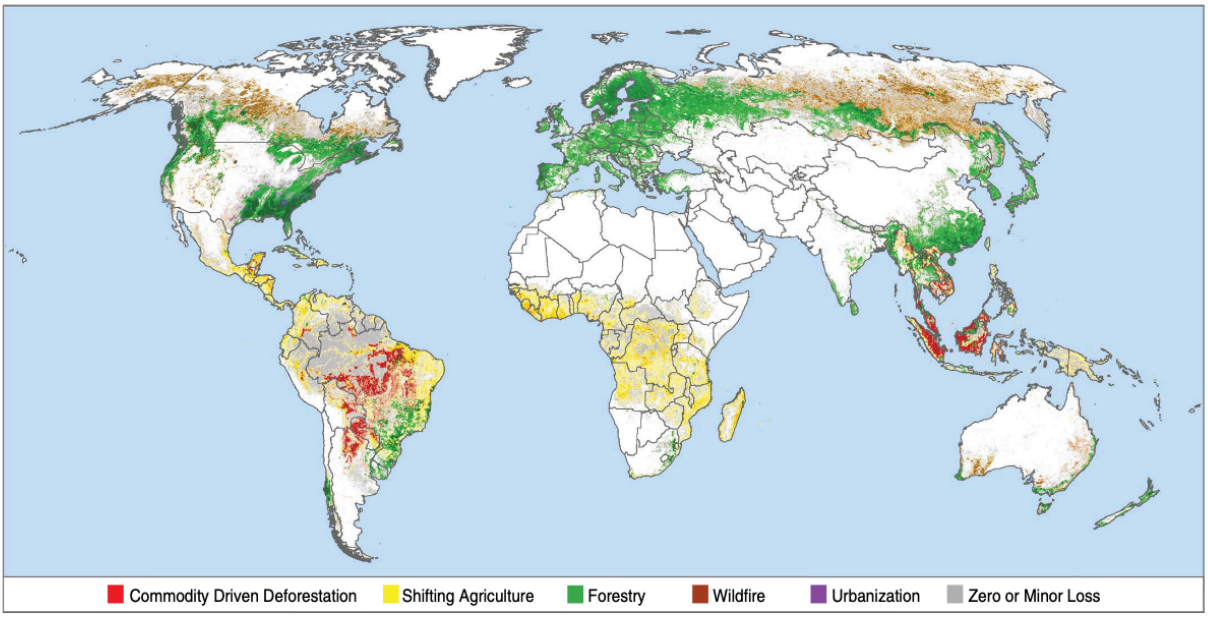

Figure 5: Primary drivers of forest cover loss for the period 2001 to 2015.Darker color intensity indicates greater total quantity of forest cover loss (Classifying Drivers of Global Forest Loss, s. d.)

Despite the few remaining forests, Mata Atlântica remains remarkably rich in biodiversity and endemic species, many of which are threatened with extinction. Sixty percent of Brazil's threatened species are found in Mata Atlântica. Due to several threats and species left in small declining fragments, a Brazilian ecologist, Antonio Rossano Mendes Pontes, called the species in Mata Atlântica: 'the living dead'.

1.5 Reforestation and conservation initiatives in the Mata Atlântica

Conservation initiatives

About 23.800 square kilometers of the Atlantic Forest is under protection. This is 23.8 % of the Mata Atlântica's remaining forest, but less than 2 percent of its historic forest range.

In Brazil there are 224 protected areas in the region, including over 100 state and national parks. These protected nature reserves include the Iguazu National Park which protects 67.000 hectares (670 square kilometers) of the Argentine region of Mata Atlântica, as well as the famous Iguazu Falls. The park has 422 species of birds, 68 mammals, 38 reptiles and 13 amphibians. There is also Serra dos Orgaos National Park in Brazil, just one hour away from Rio de Janeiro which covers 11.000 hectares (110 square kilometers). The park is home to endangered birds such as the Northern Parrot (Amazona vinacea), the Common Finch (Oryzoborus crassirostris) and the Black-fronted Guan (Pipile jacutinga).

Reforestation initiatives

Concerns about intense deforestation in the Atlantic Forest arose at the beginning of the 19th century (Dean, 1995) due to a lack of natural resources, agricultural pests and climate change, such as the city of Rio de Janeiro, which faced a water supply crisis after forest areas were converted into coffee plantations.

At the same time, the first reforestation project took place in Brazil where thousands of seedlings of native and exotic species were planted between 1862 and 1892 (Corlett, 1999).

Various reforestation projects have been carried out in the Atlantic Forest since this pioneering initiative. The objectives of reforestation projects have changed, new techniques have been developed (Rodrigues et al., 2009). The history of Atlantic Forest reforestation programs can be divided into 5 phases:

Phase 1:

Until 1982, the first restoration projects mainly concerned the planting of so-called protection plantations, whose main purpose was the protection of water and soil resources, and which were carried out by government institutions (KAGEYAMA & Castro, 1989). This phase increased especially after the 1970s. It was not until the late 1970s that restoration ecology became a formal research focus, when the first information on tree species functionality and restoration patterns was obtained (Filho et al., 1982). The ecological processes responsible for preserving the forest have been largely neglected, and the criteria for species selection have not yet been established. Therefore, although some projects have resulted in permanent forests (J.c.b, 1977), they have often required long-term maintenance activities (10-15 years) and significantly increased costs (Rodrigues et al., 2009).

Phase 2:

From 1982 to 1985, planting of native Brazilian species became widespread, although not always native to the restored area. This phase began with the integration of growing ecological knowledge about natural forest succession into restoration projects, where species are selected and distributed according to their ecological groups (Budowski, 1965). But their main motivation was to restore the forest structure quickly and with lower maintenance costs. Species knowledge was scarce, so the projects started using a small number of fast-growing species (up to 30 species) which were densely planted (low biological and functional diversity). The result was the reconstruction of forest areas at lower costs but usually without any capacity for self-perpetuation. The pioneer species reached adulthood and died rapidly, leaving little time and unfertile conditions for the establishment of non-malignant species. This phase also marked the beginning of large-scale restoration projects, mostly around hydroelectric dams or water supplies (Rodrigues et al., 2009).

Phase 3:

Between 1985 and 2000, despite the knowledge of some forest processes (e.g., the dynamics of gaps), much knowledge was still lacking. Reforestation was undertaken by reforestation of forest plots (Joly et al., 2000). In the late 1980s, projects were carried out using «restoration recipes» that reproduced the composition and structure of natural forests. Restoration began to use a greater diversity of species (Vieira & Gandolfi, 2006), and to be considered not only as a means of protecting ecosystem services, but also as an alternative to the conservation of biodiversity *in situ* (KAGEYAMA & Castro, 1989). Unlike the previous phase, many projects carried out in this phase have resulted in self-sufficiency, at least as regards the forest structure (Damanesco, 2006; de Souza & Batista, 2004). The introduction of greater functional diversity, primarily with respect to species ecological groups and longevity, has been an important change to improve restoration success. However, the lack of availability of seedlings of regional

indigenous species continued to be an obstacle for many projects. Riparian forest formations have received particular attention (Rodrigues & Gandolfi, 2000) and, for the first time, genetic issues have begun to be addressed, although they have not yet been applied (KAGEYAMA & Castro, 1989). (Rodrigues et al., 2009)

Phase 4:

Between 2000 and 2003, this phase saw significant changes in restoration objectives, no longer aiming to "reproduce" natural forests, which turned out to be an expensive practice. The great diversity of species, the local flora and the light requirements of the species remained a concern. The objective was to restore the forest's basic ecological processes by stimulating and accelerating natural succession, with the aim of recovering the forest's ability to sustain itself. Thus, restoration was now considered a non-deterministic process open to stochastic events that do not necessarily lead to a single predetermined climax (Pickett et al., 1987; Urbanska et al., 1997). Disturbances were integrated into the process and phytosociology received little attention during species selection, which started to be influenced more by the increasing knowledge on the biology of species (e.g. dispersal syndrome and pollination system). High diversity (e.g., 80-90 tree species) has been used to restore certain ecological processes (Engel & Parrotta, 2001; Reis & Xavier, 2003). (Rodrigues et al., 2009)

Phase 5:

Since 2003, this phase includes current effort to adapt to floristic and intraspecific genetic diversity, which are key factors to maintain and develop any forest system (Lesica & Allendorf, 2002). More care is taken at the origin and collection of seeds if done locally as much as possible (McKay et al., 2005). In some cases, the seeds are harvested from nearby forests and grown in local nurseries. Another strategy is to exploit existing genetic diversity through natural regeneration of already existing soil, such as soil seed banks and/or seedling transplantation (Rodrigues, 2007a; Rodrigues & Gandolfi, 2000). Maintaining this diversity over time is now considered in the spatial distribution of species, which attempt to meet their specifications on pollination and dispersal (Barbosa & Pizo, 2006; Rodrigues, 2007b). However, reproductive biology data for many native species are largely absent.(Rodrigues et al., 2009)

Massive reforestation movement has recently raised some concerns about the water balance. If reforestation is not managed properly, it may not be sustainable in the long term. Indeed, soil water dynamics are strongly affected by land use (Heo et al., 2015; Sertel et al., 2019). Sudden changes in this occupation can disrupt the water balance. Thus, if the reforestation is too intense and brutal or if it's done using monocultures, it would be possible to witness a depletion of water resources. Several studies have shown significant reductions in river flows after reforestation (Farley et al., 2005; Jackson et al., 2005). Significant water stress would then threaten the sustainability of this new ecosystem that would eventually collapse. This stress could also be exacerbated by future climate change.

1.6 Previous work

This Master thesis is in the continuity of Basile Delvoie last year Master thesis which focused on the impact of reforestation on the equilibrium of water resources in the soil. His Master thesis was subdivided into 3 objectives which were to first quantify the impact of reforestation on the hydraulic conductivity of the soil, secondly to quantify the impact of reforestation on evapotranspiration and on the dynamic of water uptake by plant and finally to quantify the impact of reforestation on the dynamic of the fluxes for the water table recharge.
He was working on two areas, a young forest of 10 years called R10, and an old forest of 40 years called R40. These areas will be described more in Materials and methods.

At the end of his Master thesis, some uncertainties remained concerning the soil properties of the soil for the two area, the cultural coefficient K_c for forest that is not very known and so lead to some uncertainties too for the evapotranspiration assessment and for the dynamic of the water uptake by the plants. To respond to these uncertainties, this Master thesis will focus on evapotranspiration assessments through remote sensing methods and through a mass balance. This will be made on the two areas R10 and R40 but also on a pasture P and an abandoned area called cleared area CA that could be closer soils in term of soil properties. This hypothesis will be addressed by Charlotte Dermauw in her Master thesis during this year 2023-2024.

This thesis is also related to the work done by INPE. Since 2023, Mauro Junior has been working on the measurement of transpiration, using sap flow measurements, of the tree *Pleroma pulchrum*, a species native to the region dominating the old forest strata. This species is commonly used during reforestation, but according to farmers, it would consume a lot of water in its juvenile state compared to other native species and could pose a risk to soil water resources. This fear has stopped reforestation in some areas. The results of his study suggest that this species does not consume more water than another native species during its juvenile state and that the high evapotranspiration rates measured are mainly due to the higher density of trees in the same area. During this year 2024, another study was conducted on soil macrofauna in this region and the impact on the chemical and physical properties of soil between R10 and R40. No significant difference in saturated hydraulic conductivity (Ks) was observed, however, R40 showed a reduction of Ks in deeper layers compared to R10. Several macrofauna taxa were positively correlated with Ks and soil carbon. The regeneration stage altered the abundance and diversity of these invertebrates in general (except for earthworms), and R40 showed high abundance of most taxa. In conclusion, our study highlights the potential of macrofauna communities as robust indicators of the restoration of soil functions in regenerating forests in the Atlantic Forest biome. The positive correlations observed between macrofauna abundance and diversity with soil water infiltration and organic carbon content highlight the key role of these invertebrates in essential ecosystem functions. (Demetrio et al., 2024; Monteiro, 2023).

2. State of the art

2.1 Definition of ET

According to the FAO, evapotranspiration (ET) can be defined as a combination of two separate processes that occur simultaneously where water is lost through evaporation from the soil surface and through transpiration from the crop (Allen et al., 1998). The part of the soil from which the roots absorb water is called the effective root zone. (Bos et al., 2009).

There are different kinds of ET: ET_0, ET_P and ET_a.
ET_0 is known as reference evapotranspiration and is a climatic parameter that represents the evapotranspiration of standardized vegetated surface which doesn't suffer from any water stress and is independent of the type of crop and the management practices.
ET_P is the potential evapotranspiration, referring to the evapotranspiration of well-managed, large, well-watered, disease-free, and well-fertilized fields that reach full production under given climatic conditions. It is specific to the soil cover and surface and can be calculated through the formula from FAO: $ET_p = K_c \times ET_0$ where K_c is the cultural coefficient of the crop.
ET_a is the actual evapotranspiration; it will be equal to ET_p during each growing stage if the crop is not water stressed. If there is water stress, it will be lower. (Allen et al., 1998; Bos et al., 2009)

2.2 Water cycle in tropical forests

Large signs of changes in precipitation or runoff indicate an intensification of the hydrological cycle in many parts of the world during the past century (Huntington, 2006). About two-thirds of global water losses are caused by surface ET (Shukla & Mintz, 1982) and ET accounts for approximately 60% of the average precipitation globally.
In the tropics, the water cycle is stronger than anywhere else on Earth. Evaporation peaks in the subtropical ocean trade winds with minimal, while water vapor is transported to lower latitudes with abundant precipitation, resulting in a very active water cycle (Roca et al., 2010).
Tropical rainforests are among the most important biomes in terms of annual carbon turnover and evapotranspiration. Although tropical rainforests cover only about 8% of the world's land surface (Woodwell & Pecan, 1973), they contain about 40% of biomass (Skole & Tucker, 1993) and account for about 50% of the biosphere's annual net primary production (Roy et al., 2001). ET of these forests has significant impacts on local climate and extratropical atmospheric circulation patterns (Shukla & Mintz, 1982; Williams et al., 1998). Change of ET affect precipitation, by altering the amount of water vapor transferred from the land to the atmosphere. ET also have an impact on temperature since a large amount of heat is removed from the Earth's surface by evaporation, imposing a direct cooling effect on the Earth. Thus, increased evaporation reduces near-surface air temperatures and acts as an important negative biophysical feedback against anthropogenic global warming. (Yang et al., 2020)

2.3 ET in the Atlantic Forest

On a global scale, the average annual total ET varies between 450 and 550 [mm/yr.] (Goss & Oliver, 2023). However, the amount of total ET varies considerably between regions and biomes. In Brazil, in deciduous evergreen forests, ET is equals to 1227 ± 102 [mm/yr.]. This value has been increasing since the early 1980s, with a trend of 0.66 ± 0.38 [mm/yr^2], equivalent to 3.7 ± 2.1%. These historical ET increases are mainly due to the greening of vegetation (increased LAI), increased atmospheric evaporation demand (AED) and increased precipitation. Together, these three factors explain 81% of the annual variation in global average evapotranspiration during the period 1982-2011. However, the positive trends in ET in Amazonia and eastern Brazil largely declined between 2001 and 2020, reflecting changes in climatic conditions and likely widespread deforestation in these regions (Hoang & Kanemoto, 2021; Sterling et al., 2013). In addition to these variations, ET changes during the year through the change in vegetation growth with an increase of the ET during the growing season.(Gaertner et al., 2019; Hwang et al., 2018; Obrist et al., 2003; White et al., 1999; Yang et al., 2020; Young et al., 2022).

Regardless of the deforestation in Brazil, ET is supposed to increase in the future in some regions due to climate change and the intensification of the hydrological cycle in warmer climate (Held & Soden, 2006; Huntington, 2006). However, ET will decrease in other regions due to climate change with the expected decrease in precipitation in these regions (Ranasinghe et al., 2021) and the decrease of the sensitivity of ET to vegetation greening as emissions increase (Lu et al., 2021), likely due to greater stomatal closure at higher CO_2 levels and/or a non-linear saturation response of ET to LAI (Yang et al., 2020)

2.4 Impact of land cover and land use change on actual ET.

Changes in land use and cover affect ET by changing plant species with different transpiration rates, radiative transfer in the canopy (Martens et al., 2000; Panferov et al., 2001) and by changing topography, albedo, soil texture, etc. of the area. (El Maayar & Chen, 2006; Zeng & Yoon, 2009).

Nobre et al. (1991), in a study they conducted, found that when the Amazonian tropical forests were replaced by degraded grass (pasture), a significant increase in the mean surface temperature (about 2.5°C) and a decrease in the annual evapotranspiration (30% reduction), precipitation (25% reduction), and runoff (20% reduction) occurred in the region.

ET for deforested areas

The effects of tropical deforestation resulting in alterations in land surface characteristics are likely to increase soil and air temperatures, reduce evapotranspiration and increase runoff (Shukla et al., 1990).

According to Shukla et al. (1990), deforested soils have less capacity to store water, their soil hydraulic conductivity decreases due to compaction induced by deforestation activities which reduces water infiltration into the soil (Malmer & Grip, 1990) and less energy is available for evapotranspiration (as more energy is reflected due to higher albedo). This gradual change in the land cover will affect the atmosphere by reducing the amount of water that is returned and the atmospheric dynamic (Werth & Avissar, 2002).

Consequently, the reduction of evapotranspiration leads to a reduction in precipitation and this decrease in precipitation can impact the flow of rivers according to the scale of deforestation. On small-scale deforestation, runoff caused by soil stripping is large enough to suppress precipitation reduction and raise river level, but on large-scale deforestation, reduced evapotranspiration with precipitation prevails and river flow is reduced (Gentry & Lopez-Parodi, 1980).

However some studies (Martens et al., 2000; Panferov et al., 2001) found an increase in ET during the land degradation process that would be justified by the change in surface properties because of human activities that contributed to the increase in soil evaporation that offsets the evaporative effect of defoliation. Evaporation increases also due to increased absorption of solar radiation as leaves and branches have been removed during land degradation, exposing previously shaded soil to vegetation, increasing soil evaporation. (Gong et al., 2017)

ET after pasture conversion

During the pasture conversion process, evapotranspiration increased significantly due to grass restoration. Since transpiration increases with the greening of the vegetation, the regrowth of grass would improve transpiration for plants fed with sufficient soil water (Li et al., 2009; Ming-yuan, 2002; Qiu et al., 2011; Sun et al., 2006; Wu, 2006; Yang et al., 2014). However, the increase in vegetation cover reduces the radiation absorbed by the soil and thus the evaporation of the soil. But the transpiration rates are high, if the affected areas remain grasslands in the coming years, groundwater levels may drop as consumption increases, gradually weakening the groundwater status for grass growth (Gong et al., 2017)

ET for forests/reforested areas

In general, forests have higher above-ground biomass and deeper roots, so they tend to use more water (Mátyás & Sun, 2014). In addition, the depth of water intake varies according to the vegetation. For example, isotopic studies in the eastern Brazilian Amazon showed that pasture took water only from the surface, while trees and lianas in tropical forests took it deeper, and deeper for trees than for lianas (Moreira et al., 2000). This depth also varies according to the seasons and increases during the dry season (Fritzsche et al., 2006).

These differences in water intake depth affect evapotranspiration. Trees, by drawing water from deep water, can better withstand droughts by continuing their evapotranspiration thanks to deep water reserves and/ or easy access to groundwater. Therefore, forests have higher evapotranspiration than other land cover types for several reasons: lower albedo, higher aerodynamic roughness, large leaf area, and deeper root systems (Giambelluca, 2002). In addition, the impact on evapotranspiration is influenced by species and forest age. For example, fast-growing species and older forests result in higher evapotranspiration (Tóth et al., 2014). Reforestation helps to restore soil properties affected by deforestation, but the dynamics of this restoration are crucial for the evolution of soil water balance. If evapotranspiration increases rapidly with reforestation, this can lead to a decrease in water reserve and groundwater levels, resulting in water stress (Peng et al., 2016).

Studies that quantify the effect of land cover and land use change on actual ET

Some studies already tried to understand the dynamic of the variation of ET due to land cover changes.

de Oliveira et al. (2018) made a study in Eastern Amazon where they tried to quantify the difference in ET for a forested and deforested areas. They found that during the wet season, ET values were quite similar for the forested and deforested area. But a decrease of the value of ET for the deforested area from 125mm/month in April (Wet season) to 50mm/month, two months later, in June (dry season) has been observed while there was nearly no change for the forested area for which the biggest difference observed between dry and wet season was 30mm between two months. The minimum ET in the deforested areas was lower than that in forested areas, and the amplitude between maximum and minimum was higher in the deforested areas. Elements of vegetation and soil can explain the variability in ET between the areas. The plants in deforested areas have shallow roots, so their access is limited to the water available in the upper layers of the soil. By contrast, forest trees can access the water table in the deeper regions of the soil, maintaining an optimum water balance and thereby avoiding a decrease in ET in the drier months or even resulting in an increase in ET in this period because of ideal atmospheric conditions (Fan & Miguez-Macho, 2010; Harper et al., 2014; Juárez et al., 2007; Williams et al., 1998).

The land use also changes the soil structure and the availability of water for plants. In soils whose original forest cover was exchanged for pasture, the amount of macropores and the water storage capacity decrease, whereas the surface and subsurface flow increases (de Moraes et al., 2006). This structure allows less water to be stored and to become available for ET, contributing to the water balance results. The compaction of pasture soil due to animal and machinery trampling can produce a considerable change and increase the surface runoff. Less water is stored in the soil, as it becomes more compact and less water can percolate through its structure(Chen et al., 2014; Gholami, 2013; Gholzom & Gholami, 2012; Santos & Augustin, 2015).
Soil characteristics may also play an important role even if vegetation type and root system depth are the primary factors responsible for these results. The soils' texture plays an important role, as this characteristic can drastically alter infiltration rate and storage capability (Saxton et al., 1986; Saxton & Rawls, 2006). In sandy soil, water can infiltrate faster than on a clayey soil (El Maayar & Chen, 2006; Mathias et al., 2015). In addition, as a clayey soil can become saturated more easily than sandy soil, the surface runoff will be greater on the clayey one.

Another study conducted in the upper reaches of the Xingu River in central Brazil attempted to simulate evapotranspiration rates based on different land cover: rainforest, pasture, and savannah. Evapotranspiration in tropical forest was measured at 1025mm/year while in savanna it was 1010 mm/year. These rates of evapotranspiration are quite close to estimates from other studies (Costa et al., 2010; Giambelluca et al., 2009; Oliveira et al., 2005; Vourlitis et al., 2002, 2008). It was therefore concluded that evapotranspiration was similar in forest and savannah watersheds. This is consistent with previous research, which suggests that transient tropical forests and savannahs may have similar evapotranspiration if surface soil water availability is sufficient. For grazing, the estimate was lower than estimates from other publications, at 567 mm/year, while the literature gives a range of 822 to 982 mm/year. (Lathuillière et al., 2012; Priante-Filho et al., 2004). Simulated evapotranspiration in pasture was approximately 39% lower than in natural rainforest and savannah ecosystems. This is comparable to evapotranspiration reductions observed of about 36% after deforestation and grazing in an area of Maranhão State (Dias et al., 2015; Oliveira et al., 2014).

In conclusion, changes in land use and land cover have a significant impact on evapotranspiration (ET). Deforestation generally results in a reduction in ET due to reduced forest cover, resulting in an increase in albedo and a decrease in energy available for evapotranspiration. In addition, soil in deforested areas often becomes compacted due to the trampling of machinery and animals, which decreases its hydraulic conductivity and reduces water infiltration. Therefore, less water is available for ET, and more is lost as runoff. This change in soil surface characteristics not only increases soil and air temperature, but also disrupts the water cycle, reducing precipitation and river flow in the long run. In contrast, conversion to pasture after deforestation initially increases ET due to the restoration of grass

that has a higher transpiration rate. Pasture tends to green quickly, which increases transpiration if there is enough water in the soil. However, this increase in vegetation cover reduces the radiation absorbed by the soil, thus reducing soil evaporation. Over time, if pasture remain and groundwater levels decrease due to increased water consumption, the ET could decrease again, which would weaken the water condition for grass growth. Reforestation typically results in higher ET than other land cover types due to several factors. Forests have higher aerial biomass, deeper root systems, lower albedo, higher aerodynamic roughness, and larger leaf areas. Some of these features allow forests to draw water from deeper soil layers, maintaining higher ET even during dry seasons. Restoration of soil properties after reforestation helps to rebuild water storage capacity and soil macropore structure, allowing better water infiltration and availability for plant use. However, if reforestation causes a rapid increase in ET, it can deplete water supplies and lower groundwater levels, which could cause water stress.

2.5 Remote sensing technology to assess evapotranspiration.

Remote sensing technology is recognized as the only viable means to map regional- and meso-scale patterns of ET on the Earth's surface in a globally consistent and economically feasible manner and surface temperature helps to establish the direct link between surface radiances and the components of surface energy balance (Allen et al., 1998). Remote sensing technology has several marked advantages over conventional “point” measurements:

- it can provide large and continuous spatial coverage within a few minutes.
- it costs less when the same spatial information is required.
- it is particularly practical for ungauged areas where man-made measurements are difficult to conduct or unavailable (RANGO, 1994). Remotely sensed surface temperature can provide a measure of surface temperature from a resolution of a few cm^2 from a hand-held thermometer to about several km^2 from certain satellites.(Li et al., 2009).

The majority of remote sensing models that estimate actual ET do so through the estimation of land surface energy fluxes. This requires both knowledge of the state of vegetation (e.g. LAI or fraction of green vegetation) and of land surface temperature (LST) which acts as one of the model boundaries. Therefore, remote sensing observations using both visible/near-infrared and thermal infrared sensors serve as an important source of input data for such models.
There are different ET datasets utilizing remote sensing observations but none of them fully satisfies the need for an accurate, operational, and field-scale flux estimates.

Moderate Resolution Imaging Spectroradiometer (MODIS)

MODIS Global Evapotranspiration Project (MOD16) is one of the widely available datasets suitable for regional and/or scientific applications (with an 8-day temporal and 500m spatial

resolution)(ESA, 2020). It's an instrument onboard NASA's Terra and Aqua satellites (Justice et al., 2002) that provides detailed information on vegetation and surface energy to estimate evapotranspiration on a regional and global scale in near real-time (Los et al., 2000). It works by measuring the reflectance of light emitted by the Earth in different spectral bands recorded by sensors, ranging from visible to thermal infrared. Each band corresponds to a specific range of wavelengths. It captures images of the Earth by scanning the surface in transverse bands and offers moderate spatial resolution. The raw data collected are processed to correct atmospheric, geometric, and radiometric effects. This allows accurate measurements of the reflectance of the Earth's surface. A first algorithm (2007) was created but as then being improved in different ways with a simplification of the calculation to assess vegetation cover fraction, a sum of the daytime and nighttime components to provide a more comprehensive assessment of evapotranspiration processes, a calculation of soil heat flux to better understand the energy balance and water exchange at the land surface. The new algorithm (2011) is also capable of distinguishing dry and wet canopy surfaces, allowing for a more detailed assessment of canopy water loss through evaporation and transpiration (Mu et al., 2011). The flowchart of the new algorithm is visible on Figure 6.

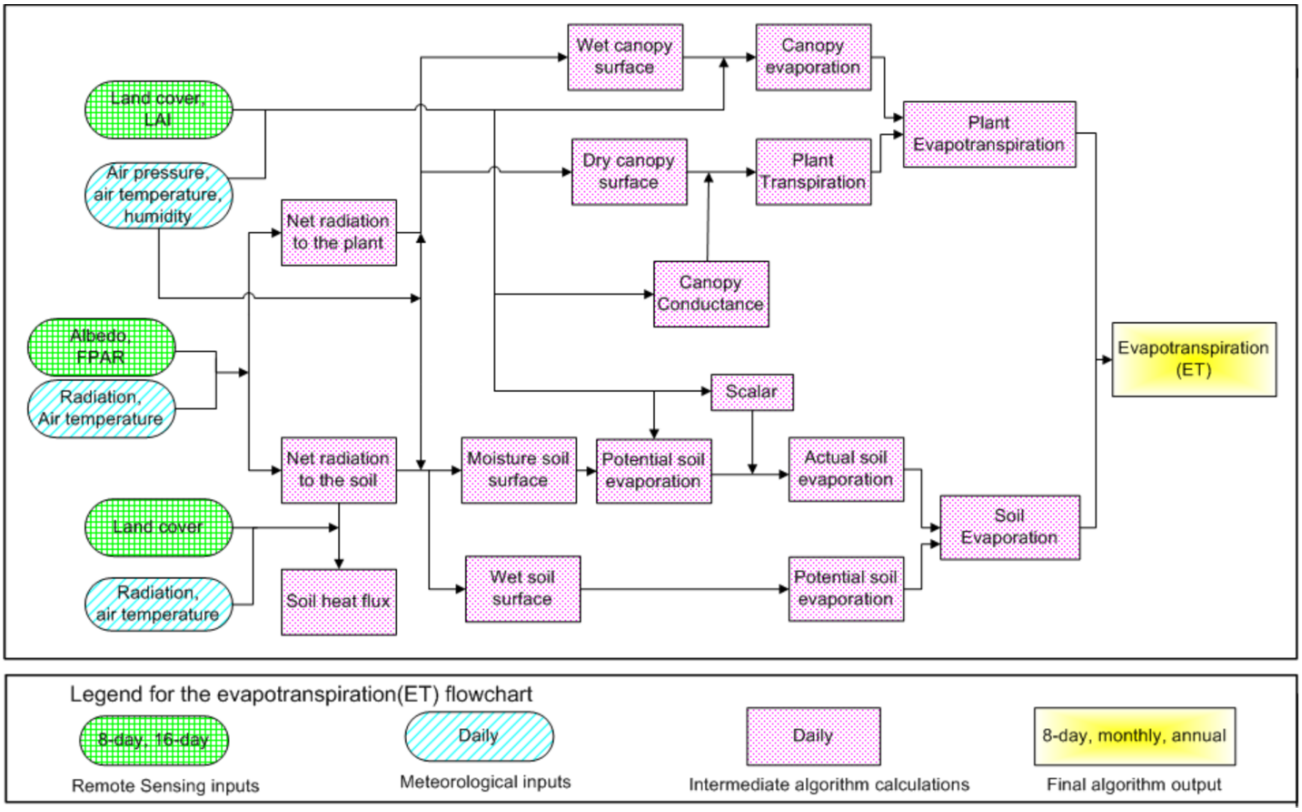

Figure 6: Flowchart of the improved MODIS Evapotranspiration (ET) algorithm (Mu et al., 2011)

The results obtained by this algorithm have been compared with ET measurement based on fluxes tower and a correlation coefficient of 0.86 was measured (Friedl et al., 2002). This coefficient is higher than the one based on the older algorithm which was 0.83.

Sentinels for evapotranspiration (SEN-ET)

The recent launches of the Sentinel-2A, Sentinel-2B and Sentinel-3A satellites (and upcoming launch of Sentinel-3B) present new opportunities for accurate and operational modelling of actual ET using of remote sensing data. The Sentinel satellites were designed to serve the operational needs of diverse user communities and fields of application. In the field of agriculture this aim is already partially realized with ESA projects such as "Sentinel-2 for Agriculture" providing a system which utilizes high spatial and temporal resolution optical data from Sentinel-2 satellites (and Landsat-8) for estimating growing area extent for main crop types as well as crop status from temporal evolution of Leaf Area Index (LAI) over a growing season. Time-series of Sentinel-1 Synthetic Aperture Radar observations have also been used to operationally map rice crop evolution or to discriminate between different crop types. The Sentinel-3 satellite has added the capacity of acquiring thermal observations to the existing suite of Sentinels' capabilities. This should allow for operational modelling of ET and of other land surface energy fluxes. However, for many agricultural applications the resolution of the modelled fluxes should be smaller than the typical field size. In the European Union agricultural context, where the Agricultural Census 2010 reported that the average farm size was 14.2 hectares and that 6 million farms were smaller than 2 hectares, this requires model outputs with a pixel size on the order of tens of meters. This is not possible when using Sentinel-3 alone (Sentinel-3 thermal sensor SLSTR has a spatial resolution of 1000 m) but might be achievable if synergies between Sentinel-3 and Sentinel-2 are utilized. The Multi Spectral Instrument (MSI) on board Sentinel-2, with its high spatial resolution (up to 10 m) and red-edge spectral bands, could allow for the disaggregation of ET model inputs and/or outputs to higher spatial resolution. By utilizing the synergies between the sensors of those two satellites it might be possible to derive accurate flux estimates at high spatial resolution (ESA, 2020). Evapotranspiration is estimated from the latent heat flux LE by a conversion into instantaneous quantity of evaporated water (in mm/second) divided by the latent heat of vaporization. This can then be converted into daily evapotranspiration in mm/day by multiplying by the ratio of instantaneous to average daily solar irradiance. SEN-ET will be used in this thesis, it is explained in more detail in the Materials and methods (4.5.2) (ESA, 2020).

The uncertainties related to its use were evaluated at the turbulent heat flux (sensitive and latent) measured at validation sites. These were estimated at 20-30%. Furthermore, based on the validation of the SEN-ET model at 11 sites covering a range of land use and climate conditions, the expected relative square error (rRMSE) for the sensitive thermal flux (H) is about 0.45 and the correlation (r) about 0.67. For grasslands, these values improve at a rRMSE of 0.37 and a correlation of 0.79. Based on the same validation set used for H, the expected rRMSE for LE is about 0.46 and r of 0.76 with the best performance obtained in cropland (herbaceous and woody) where rRMSE was 0.32 and r of 0.75 (ESA, 2020).

3. Objectives

The impact of reforestation on water resources depends on previous results on the alteration of transpiration with land cover. Previous results have shown that there were many uncertainties regarding the evapotranspiration measurement in the study area (Delvoie, 2023). To resolve this uncertainty, the main objective of this Master's thesis is to answer the following question:

What is the impact of reforestation on evapotranspiration? How can we better assess evapotranspiration in the Atlantic Brazilian Forest?

To answer question, two estimates of evapotranspiration will be used in this Master thesis:

1) Mass balance equation. The mass balance will be assessed based on the following fluxes: Water stock variation (ΔS), precipitation (P), drainage (D) and capillary rise (CR) to estimate actual evapotranspiration (ET_a)
2) SEN-ET remote sensing method. SEN-ET will provide actual evapotranspiration ET_a with a spatial resolution of 20m and a temporal resolution of 10 days.

These two methods will be compared with a reference evapotranspiration ET_0 using weather station measurements to first, understand the periodicity and the variability of evapotranspiration in the study area based on the ET_0. Then the two methods will be compared to identify the possible differences and errors in terms of estimation of evapotranspiration. The final objective will be to compare evapotranspiration between the different study plots to answer the following question:

Does a regenerating forest transpire more than an older forest? Could it have an impact on soil water resources?

4. Materials and methods

4.1 Description of the area under study

4.1.1 Region

This study focuses on the Atlantic Forest region (Figure 7a), which has experienced intense deforestation in the last decades. The climate is subtropical humid with dry winter, from May to September, and a hot summer, from October to April. The mean precipitation is 1900 mm (IMNET).

The map below (Figure 7b) illustrates the land cover of a region of the Brazilian Atlantic Forest in 2017 and shows the different proportions of land cover and which are dominant. In yellow, most of the land is given over to agriculture and grassland. In dark green are areas where forests are growing naturally, and in khaki are areas where new forests are being planted (Wagner et al., 2020).

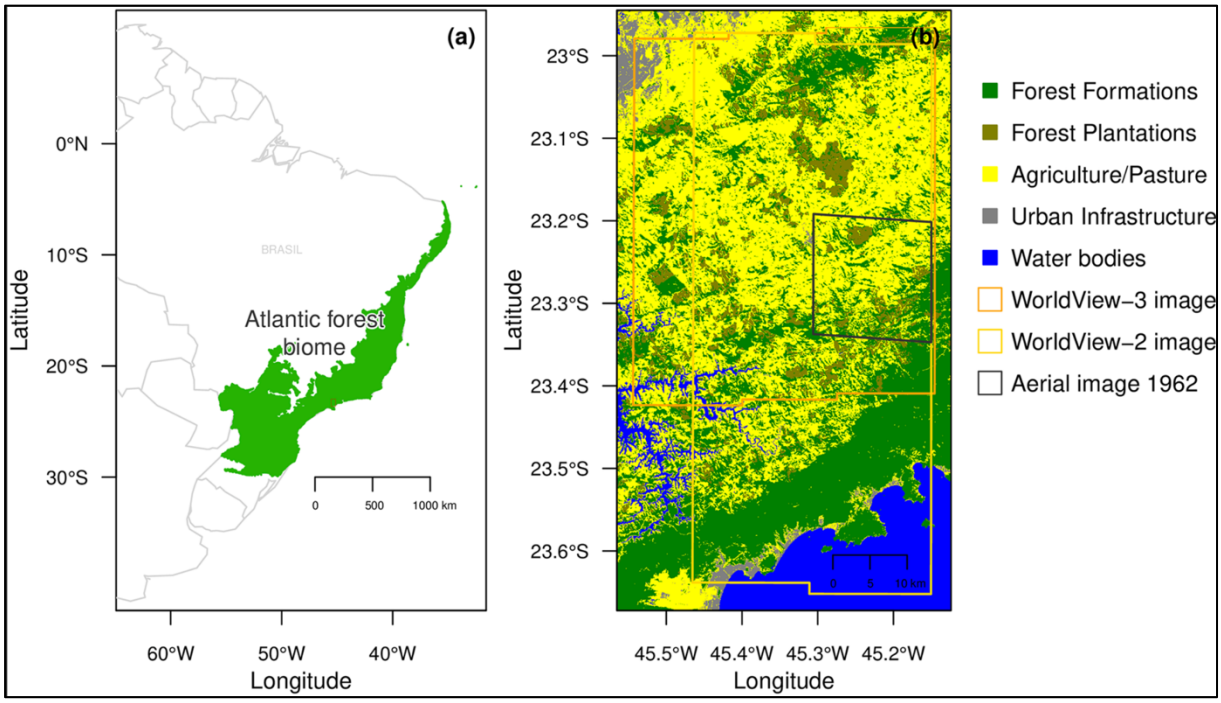

Figure 7 : Maps from the research article "Mapping Atlantic rainforest degradation and regeneration history with indicator species using convolutional network" (Wagner et al., 2020). Map (a) shows the geographical location of the Brazilian Atlantic Forest. Map (b) illustrates the different land covers of one part of the Brazilian Atlantic Forest in 2017, taken from the MapBiomas project.

INPE (Brazilian National Institute for Space Research) has set up a research project in this region where different contrasted plots have been defined and equipped with sensors. This data set was collected at the São Francisco Xavier Ecohydrological Experimental Station (EES-SFX). Located at around 1100 m above mean sea level. EES-SFX is the experimental branch of the INPE's Laboratory of Isotopic Ecohydrology (LabEcoh).

4.1.2 Experimental plots

EES-SFX comprises 4 distinct plots nestled in the historical landscape of the Atlantic Forest, situated within the protected confines of APA-São Francisco Xavier. These plots are situated on a privately owned estate within the São José dos Campos district of São Francisco Xavier, in São Paulo state.

After intense occupation of the Atlantic Forest in the early twentieth century, the areas of these plots, initially deforested, were subjected to different types of use and occupation. Area R40 comprises a mature forest, regenerated in a coffee plantation area over 40 years ago. Located on a hilltop with a slope of about 15 degrees, this plot is now located in a more intensive protection zone called the Alto do Deco Private Natural Protection Reserve (RPPN) (Figure 8a). Area R10 is situated in a riparian area, predominantly flat (~5 degrees of slope), which has undergone a reforestation process for over 10 years (Figure 8b). The CA (cleared area) area is located on the same slope as R40 (also with a slope of ~15 degrees), but outside the boundary of the Alto do Deco RPPN. This area was not reforested, but grazing activities were less intense than in the lower areas. Today, this area is predominantly occupied by shrubs and grasses, with tall trees scattered sparsely (Figure 8c). Finally, the P (pasture) area comprises a pasture area situated on a slope of ~10 degrees, still used for grazing and covered by grass (brachiaria) (Figure 8d).

Table 1: Different characteristics of the areas P, CA, R10 and R40: Surface, slope, state of vegetation and status

Parcel	Surface of the area m^2	Slope	State of vegetation	Status
P	80	10°	Pasture	Not protected
CA	100	15°	Cleared area covered with bushes	Not protected
R10	450	5°	Young forest of 10 yrs	Riparian area
R40	370	15°	Old forest of 40 yrs	Protected

These four areas can be seen on these following pictures, taken by Charlotte Dermauw when she was in Brazil:

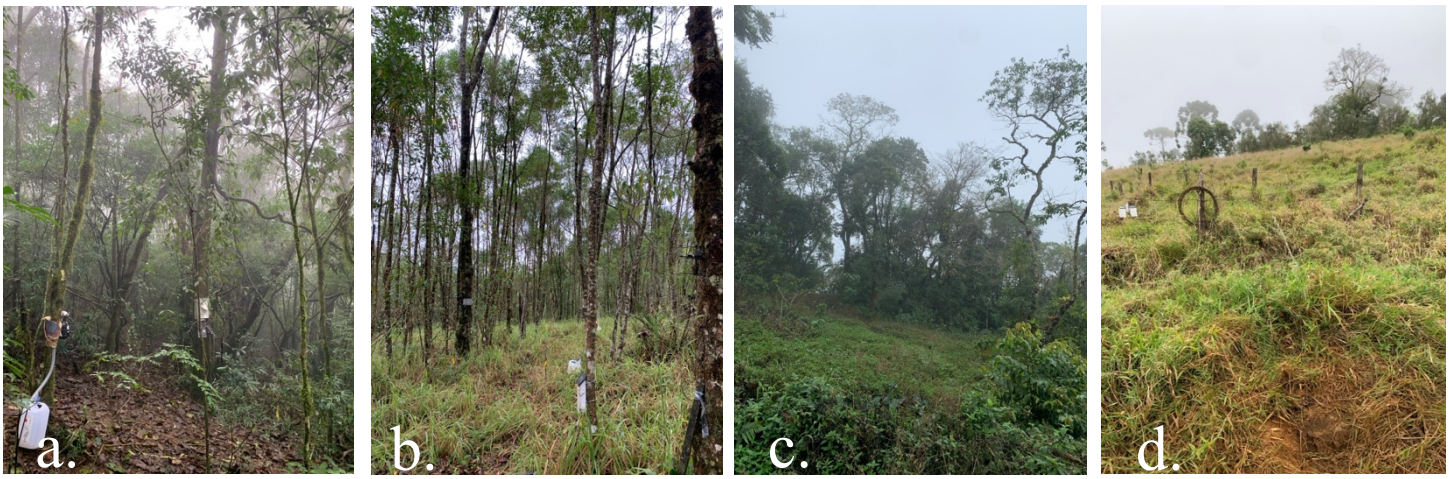

Figure 8:Pictures of the four study areas to illustrate the different landscapes and stages of reforestation. These are placed in order of reforestation stage, with R40, R10, CA and finally P corresponding to pictures a, b, c and d (Figures authored by Charlotte Dermauw, in 2023).

4.1.3 Climatic Data

Weather data were collected from January 2019 to August 2023 using a HOBO meteorological station, model U30 equipped with a rain gauge S-RGF-M002 and ATMOS 41. These stations were installed at São Francisco Xavier, in the study area and covered different periods. HOBO took measurements from January 2019 to January 2022 while ATMOS was implemented in January 2023 and the data available for this master thesis are until August 2023. A rain gauge ECRN-100 was used between July 2022 and January 2023. The data provided by these weather stations are hourly:

- rainfall [mm],
- temperature [°C],
- dew point temperatures [°C],
- relative humidity [%],
- wind speed [m/s],
- gust speed [m/s],
- cloud height [m],
- solar radiation [W/m2]
- pressure [mbar].

All these data were used to assess reference evapotranspiration ET_0 as explained in 4.5. For periods in which no data were available (i.e. January to July 2022), rainfall data were obtained from an INMET (acronym in Portuguese for National Institute of Meteorology) station, located in the municipality of Monte Verde, at around 60 km northwest from our study area. The data from this station are aligned with another time network, no doubt enabling INMET to standardize their data across the whole of Brazil, and therefore had to be brought forward by 4 hours. Subsequently, from July 01, 2022, to January 08, 2023, rainfall was measured using a rain gauge, model ECRN-100 (METER Group).

Figure 9: ATMOS meteorological station, São Francisco Xavier

Daily precipitation can be seen on Figure 10 where precipitation during the dry period are represented in yellow while precipitation during the wet period are represented in blue.

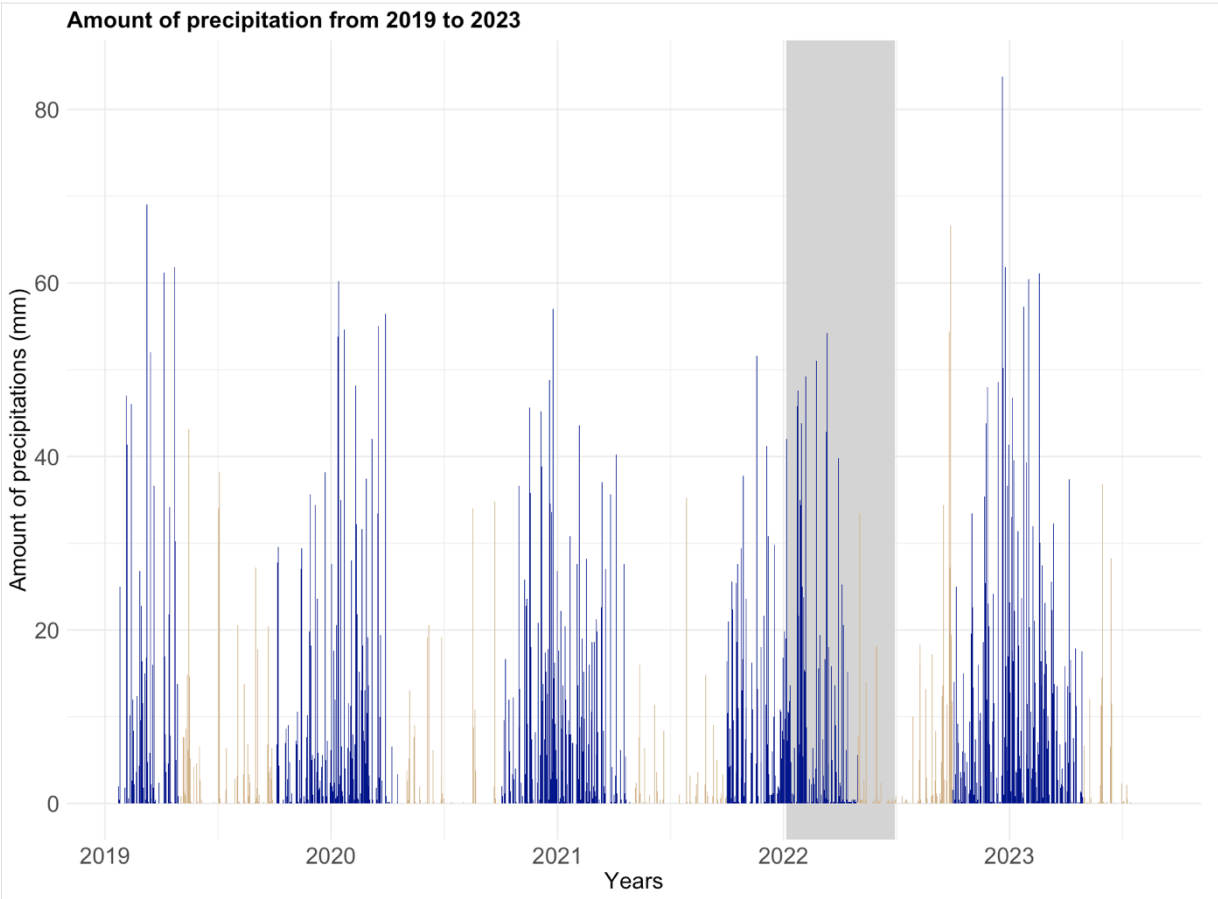

Figure 10: Daily precipitation measured at INPE in mm per day. The data available during the dry season are represented in yellow and the data available during the wet period are represented in blue. The time cover is from January 2019 to August 2023. The grey rectangle represents the moments where there are no meteorological data available except rainfall measured by the rain gauge (July 2022 to January 2023).

4.2 Water content and water potential time series

4.1.4 Data Acquisition

Soil water potential (h) and volumetric water content (θ) were monitored in the 4 plots at 7 different depths: 0.1, 0.2, 0.3, 0.5, 1, 1.5 and 2 m-depth using MPS-6 sensors from METER group for h while GS1 capacitance sensors (Meter Group) were used for volumetric water content θ. The sensors' measurements were automatically recorded in datalogger models Em50 or ZL6 (*ZL6*, 2021) at user-defined intervals. Eventually, defective sensors were substituted by the same sensor model when available, or similar models, such as the TEROS 10 model for the GS1 water content sensor and TEROS 21 for the MPS-6 matric potential sensor, from the same manufacturer (*TEROS 10 - Meter Group*, s. d.; *TEROS 21*, 2021). It is important to mention that the sensors have not been calibrated by INPE and that those used to measure water potential, TEROS 10, sometimes take longer to react than TEROS 21 sensors used to measure water content. This discrepancy is visible on several retention curves shown (Appendix 3). Installation of the sensors took place in different years for each plot, as presented on Table 2 representing all the data used for this thesis.

Table 2 : Periods of measurements studied for the 4 areas, the old forest of 40 years (R40), the young forest of 10 years (R10), the cleared area (CA) and the pasture (P) for θ and h.

Area	Beginning of the measurements	End of the measurements
R40	20/02/19	15/08/23
R10	12/02/19	04/08/23
CA	02/06/21	15/08/23
Pasture	16/07/21	15/08/23

4.1.5 Data filtering

Data treatment of the data has been done on R Studio.

First, θ and h were not recorded at the same timescale during the period of measurements. Most of the time, the values were available every hour, but for a short period, they were available every 15 minutes, but not at the same time, depending on the depth and the study area. For the sake of consistency, an hourly average was calculated.

Next, θ values at each depth were treated as follow:

- If two consecutive values had a difference of more than 0.05cm³/cm³/hour in the measurement, the second value was disregarded and replaced by a NA (No available).
- A normal distribution was drawn for each depth, allowing values outside the 5% confidence interval on either side of the distribution to be removed.

For h data, they were treated as follow:

- If two consecutive values had a difference of more than 0.01 of pF between two consecutive hours, the second value was disregarded and replaced by a NA.
- A normal distribution was also drawn like θ and values outside the 5% confidence interval on either side of the distribution were removed.

The confidence intervals for each depth and study zone are shown in Table 3 and the normal distributions are shown in Appendix 1.

Table 3: Intervals of normal distributions of θ and h for each plot and each depth: 0.1, 0.2, 0.3, 0.5, 1, 1.5 and 2m. A confidence interval of 5% on each side of the distribution was taken. Any value outside this confidence interval was replaced by NA.

		0.1	0.2	0.3	0.5	1	1.5	2
P	θ [cm³/cm³]	0.298-0.445	0.367-0.441	0.313-0.399	0.354-0.405	0.296-0.358	0.311-0.364	0.308-0.371
	h [pF]	1.995-2.694	1.972-2.694	2.025-2.457	2.087-2.475	2.080-2.423	2.050-2.861	2.054-2.449
CA	θ [cm³/cm³]	0.360-0.462	0.372-0.438	0.398-0.441	0.398-0.438	0.337-0.396	0.351-0.397	0.340-0.364
	h [pF]	1.895-2.381	1-1	1.977-2.324	2.105-2.496	2.046-2.275	1.999-2.196	2.017-2.288
R10	θ [cm³/cm³]	0.129-0.285	0.200-0.382	0.257-0.396	0.350-0.427	0.356-0.403	0.245-0.393	0.376-0.425
	h [pF]	2.013-3.578	1.995-3.746	2.004-3.771	1.962-3.172	2.008-2.627	1.986-2.449	1.927-2.357
R40	θ [cm³/cm³]	0.225-0.405	0.266- 0.433	0.287- 0.406	0.369- 0.459	0.354- 0.447	0.309- 0.439	0.341- 0.440
	h [pF]	2.057-3.780	2.025-3.782	2.025-3.618	2.042-3.368	2.042-3.342	2.042-3.182	2.017-2.778

As many data are missing initially and after these filtering's for θ and h, one method was used to fill the gaps.

An interpolation between different depths will be performed to assess the correlation between them and to see if it is possible to estimate a value at one depth based on values available at other depths. The goal is to see the correlation between different depths in term of spatial and temporal dimensions to see when and based on which depth could another depth be assessed and have the better R^2.

Unfortunately, there will still be missing data after that.

4.3 Soil properties

28 soil samples were collected from the four plots at seven different depths by the Agronomic Campinas Institute (IAC) in May 2023. These samples were used to identify the texture based on a granulometry analysis of the soil. This analysis was carried out by INPE.

The different types of soil identified are shown in Table 4.

Table 4: Main texture of horizons 0.1, 0.2, 0.3, 0.5, 1, 1.5 and 2 for the four study areas, the old-growth forest R40, the reforested forest of ten years (R10), the cleared area (CA) and the pasture (P). Estimation based on IAC textural triangles.

	R40	R10	Cleared area	Pasture
0.1	Clay	Sandy clay loam	Clay	Sandy clay
0.2	Clay	Clay	Sandy clay	Sandy clay
0.3	Clay	Sandy clay loam	Clay	Clay
0.5	Clay	Sandy clay loam	Clay	Clay
1	Clay	Sandy clay loam	Clay	Clay
1.5	Clay	Sandy clay loam	Clay	Clay
2	Clay	Sandy clay loam	Clay	Sandy clay loam

4.3.1 Laboratory

The samples were then subject to evaporation to assess soil hydraulic properties using the HYPROP system. This system allows one to characterize soil retention and conductivity curves.

The retention curve was assessed using the following multimodal van Genuchten equation:

$$S_e(h) = \sum_{i=1}^{k} w_i \left[\frac{1}{[1 + (\alpha|h|)^{n_i}]}\right]^{m_i} \qquad Equation\ 1$$

Where $S_e(h) = \frac{\theta(h) - \theta_r}{\theta_s - \theta_r}$ and $m_i = 1 - \frac{1}{n_i}$

With Se: Saturation rate [-]

θ: Water content [cm^3/cm^3]

h: Water potential [kPa]

θ_r: Residual water content [cm^3/cm^3]

θ_s: Saturate water content [cm^3/cm^3]

α: Parameter linked to the inverse of the air entry point [cm^{-1}]

n: Parameter linked to the pore size distribution and determining the slope of the curve [-]

w_i: Weighting factor between the two curves i=1 and i=2 [-]

Depending on if the soil is unimodal or bimodal, k is equal to 1 or 2. The conductivity curve equation is:

$$K(S_e) = K_s \sum_{i=1}^{k} (w_i S_{e,i})^{\tau} \left[\frac{\sum_{i=1}^{2} w_i \alpha_i \left[1 - \left(1 - S_{e,i}^{1/m_i} \right)^{m_i} \right]}{\sum_{i=1}^{2} w_i \alpha_i} \right]^2 \qquad Equation\ 2$$

Where:

- K is the hydraulic conductivity [cm/j].
- S_e is the saturation rate [dimensionless]
- K_s is the hydraulic conductivity at saturation [cm/j].
- τ : is a parameter link to the tortuosity, often equals to 0.5 [-].

(Priesack & Durner, 2006)

K_S (or Ksat) was measured by the INPE for plots R10 and R40 and then put as a fix value in LABROS with the use of the Van Genuchten Mualem relation in order to obtain $\alpha_1, \alpha_2, \theta_r, \theta_{sat}, n_1, n_2\ and\ w_2$(Appendix 6). Since no measurements have been recorded for CA and P, the mean of the measured values for R40 and R10 was used as the Ksat value for P and CA after validation of the hypothesis by performing a comparison of the measured conductivity values for the 4 zones. (Appendix 8)

The final Ksat values in cm/h can be found in the table below:

Table 5: Table with the measured Ksat value for R10 and R40, measured by INPE, and the Ksat value of P and CA based on the mean of the Ksat value of R10 and R40.

Parcels	Ksat value at 1.5m [cm/h]	Ksat value at 2m [cm/h]
P	33.125	58.8
CA	33.125	58.8
R10	53.25	24
R40	13	93.5

4.3.2 Field soil characteristic

In situ measurements of θ-h can be used to retrieve a field retention curve, by plotting pairs taken at the same depth and time (Appendix 3).

To check the general appearance of the curve, a retention curve obtained from the various parameters of the Van Genuchten equation will be fitted to the point cloud (van Genuchten, 1980).

4.4 Mass balance

The first subobjective of this thesis is to assess the evapotranspiration through a mass balance equation. We defined the hourly mass balance equation over 1.75 m depth as:

$$0 = -\frac{\Delta S}{\Delta t} + P - ET_a + BF \ \left[\frac{mm}{hour}\right] \qquad Equation\ 3$$

Where

- $\Delta S/\Delta t$ is the variation of the water stock in the soil between 0 and 1.75m [mm/hour],
- P is recharge of the soil in water due to precipitations [mm/hour],
- ET_a is the actual evapotranspiration [mm/hour],
- BF represents that Bottom Flux at 1.75m, negative when drainage occurs and positive for capillary rise[mm/hour].

In the following, we define each term of this equation:

4.4.1 Water Stock

The variation in water stock for the 4 areas studied could be calculated using the following formula:

$$S = \sum_{i}^{n} (Pi \times \theta i) \ \left[\frac{mm}{\text{hour}}\right] \qquad Equation\ 4$$

Where:

- P_i is the width of layer i
- θ_i is the water content in layer i
- S is the hourly water stock

The width of the layer is based on the location of the probes.

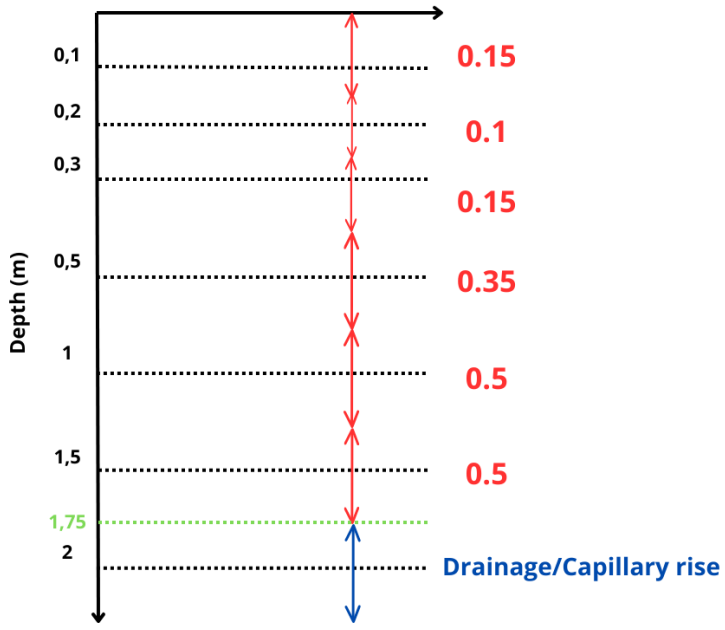

Figure 11: Scheme showing the width of the different layers measured for each depth. The width of the layer is shown in meters.

4.4.2 Drainage and capillary rise

Drainage or capillary rise q can be calculated based on Darcy equation:

$$q = -K(h) \times \nabla H \quad \left[\frac{m}{s}\right] \qquad Equation\ 5$$

Where:

K(h) is the vertical soil hydraulic conductivity [m/s] at suction h.

∇H is the vertical gradient of total water head , i.e. is the sum of the matrix and gravitational heads [-] (Neuman, 1977).

The equation uses to calculate ∇H between 2 and 1,5 m depth is:

$$\nabla H = \frac{\Delta H}{\Delta z} = \frac{(h_{2m} - 2) - (h_{1.5m} - 1{,}5)}{(-2 + 1{,}5)} \qquad Equation\ 6$$

where ΔH is the difference between H_2 and H_1, h is the water potential [cm]. Positive values of ∇H (i.e. negative q) mean that there is drainage, while negative ∇H mean capillary rise.

Soil hydraulic conductivity is function of the soil type and defined in section 4.3.1. K(h) in Eq. 5 is provided by the value of K at the mean $h=(h_{2m}+h_{1,5m})/2$.

4.5 Evapotranspiration

Different methods have been used to estimate actual evapotranspiration time series.

The Penman-Monteith equation provides potential evapotranspiration (ET_0) based on commonly measured meteorological data such as solar radiation, air temperature, vapor content or wind speed (Allen et al., 1998). It will be used to understand the variability and seasonality of evapotranspiration in the study area and to compare with actual and potential evapotranspiration that will be assessed. Potential ET (ET_p) can be calculated by multiplying the ET_0 by a cultivation coefficient, K_c, where K_c represents the ratio between the potential ET and ET_0.

MODIS provides ET_p and ET_a and can be used by comparison to PM to provide K_c values. The value of soil K_c varies according to the level of water content. (Allen, s. d.)

4.5.1 MODIS (MODerate Resolution Imaging Spectroradiometer)

The MODIS MOD16 (MOD16A2GF.061) global evapotranspiration products can be used to calculate regional water and energy balance, soil water status; hence, they provide key information for water resource management. The MOD16 ET datasets are estimated using Mu et al.'s improved ET algorithm (Mu et al., 2007).

The ET algorithm is based on the Penman-Monteith equation (see Appendix 11) and considers both the surface energy distribution process and environmental constraints on ET. It uses

ground-based meteorological observations and remote sensing data from MODIS to estimate global ET by:
(1) adding vapor pressure deficit and minimum air temperature constraints on stomatal conductance.
(2) using leaf area index as a scalar to estimate canopy conductance.
(3) replacing the normalized difference vegetation index with the enhanced vegetation index, which also changes the equation for calculating the fraction of vegetation cover (FC).
(4) adding a soil evaporation calculation to the previously proposed RS-PM method.
With a spatial resolution of 500m and a temporal resolution of 8 days, it was the more precise available. Two bands of evapotranspiration are available: ET and PET. ET correspond to the total evapotranspiration and so the actual evapotranspiration while PET corresponds to the potential evapotranspiration. Based on these two data, the cultural coefficient could be assessed.

The data obtained are given in [Kg/m^2/8 days] so to compare the evapotranspiration measured a unit conversion to [mm/8 days] has been done. The value of the pixel obtained is equal to the sum of the evapotranspiration over 8 days.

$$ET_p = \left(\frac{ET_p \left[\frac{Kg}{m^2} \right] \times 1000}{Water\ density \left[\frac{kg}{m^3} \right]} \right) \left[\frac{mm}{8\ days} \right] \qquad Equation\ 7$$

Where:

- 1000 is used to convert meter into millimeter.
- The water density is equal to 1000 kg/m^3.

Since the resolution is very low, the results expected will not be very precise but will help in the comparison of ET measurements.

4.5.2 SEN-ET (Sentinels for Evapotranspiration)

The aim of SEN-ET, developed by the ESA (European Space Agency), is to estimate real evapotranspiration at ground level using observations from the Sentinel-2 and Sentinel-3 satellites.

Sentinel-2 provides optical data with high spatial and temporal resolution thanks to the multi-spectral instrument (MSI) with a high resolution of up to 10m and red-edge spectral bands. Sentinel-2's MSI optical data is used to characterize the biophysical state of the Earth's surface at a resolution of 20m. This resolution was chosen because it corresponds to the native resolution of the MSI bands in the red and short infrared and is also sufficient to capture most

of the landscape features of interest. MSI data can also be used to refine lower resolution SLSTR data.

Sentinel-3 provides thermal observations based on the SLSTR sensor and has a lower resolution of 1 km compared to Sentinel-2. Sentinel-3's SLSTR thermal data are used to establish the lower boundary condition of the Earth's surface energy model. As the LST data are acquired at a spatial resolution of around 1 km, they are refined using a machine learning model down to 20 m.
The data acquired by Sentinel-2 and Sentinel-3 do not necessarily have to be on the same timescale and can be separated by up to 10 days. Energy fluxes at the Earth's surface are always modeled at the time of the S3 passage. This is because vegetation changes are not as dynamic as LST changes. However, the smaller the time difference between the two passes, the lower the risk that abrupt changes in vegetation conditions will introduce errors into the model.

Meteorological data available in the Copernicus Climate Data Store (CDS) are also used. These are needed to establish the conditions that drive and modulate the transfer of energy between the surface and the atmosphere. ERA-5 data, a specific CDS product, is used in this case and provides meteorological data with high spatial and temporal resolution. such as temperature at 2m, dew point temperature at 2m, surface pressure, etc.

In addition to meteorological and Sentinel data, the land cover map is used to define parameters that are not easily retrievable from optical images, such as vegetation height, and a digital elevation model is used to adjust the air temperature to the correct elevation.
Four different energy flows modelled at the soil surface (W/m^2) can be obtain from SEN-ET:

- Latent heat (LE), which is the energy used during evapotranspiration to convert water from the liquid to the gaseous phase. Latent heat is obtained via the 3 other products.

$$LE = R_n - G - H \quad \left[\frac{W}{m^2}\right] \qquad Equation\ 8$$

- Sensible heat flux (H), which is the temperature transfer from the surface to the overlying air, determined by the temperature difference between the surface and the air and depends on surface and meteorological conditions (roughness, wind speed, etc.). H is obtained through Sentinel-3 and RA5 data.
- Soil heat flux (G), which is the heat transfer from the surface to the deepest layers of the soil. G is the flux with the greatest uncertainty because of the high spatial variability of the flux and the mismatch in scale between old measurements and model outputs. G is obtained through Sentinel-2 data.
- Net radiation (R_n) includes net shortwave radiation (dependent on solar irradiance and surface albedo) and longwave radiation (dependent on surface and air temperatures and emissivity). R_n is obtained through RA5 and Sentinel-2 data.

LE can then be converted into daily evapotranspiration (mm/day) by dividing LE by the latent heat of vaporization and multiplying by the ratio between instantaneous solar irradiation and average daily solar irradiation.

$$ET_a = \left(\frac{LE}{LH}\right) \times \left(\frac{I}{I_{avg}}\right) \quad \left[\frac{mm}{day}\right] \qquad Equation\ 9$$

Where:

- LH, latent heat of vaporization, is the amount of energy required to vaporize a unit mass of water, generally expressed in joules per kilogram (J/kg) or watts per square meter (W/m²). It is a constant that depends on temperature and pressure. The latent heat of vaporization of water is about 2260 J/kg.
- I, instantaneous solar irradiance, is the solar energy flux incident on a surface per unit area and time, generally expressed in watts per square meter (W/m²). It represents the quantity of solar energy received at a given moment.
- I_{avg}, average daily solar irradiance, is the average solar energy flux incident on a surface over a whole day, also expressed in watts per square meter (W/m²). It represents the average amount of solar energy received over the course of a given day.

So far, SEN-ET has only been validated for cultivated areas and never for forests. One of the sub-objectives of this master's thesis is to use it in forests and see how accurate and precise it is by comparing it with other evapotranspiration measurements (ESA, 2020).

5. Results and discussions

5.1 Meteorological data

Based on meteorological data, two fluxes have been assessed: i) Monthly precipitation (blue in Figure 12) directly measured by the meteorological station at INPE and ii) Monthly reference evapotranspiration ET_0 (red in Figure 12) assessed based on the Penman-Monteith equation (Appendix 11) and the use of the meteorological variables at EES-SFX obtained from the different meteorological stations. (4.1.3)

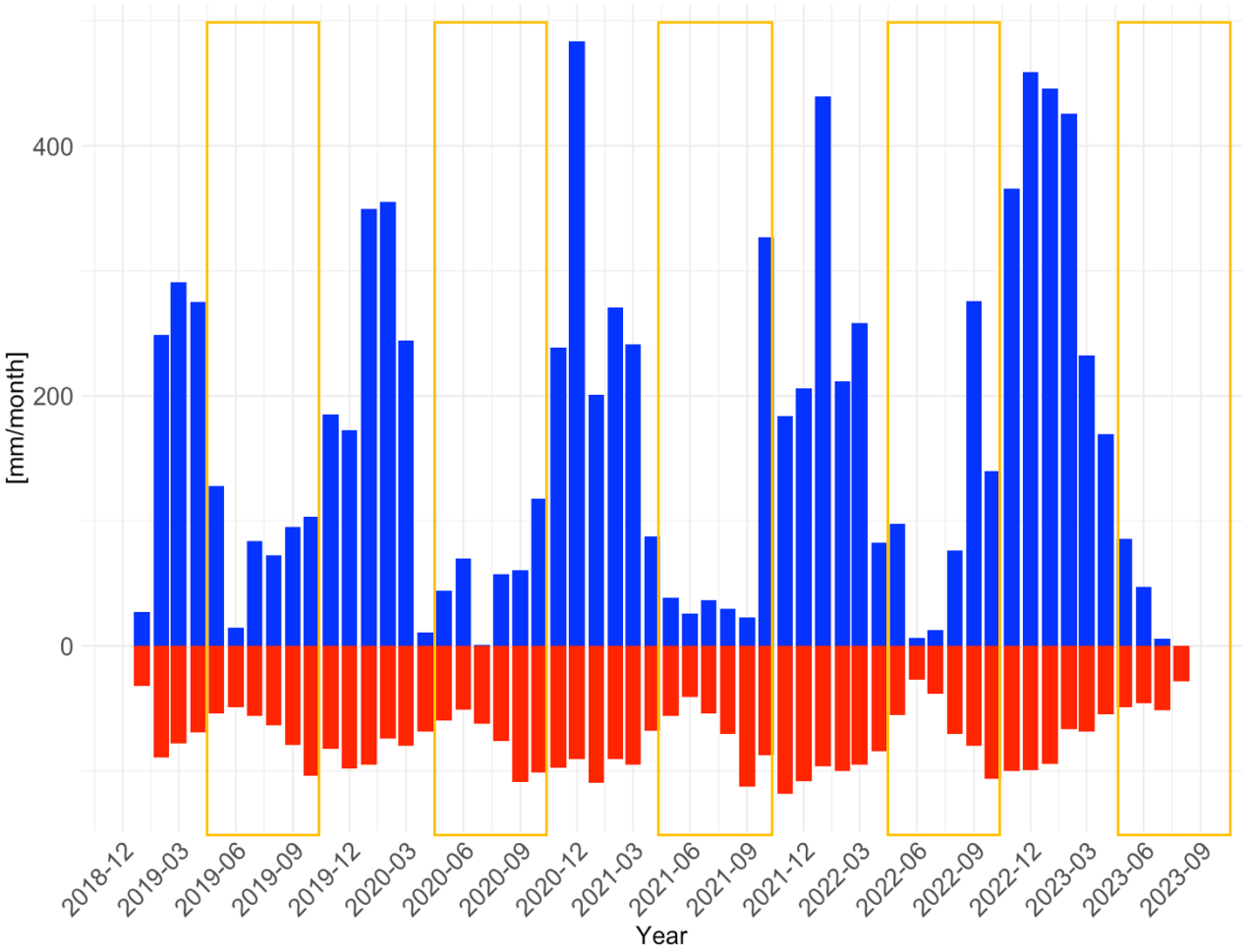

Figure 12: Graphic of measured precipitations (blue) and calculated reference evapotranspiration (red), cumulated for each month from January 2019 to August 2023. Dry seasons are in yellow.

Figure 12 illustrates the seasonal variability of monthly precipitation and ET_0 in the study area. Precipitations and ET_0 are both higher during the wet period (from October to April) than during the dry season (from May to September (yellow rectangle)). It can also be seen on Figure 12 that sometimes dry season starts or finish earlier than in theory with for example during year 2020 an early dry season that started one month earlier, in April.

For all the studied years, June is the month with the least precipitation (1.09 mm/day) and ET_0 (1.42 mm/day). June 2022 was the lowest of the 4 years with 0.89 mm/day of evapotranspiration and 0.21 mm/day of precipitation.

The higher ET_0 is found in October (3.21 mm/day compared to 5.54 mm/day of precipitation on average) while higher precipitation occurs in January (9.43 mm/day).

Comparing year to year, we can see that rainfall seems to be increasing in recent years and especially during the wet season from October 2022 to April 2023 where half of the months exceeded 400 mm of precipitation per month. However, ET_0 doesn't seem to be affected in the same way. In fact, 2022 was a wet year with nearly 300 mm of precipitation in September, which is normally quite a dry month.

5.2 Soil data

As explained in Materials and Methods (4.1.5), the initial θ and h data had to be filtered to remove outliers. The number of filtered values for θ and h for each area is shown in the following table:

Table 6:Table showing the total number of initial values, the number of values filtered by the normal distribution (5% confidence interval) and the number of values filtered by the slope for all 4 study areas for water content θ and water potential h.

Parcels		Total values	Outliers removed by the normal distribution	Outliers removed by the slope
P	θ	127.645	17.481	0
	h	127.680	46.763	484
CA	θ	113.883	20.865	0
	h	124.152	20.677	0
R10	θ	224.308	82.062	0
	h	241.710	44.707	9.849
R40	θ	254.870	68.097	2.060
	h	219.604	104.267	5.905

Filtering through the normal distribution removed most values from plot R40 for h and plot R10 for θ. The removal of outliers via the slope was especially useful for h of plot R10 and for θ and h of plot R40. It can be deduced that most outliers, evaluated based on the precise criteria of this thesis, were present in plots R10 and R40. Retention curves with these field data have been made and are visible in Appendix 3. The next two sub-points will present the θ and h data after these filters for the four study areas.

5.2.1 Water content

The final θ data after filtering is presented in Figure 13 for each of the four areas under study. These graphs highlight the variation of θ within the same area according to the depth of the soil and to visualize the seasonality of θ in the soil. They also allow for the comparison of θ between the four study areas and to deduce certain behaviors, certain trends.

Within the same study area, the different θ values vary according to depth. For the R10 and R40 areas, θ in the soil tends to increase with depth, with θ at 2m depth is often the highest. However, the depths of 0.3 and 1.5 stand out from the others, 0.3m being much wetter and 1.5m being much drier than their surrounding layers. For these two areas, a very pronounced seasonality is visible, with much lower θ values during the dry seasons (from May to September). The seasonality of these zones could be described as highly dynamic, and this dynamic is probably linked to the consumption of water for evapotranspiration and a significant amount of water withdrawn from the roots of the trees. These high rates of water uptake occur during the dry period while ET is the lowest. This seasonality and variation are especially visible for R40, which is the study area where the most data are available. And in general, the greatest variations in θ occur near the surface (at depths 0.1, 0.2 and 0.5m)

For plots P and CA, which are not covered by forests, the seasonality of θ is much lower and therefore the dynamics are less pronounced. θ value at most depths varies by about 10% for CA and 20% maximum for P where it varies between 40% and 50% for some depths of R10 and R40 (the depths closest to the surface). These small variations could be related to the fact that CA and P are probably areas saturated with water continuously and less evapotranspiration rates. However, since very few data are available, it is difficult to draw conclusions. As for the variation of θ as a function of depth, the depths of soil closest to the surface are richest in water content, and θ gradually decreases as it goes deeper into the soil.

By comparing the 4 zones, it can be deduced that plot R10 is the most dynamic plot in terms of variation of θ in the soil, especially since R10 is a riparian zone. These large variations could be explained by the presence of many roots and macropores that would induce a saturation of the soil, in the dry season, as soon as it rains. For P and CA, it would be better to have more data available to confirm some hypotheses since sensors have only been placed in June 2021, one year and a half after the sensors for R10 and R40.

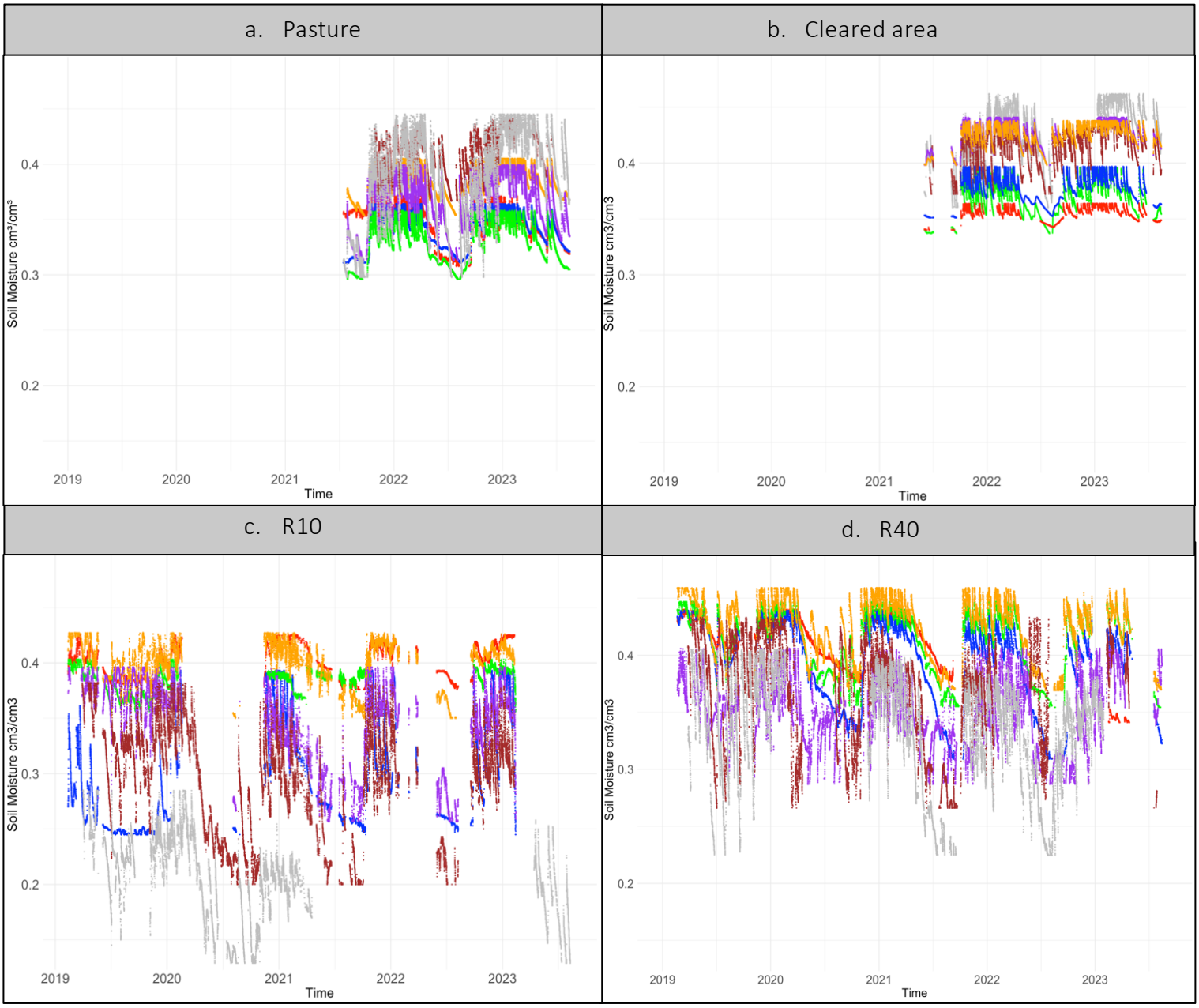

Figure 13: Evolution of water content measurements (cm3/cm3) over time for each depth from January 2019 to August 2023 for a. Pasture (P), b. Cleared area (CA), c. The young forest of 10 years (R10) and d. The old forest of 40 years (R40) (hourly data after filtering and outliers' removal). Depths are represented as follow: 2m in red, 1.5m in blue, 1m in green, 0.5m in orange, 0.3m in purple, 0.2m in brown and 0.1m in

5.2.2 Water potential

The final h time series after filtering is presented in Figure 14 for each of the four area under study. These graphs highlight the variation of h within the same area according to the depth of the soil and the seasonality of the water potential in the soil. They also allow for the comparison of h between the four study areas and the deduction of certain behaviors and trends. An important point to note is that for each of the studied area, the h data seems to be limited to pF2 due to the limitation of the sensors (*TEROS 21*, 2021). This means that the wettest states of the soil were not able to be measured and analyzed in this report.

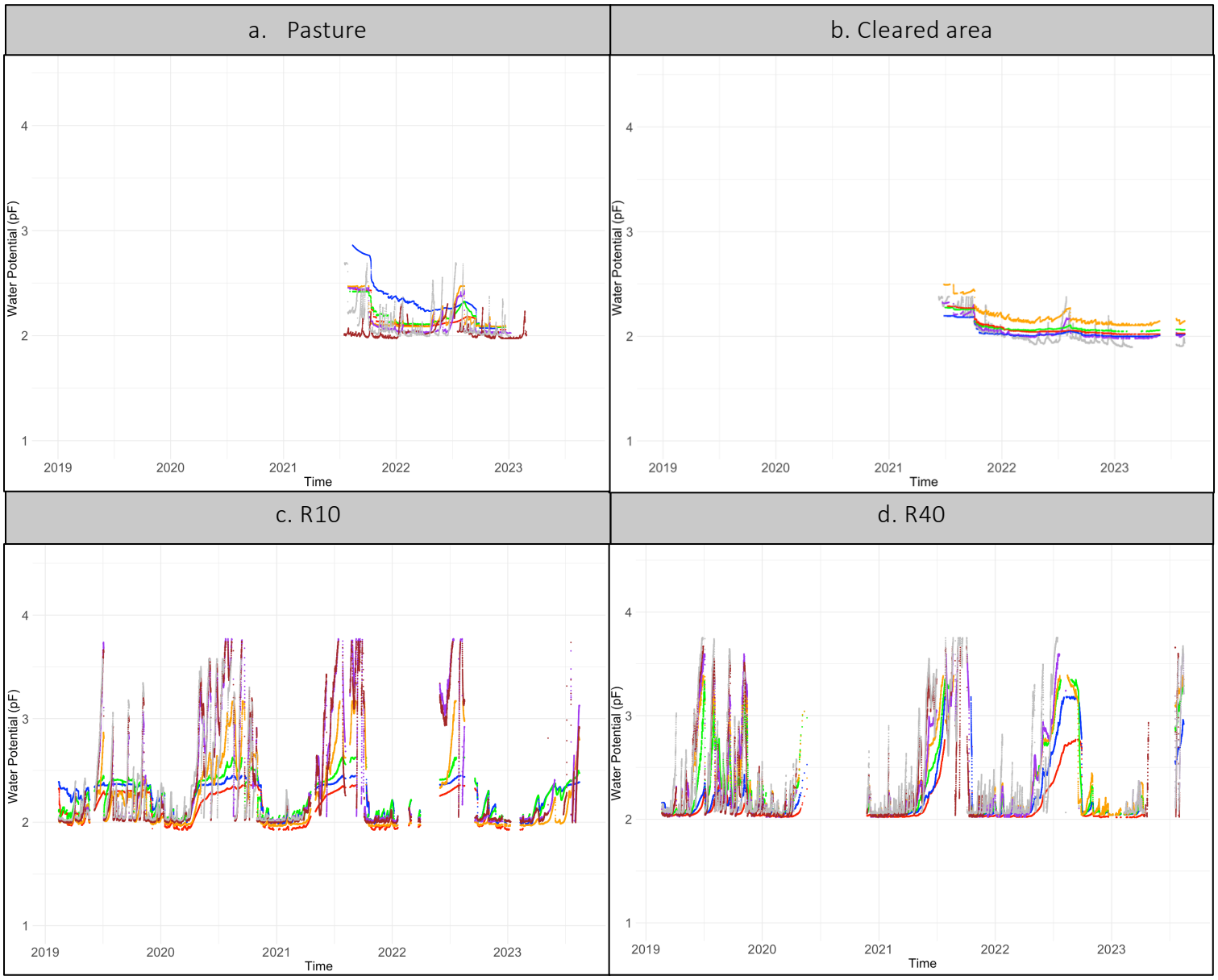

Figure 14: Evolution of water potential measurements (pF) over time for each depth from January 2019 to August 2023 for a. Pasture (P), b. Cleared area (CA), c. The young forest of 10 years (R10) and d. The old forest of 40 years (R40) (hourly data after filtering and outliers' removal). Depths are represented as follow: 2m in red, 1.5m in blue, 1m in green, 0.5m in orange, 0.3m in purple, 0.2m in brown and 0.1m in grey.

For areas R10 and R40, the variations in h are greater at shallow depths and decrease with depth. The variation in water potential is very pronounced in the dry season, with continuous peaks ranging from pF 2 to pF 3-4 are visible. A significant drying at the depth of 2m is visible mainly for R40 during the year 2022. However, for R10 this drying is weaker, which can be explained by the fact that R10 is a riparian area. The depth of the water table in this area may be responsible for the increase in moisture conditions at the higher depths. Similarly to what happened with the water content of the soil, the seasonality in water potential is much less visible for the P and CA areas. This could also confirm the hypothesis that these two areas tend to maintain the soil moisture throughout the year, but since there is very few data available, it is quite difficult to draw conclusions and see a tendency. The shape of h raw data for CA and P is quite surprising and abnormal due to the saturation at pF2 of the sensors. Large falls are visible just after June 2021 for these two areas, that could be related to the installation of

sensors and the time required for them to be effective. It is important to note that not all h or θ sensors were calibrated at or after installation. These jumps in h values could also be related to a change in soil structure when installing sensors at different depths and the time it takes for the soil to recover after installing the sensors.

5.2.3 Interpolations to fill the gaps.

To fill the many gaps in the initial data and after filtering, one method was considered (4.1.5). This filling of the gaps was done for the data θ, which are used to estimate the water stock in the soil and its variation, to have the most stock values available.

The method for filling the gaps is based on estimating the value of θ at one depth (missing value) based on the value of θ available at another depth. To perform this interpolation, it was first necessary to establish the correlation between one or more depths (spatial correlation) and the time t at which the correlation is highest (temporal correlation).

For this, various combinations of depths and time (from 1 to 10 hours before/after) have been combined and are included in Table 7 and Table 8 with correlations from one and two depths. The data used for interpolation are the water content data measured from 2021 to 2023, a period common to all zones and correlations were tested over different durations taking first one month in the dry season and one month in the wet season, a full dry season, and a full wet season and two full years to see if correlations could be higher depending on seasonality. After testing all the combinations, better correlation coefficients were obtained by taking the complete data of the two years.

Table 7: Table showing all the depths and measurement times that have been tested to find the best correlation from one depth so that interpolations can be made for θ.

Depth predicted	Depth use to predict	Values of t tested
0.2 (t0)	0.1	From t_0 to t_{-10}
0.2 (t0)	0.3	From t_0 to t_{+10}
0.5 (t0)	0.3	From t_0 to t_{-10}
1 (t0)	0.5	From t_0 to t_{-10}
1.5 (t0)	1	From t_0 to t_{-10}
2 (t0)	1.5	From t_0 to t_{-10}

Table 8: Table showing all the depths and measurement times that have been tested to find the best correlation from two depths so that interpolations can be made for ϑ.

Depth predicted	1st depth used to predict	Values of t tested	2nd depth used to predict	Values of t tested
0.2 (t0)	0.1	From t_0 to t_{-10}	0.3	From t_0 to t_{+10}
0.3	0.2	From t_0 to t_{-10}	0.5	From t_0 to t_{+10}
0.5	0.3	From t_0 to t_{-10}	1	From t_0 to t_{+10}
1	0.5	From t_0 to t_{-10}	1.5	From t_0 to t_{+10}
1.5	1	From t_0 to t_{-10}	2	From t_0 to t_{+10}

The best possible combinations of depths and time, taking the years of data measured from 2021 to 2023 were retained for each of the 4 zones and are included in Table 9Table 10Table 11 Table 12 also showing the correlation coefficient values obtained from R2, the Root Mean Square Error RMSE and the equation that was used to estimate the missing depth values.

Table 9: Table with the depths used to interpolate ϑ, the R2 and the RMSE associated to the interpolations and the equation used for R10.

Depth	Depth used to predict	Depth used to predict	R2	RMSE	Equation for interpolation
0.1	0.2	/	0.855	+/- 0.036 cm^3/cm^3	= $(\theta_{0.2} + 0.004)/1.507$
0.2	0.1	0.3	0.889	+/- 0.032 cm^3/cm^3	= $0.74 * \theta_{0.1} + 0.26*\theta_{0.3}$
0.3	0.2	0.5	0.833	+/- 0.037 cm^3/cm^3	= $0.6 * \theta_{0.2} + 0.4*\theta_{0.5}$
0.5	0.3	/	0.634	+/- 0.044 cm^3/cm^3	= $0.455 * \theta_{0.3} + 0.248$
1	0.5	1.5	0.016	+/- 0.25 cm^3/cm^3	= $0*\theta_{0.5} + 1*\theta_{1.5}$
1.5	1	2	0.650	+/- 0.043 cm^3/cm^3	= $0.38*\theta_1 + 0.62*\theta_2$
2	1.5	/	0.646	+/- 0.043 cm^3/cm^3	= $0.278 * \theta_{1.5} + 0.319$

Table 10: Table with the depths used to interpolate ϑ, the R2 and the RMSE associated to the interpolations and the equation used for R40.

Depth	Depth used to predict	Depth used to predict	R2	RMSE	Equation for interpolation
0.1	0.2	/	0.566	+/- 0.052 cm^3/cm^3	= $(\theta_{0.2} - 0.177) / 0.578$
0.2	0.1	/	0.566	+/- 0.052 cm^3/cm^3	= $0.578 * \theta_{0.1} + 0.177$
0.3	0.2	/	0.176	+/- 0.087 cm^3/cm^3	= $0.657 * \theta_{0.2} + 0.134$
0.5	1	/	0.927	+/- 0.024 cm^3/cm^3	= $0.928 * \theta_1 + 0.04$
1	0.5	1.5	0.956	+/- 0.019 cm^3/cm^3	= $0.71*\theta_{0.5} + 0.29*\theta_{1.5}$
1.5	1	2	0.992	+/- 0.006 cm^3/cm^3	= $0.05*\theta_1 + 0.95*\theta_2$
2	1.5	/	0.992	+/- 0.006 cm^3/cm^3	= $0.515 * \theta 1.5 + 0.215$

Table 11: Table with the depths used to interpolate ϑ, the R2 and the RMSE associated to the interpolations and the equation used for CA.

Depth	Depth used to predict	Depth used to predict	R2	RMSE	Equation for interpolation
0.1	0.2	/	0.586	+/- 0.051 cm^3/cm^3	= $(\theta_{0.2} - 0.180)/0.549$
0.2	0.1	0.3	0.892	+/- 0.029 cm^3/cm^3	= $0.01 * \theta_{0.1} + 0.99 * \theta_{0.3}$
0.3	0.2	0.5	0.964	+/- 0.017 cm^3/cm^3	= $0.24 * \theta_{0.2} + 0.76 * \theta_{0.5}$
0.5	0.3	1	0.966	+/- 0.016 cm^3/cm^3	= $0.78 * \theta_{0.3} + 0.22 * \theta 1$
1	0.5	1.5	0.966	+/- 0.016 cm^3/cm^3	= $0.28 * \theta_{0.5} + 0.72 * \theta_{1.5}$
1.5	1	2	0.982	+/- 0.008 cm^3/cm^3	= $0.25 * \theta_1 + 0.75 * \theta_2$
2	1.5	/	0.952	+/- 0.021 cm^3/cm^3	= $1.911 * \theta_{1.5} - 0.299$

Table 12: Table with the depths used to interpolate ϑ, the R2 and the RMSE associated to the interpolations and the equation used for P.

Depth	Depth used to predict	Depth used to predict	R2	RMSE	Equation for interpolation
0.1	0.2	/	0.707	+/- 0.038 cm^3/cm^3	= $(\theta_{0.2}$- 0.250)/0.416
0.2	0.1	0.3	0.908	+/- 0.024 cm^3/cm^3	= 0.19 * $\theta_{0.1}$ + 0.81 * $\theta_{0.3}$
0.3	0.2	0.5	0.923	+/- 0.024 cm^3/cm^3	= 0.36 * $\theta_{0.2}$ + 0.64 * $\theta_{0.5}$
0.5	0.3	1	0.946	+/- 0.022 cm^3/cm^3	= 0.64 * $\theta_{0.3}$ + 0.36 * $\theta 1$
1	0.5	1.5	0.972	+/- 0.015 cm^3/cm^3	= 0.32 * $\theta_{0.5}$ + 0.68 * $\theta_{1.5}$
1.5	1	/	0.949	+/- 0.022 cm^3/cm^3	= 1.035 * θ_1 - 0.024
2	1.5	/	0.222	+/- 0.082 cm^3/cm^3	= 0.512 * $\theta_{1.5}$ + 0.174

More than the half of the R^2 obtained are above 0.7. Some depths even have correlations of 0.992 as R40 for depths 1.5 and 2m which contrasts with the R^2 of 0.176 obtained for depth 0.3m, for the same area.

Even if many of the R^2 obtained are very good, to be able to fill the most hole it is necessary that when the value that one seeks to predict is absent, that from which one seeks to estimate it is present. In this thesis, most of the data that are missing are generally missing for several depths at the same time, which limits the number of values that can be predicted. And the values where R^2 is low correspond to places where there is very little data available. All the values that have been predicted for the four study areas are shown in Table 13 for each depth individually:

Table 13: Table that contains the total number of ϑ values for each area under study, the total number of values interpolated for each area and the total number of values inteprolated by depths for each area P, CA, R10 and R40.

Parcels	Total values	Total values interpolated	0.1m	0.2m	0.3m	0.5m	1m	1.5m	2m
P	127.645	66.118	11.885	3.991	9.624	8924	12.401	9.292	10.001
CA	113.883	10.933	3.837	701	3.010	61	93	62	3.169
R10	224.308	19.016	9.966	277	1.126	907	4.288	938	1.514
R40	254.970	29.770	0	8.705	6.867	1.576	1.086	770	10.766

5.3 Results of the different methods used to assess ET.

5.3.1 Mass Balance

Water stock

The soil water stock for the four study areas was calculated (4.4.1) and is presented in Figure 15. By comparing the 4 areas, we can see that R40 can reach a total stock of water in the soil up to nearly 800mm where the other 3 areas reach almost 650mm. The old forest (R40) therefore has access to larger water resources. Moreover, R40 also shows very significant stock decreases during dry season periods probably testifying to a very important water catchment by the roots and therefore possible important capillary rises. This hypothesis will be validated at the following point analyzing drainage/capillary rise graphs. This water could be used through the evapotranspiration process.

Apart from R40 which has a lot of data on the water stock, R10 is quite poor. This lack of data does not allow us to draw conclusions about the water consumption of the young forest even if we can still observe some slightly lower peaks indicating a probable decrease in the water stock in the soil during the dry season.

For CA and P, there is enough data available to see the overall trend of water stock in the soil. We can see that here too the stock tends to decrease during the dry season, but the decrease is much smaller than for R40, which could mean that CA and P pump less water from the soil during the dry seasons and therefore transpire less.

To better visualize changes in stock over time, the change in water stock for the dry and wet seasons for each of the four areas (Figure 16) was calculated by differentiating the value of the water stock on the first day of the wet season from the value of the stock on the last day of the wet season (i.e. water stock value on October 1 – water stock value on April 30) and the same for the dry season. This allows to see the tendency of the water stock and if the total amount of water available is decreasing each year.

We can see that the water stock is either increasing during the dry or wet season depending on the year probably due to precipitations. A significant increase is visible in year 2022 with positive variation of the water stock during the dry and wet seasons, especially for R10 with a total increase in the water stock of nearly 300mm over the year. In contrast, 2021 seems to be a year where the water stock in the soil has decreased during dry and wet period for R40 and R10. Since R40 has a lot of data available, the variation of the water stock for the dry and wet seasons is available for nearly all the 4 years (except 2023 Dry season). This allows us to see a general decrease of the water stock over time and therefore a decrease in the amount of water available. For R10, a general increase in the water stock is shown in the last year.

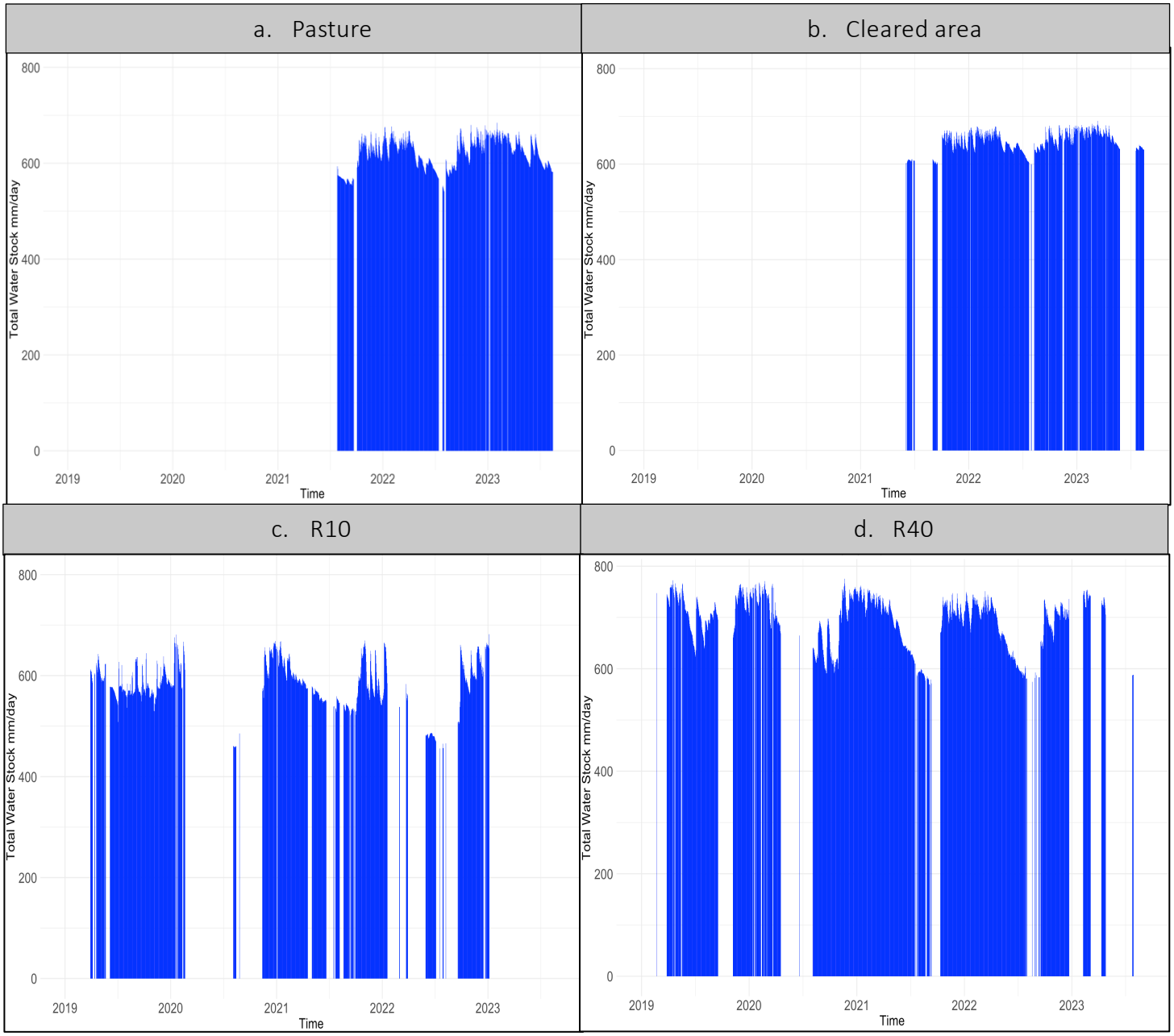

Figure 15: Graphics of the evolution of the total water stock [mm]per day for the four areas under study a. Pasture (P), b. Cleared area (CA), c. The young forest of 10 years (R10) and d. The old forest of 40 years (R40) for 2019 to 2023

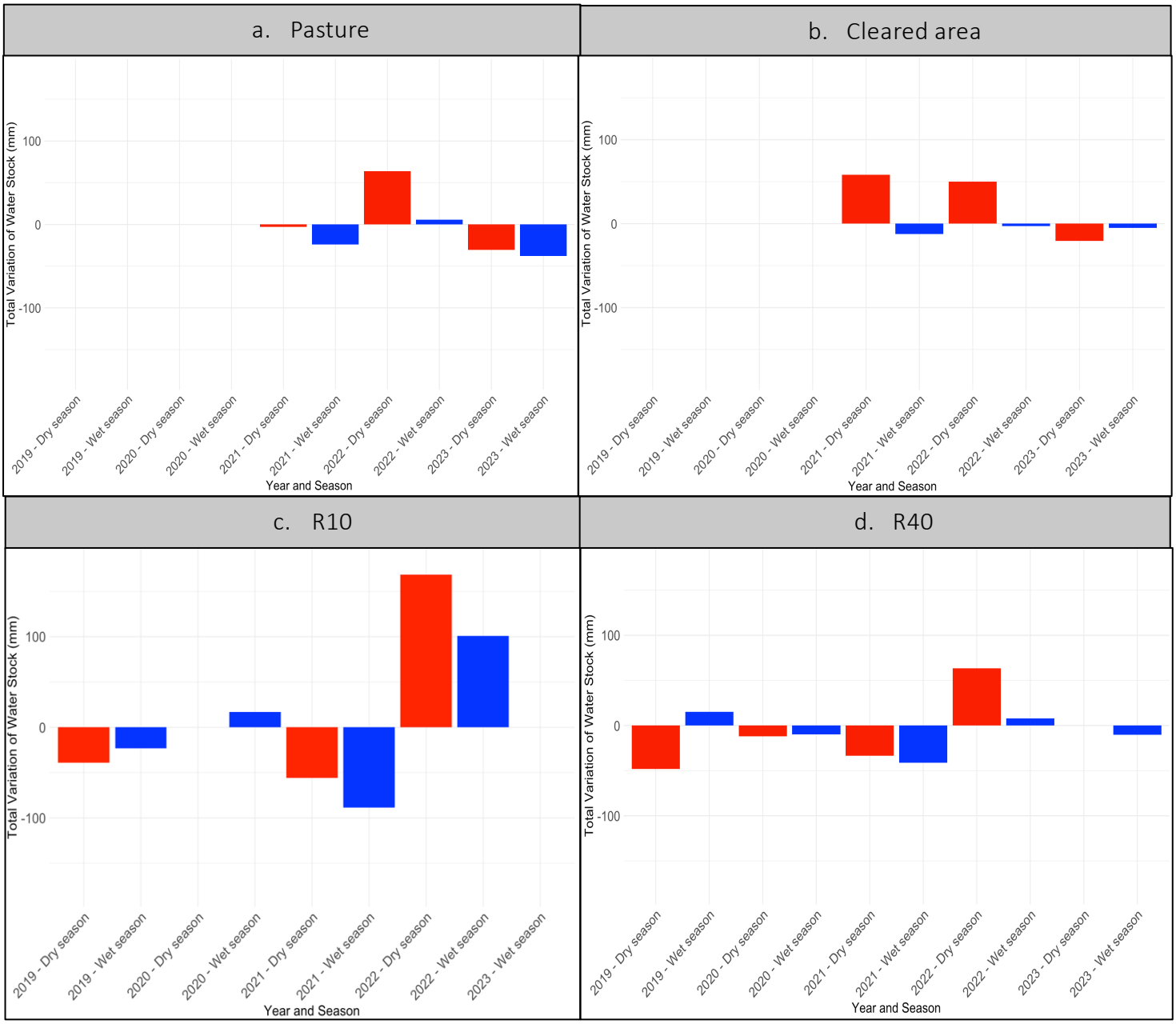

Figure 16: Variation of the water stock per season over 2019 to 2023 for each of the four areas under study a. Pasture (P), b. Cleared area (CA), c. The young forest of 10 years (R10) and d. The old forest of 40 years (R40). The dry periods have been shown by the red bars while the wet period are shown by the blue bars. The variation of the water stock for each season have been measured based on the value of the water stock of the first day of the season to which to value of the water stock of the last day of the season have been removed.

Drainage/Capillary rise

To calculate vertical fluxes at the bottom of the soil profile, the gradient of H and conductivity were calculated (4.4.2).
The gradient of H was calculated from h field data at 1.5 and 2m while the conductivity K(h) was calculated from the average of h field data at 1.5 and 2m using the hydraulic conductivity curve. Graphics representing the gradient of H and the conductivity K(h) are in Appendices 4 and 5 and the various parameters of Van Genuchten $\alpha_1, \alpha_2, \theta_r, \theta_{sat}, n_1, n_2 \; and \; w_2$ are visible in the table in Appendix 6.

The drainage obtained from Darcy's law is shown in Figure 17. For R10 and R40, a seasonality of drainage can be observed. During the dry season, R40 has capillary rise peaks (i.e. 2021, 2022) indicating significant absorption by water roots. In view of this significant amount of capillary rise, it is interesting to balance the annual flows of drainage and capillary rise to see if R40, an old forest, consumes more water by its capillary rises than it provides through its drainage, making this old forest a water user rather than a producer. This assessment was carried out and is visible in Appendix 7. It can be deduced that the water consumption of R40 was higher than its production, especially in 2022. This intensive withdrawal could affect, in the long term, the stock of water available (water resources) in the soil and the vegetation. This observation also contrasts with the basic hypothesis that a young forest (i.e. R10) consumes more water than an older forest (i.e. R40) and could affect the water balance of the soil. The large amount of water absorbed is probably used for evapotranspiration.

In comparison, R10 does not seem to experience capillary rises as large as R40, according to available data, but these are rather frequent during wet seasons. R10 seems to be more prone to drainage, especially in the dry season. For P and CA, it is quite difficult to see any seasonal variation. P seems to experience very strong capillary rises almost continuously while CA on the other hand only seems to have drainage all the time. These differences in drainage and capillary rise will have a significant impact on the water balance and so on actual evapotranspiration assessment. However, it is important to remember the h raw data for P and CA illustrated in 5.2.2 and to be cautious with both the raw data and the drainage/capillary rise assessment.

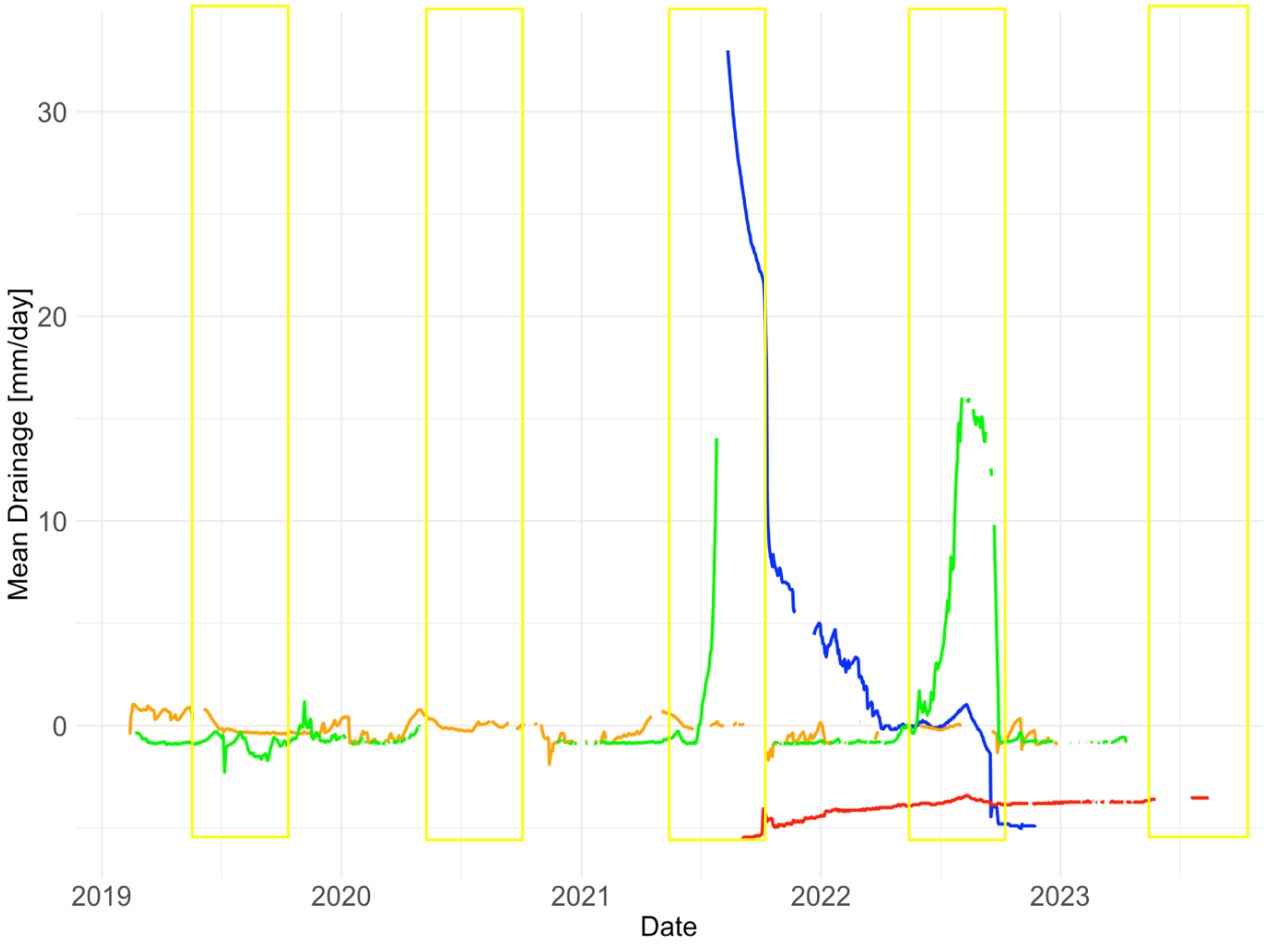

Figure 17: Graphics representing the total drainage per day [mm/day] for each of the four areas under study Pasture (P) in blue, Cleared area (CA) in red, the young forest of 10 years (R10) in orange and the old forest of 40 years (R40) in green. The drainage has been assessed based on the Darcy's law where the Van Genuchten parameters for the conductivity K(h) have been optimized through LABROS based on the Van Genuchten Muallem relation.

Water Balance

Combining water stock variation, precipitation, drainage and capillary rise, the actual evapotranspiration can be estimated (4.4).

The monthly water balance is visible for each of the 4 plots studied in Figure 18Figure 19Figure 20 Figure 21. Inputs to the soil are positive (e.g., precipitation or capillary rise), while outputs (like drainage or ET) are negative. The change in stock is represented as a negative term when there is an increase in water and a positive term when the soil dries out (see Equation 3).
Rain is represented by the blue bars, variation of the water stock by the pink bars, drainage or capillary rise by the red bars and evapotranspiration deduced from its different terms by the green bars. The water stock in the soil is also represented by the light blue dots, and the dry seasons are represented by the yellow rectangles. Evapotranspiration has not been estimated if one of the 4 incoming or outgoing flows could not be calculated due to lack of data, these areas where one of the flows is missing are represented by the gray rectangles.

For Figure 18 and Figure 21, the red rectangles represent moments where some incoming fluxes have not been identified, either due to the imprecision of the drainage and the capillary rise that have been supposed to be at 1.75m of depth or to the raw data measurements based on sensors. Positive ET values were obtained in this case, which is not possible, so the water balance has been assessed as not reliable and ET wasn't assessed.
The daily mass balance is presented in Appendix 9.

The water balance of CA is represented in Figure 18. For CA, only drainage is present as a bottom flux. There is no capillary rise. Even when there is nearly no precipitation, a lot of drainage still occurs. This could be linked to the shape of the raw data and could affect the actual value of ET assessed. Therefore, the water balance for CA will be considered as not trustable and will not be used for this thesis.

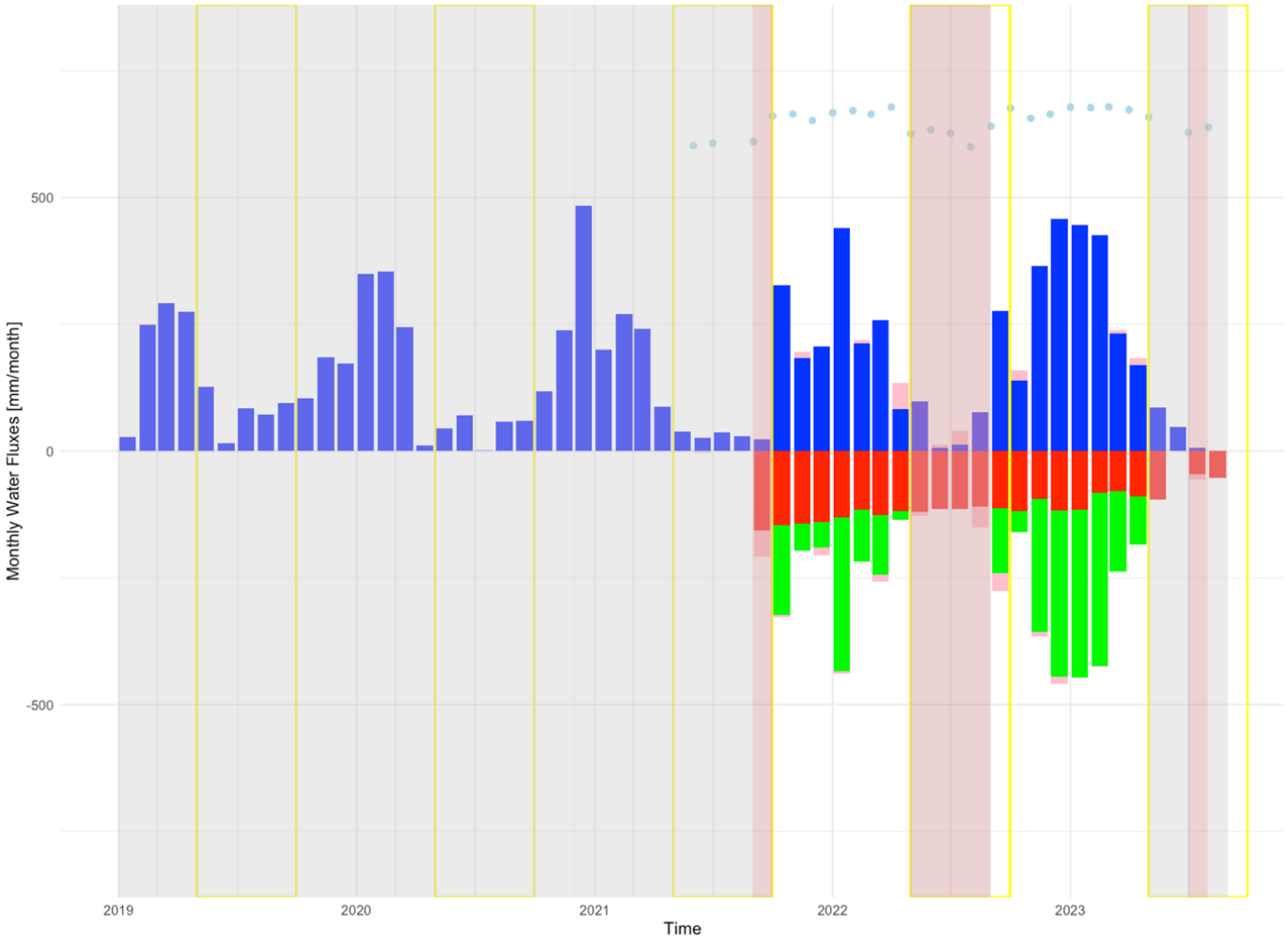

Figure 18: Water balance for Cleared area (CA) from 2019 to 2023. The different water fluxes are represented as follow: precipitation by the blue bars, drainage (-)/capillary rise (+) by the red bars, the variation of the water stock by the pink bars and actual evapotranspiration by the green bars. The water stock of the soil is represented by the blue points and the dry seasons are the yellow rectangles. Actual evapotranspiration has not been assessed if precipitation, variation of the water stock or drainage/capillary rise was missing, missing fluxes area are represented by the grey rectangle. The red rectangles represent moments where the water balance is not reliable because some incoming fluxes that are not measured false the estimation of the actual evapotranspiration.

Figure 19 represents the water balance of P. The main bottom fluxes are capillary rise, which is high in September and October 2021, at the end of dry season period with less rainfall.
Drainage is mostly visible in late 2022 and is higher during the wet season, it is much lower than capillary rises. The water stock appears to vary greatly between positive and negative values, contributing to other water flows. It increases with drainage and decreases with capillary rise. We can see a higher water stock before the beginning of the dry season (yellow rectangle) and just after. Actual ET, deduced from all other flows, is high at the end of 2021 corresponding to the time when we have a strong capillary rise. ET increases as the water stock increases and is lower when the water stock is at a minimum, probably due to the lack of available water. At this time, there is almost no precipitation.
In general, ET is lower in the dry season and higher in the wet season, except in August and September 2021. High precipitation leads to an increase in the water stock in the soil and to high ET.

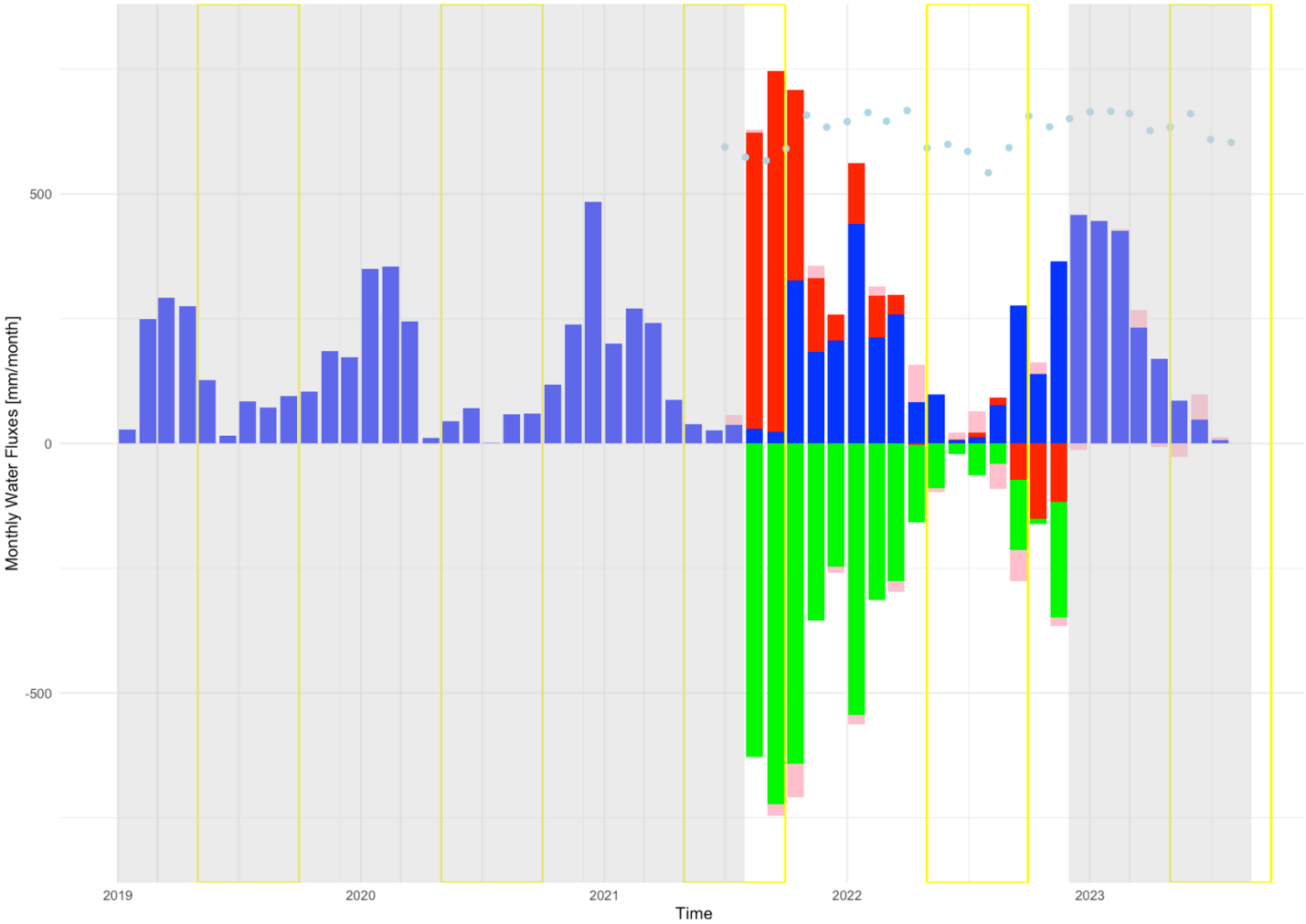

Figure 19 : Water balance for Pasture (P) from 2019 to 2023. The different water fluxes are represented as follow: precipitation by the blue bars, drainage (-)/capillary rise (+) by the red bars, the variation of the water stock by the pink bars and actual evapotranspiration by the green bars. The water stock of the soil is represented by the blue points and the dry seasons are the yellow rectangles. Actual evapotranspiration has not been assessed if precipitation, variation of the water stock or drainage/capillary rise was missing, missing fluxes area are represented by the grey rectangle. The red rectangles represent moments where the water balance is not reliable because some incoming fluxes that are not measured false the estimation of the actual evapotranspiration.

For R10 (Figure 20), there is small drainage and capillary rise. Most of the drainage occurs during the wet season, but there is also some very small drainage in the dry seasons of 2019 and 2020. Capillary rise mostly appears in the dry season, except for February, March and April 2019 corresponding to the wet season. Higher water stock variation is visible than in P, but the tendency is the same. The water stock is at its maximum just before and after the dry season and is decreasing during the dry season. When the water stock is at its minimum, ET is the lowest. The ET tendency is also the same as in P with lower ET in the dry season and higher ET in the wet season. Water stock data seems to be the limiting factor to assess ET as the grey areas show.

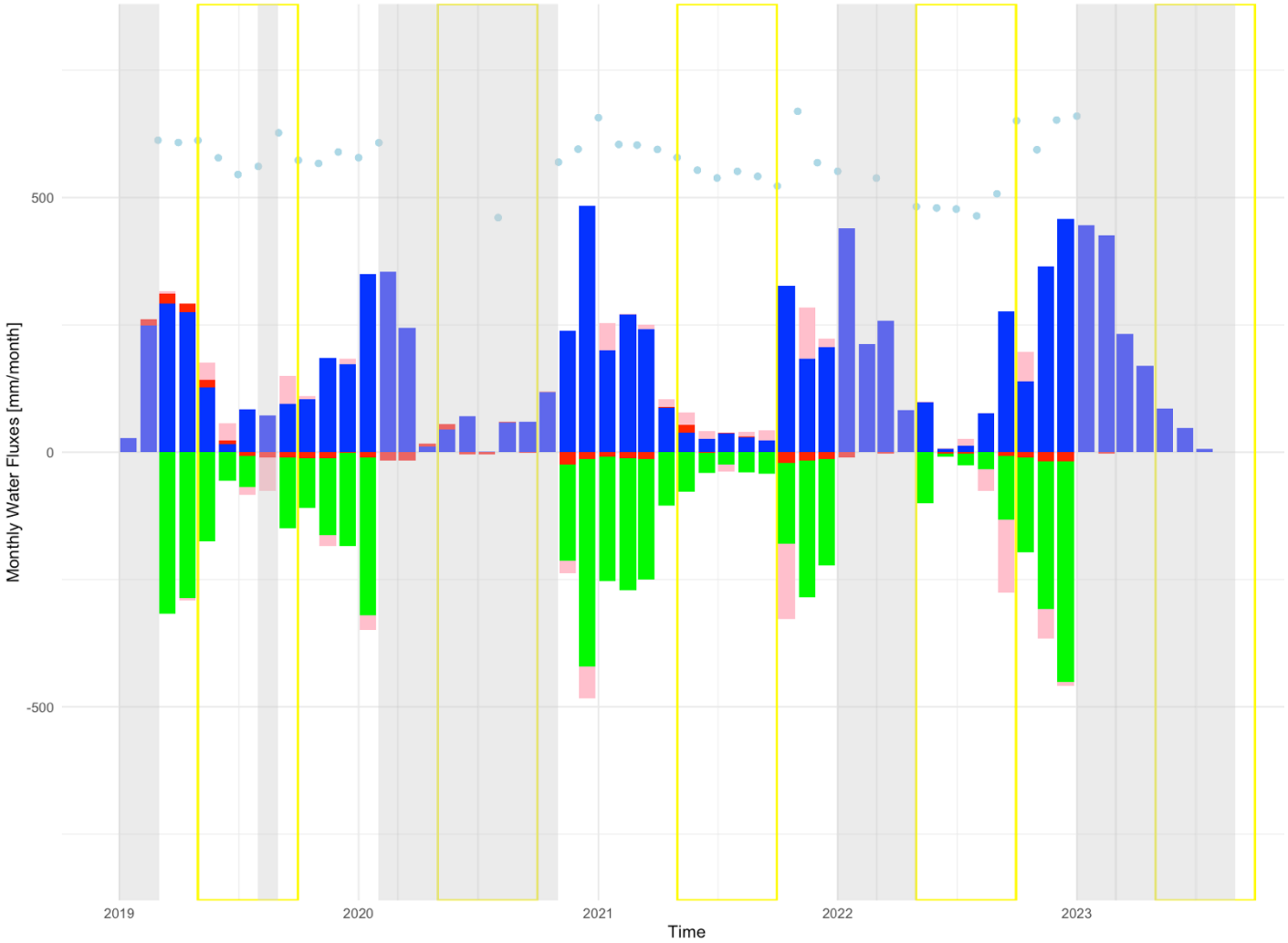

Figure 20: Water balance for the young forest of 10 years (R10) from 2019 to 2023. The different water fluxes are represented as follow: precipitation by the blue bars, drainage (-)/capillary rise (+) by the red bars, the variation of the water stock by the pink bars and actual evapotranspiration by the green bars. The water stock of the soil is represented by the blue points and the dry seasons are the yellow rectangles. Actual evapotranspiration has not been assessed if precipitation, variation of the water stock or drainage/capillary rise was missing, missing fluxes area are represented by the grey rectangle. The red rectangles represent moments where the water balance is not reliable because some incoming fluxes that are not measured false the estimation of the actual evapotranspiration.

Finally, R40 (Figure 21) is the water balance that allows for more understanding since it's the area where more data is available.

Like R10 and P, there is drainage and capillary rise. Capillary rise seems to occur only during the dry season while there is drainage both in the dry and wet seasons. A lot of variations in the water stock are also visible as for the three other areas, with higher water stock just before and at the end of the dry season and it decreases during the dry season. Minimum water stock value is usually correlated with lower ET, except in August 2021 as there is capillary rise. ET follows the same seasonality as P and R10 and the values are close to those from R10. P is the area where ET is the highest. As for CA, the water balance was not reliable, at one point in this case, as the red rectangle shows.

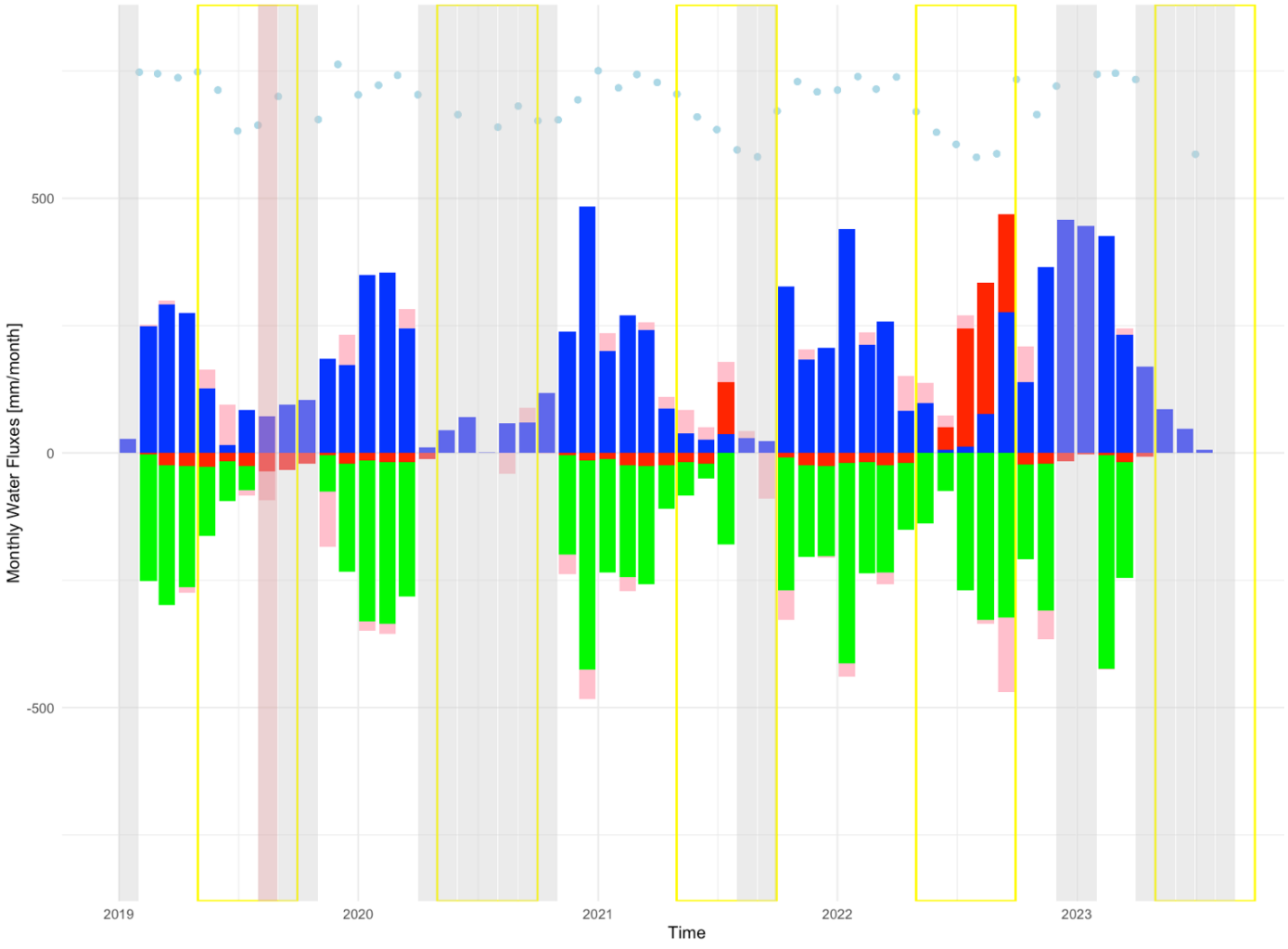

Figure 21: Water balance for the old forest of 40 years (R40) from 2019 to 2023. The different water fluxes are represented as follow: precipitation by the blue bars, drainage (-)/capillary rise (+) by the red bars, the variation of the water stock by the pink bars and actual evapotranspiration by the green bars. The water stock of the soil is represented by the blue points and the dry seasons are the yellow rectangles. Actual evapotranspiration has not been assessed if precipitation, variation of the water stock or drainage/capillary rise was missing, missing fluxes area are represented by the grey rectangle. The red rectangles represent moments where the water balance is not reliable because some incoming fluxes that are not measured false the estimation of the actual evapotranspiration.

Comparing P, R10 and R40, we can see that a certain seasonality of evapotranspiration is present, with higher evapotranspiration values during the wet seasons and lower in the dry seasons.
This seems to follow the trend given by the ET0 (5.1) The mean monthly evapotranspiration values observed during the dry and wet seasons for the four zones are shown in Table 14.
P seems to be the area that evaporate the most, whether in the wet or dry season, while R10 appears to be the area with the lowest rates of evapotranspiration in the dry season and R40 in the wet. R10 and R40 seem to follow a similar trend in terms of evapotranspiration in the wet season, but R10 has a mean evapotranspiration twice lower in the dry season.

For comparison, the evapotranspiration of P in the dry season is on average four times that of R10 and almost twice that of R40.

These results are still to be qualified, especially for the P which have shown in its raw data rather strange values of h, as CA, that can induce strange values in terms of drainage and capillary rise and therefore in real evapotranspiration. Monthly evapotranspiration data derived from the mass balance are presented in Figure 22.

Table 14: Mean monthly evapotranspiration based on the water balance for Pasture (P), the young forest of 10 years (R10) and the old forest of 40 years (R40) for the dry and the wet period The number of months for which data were available and thus the mean has been calculated in ().

Area	Mean evapotranspiration dry season [mm/month]	Mean evapotranspiration wet season [mm/month]
P	243.944 (Based on 7 month)	308.568 (Based on 9 month)
R10	67.456 (Based on 14 month)	240.809 (Based on 15 month)
R40	151.759 (Based on 11 month)	239.863 (Based on 23 month)

The same table has been created for drainage and capillary rise (Table 15). The negative mean corresponds to drainage and the positive mean corresponds to capillary rise. P and R40 are the areas presenting mainly strong capillary rise in the dry season, P being twice higher than R40. However, only P has also mainly capillary rise in the wet season.

Table 15: Mean monthly drainage based on the water balance for Pasture (P), the young forest of 10 years (R10) and the old forest of 40 years (R40) for the dry and the wet period. The number of months for which data were available and thus the mean has been calculated is in ().

Area	Mean drainage/Capillary rise dry season [mm/month]	Mean drainage/Capillary rise wet season [mm/month]
P	52.827 (Based on 7 month)	17.487 (Based on 9 month)
R10	0.049 (Based on 14 month)	-6.107 (Based on 15 month)
R40	27.223 (Based on 11 month)	-15.678 (Based on 23 month)

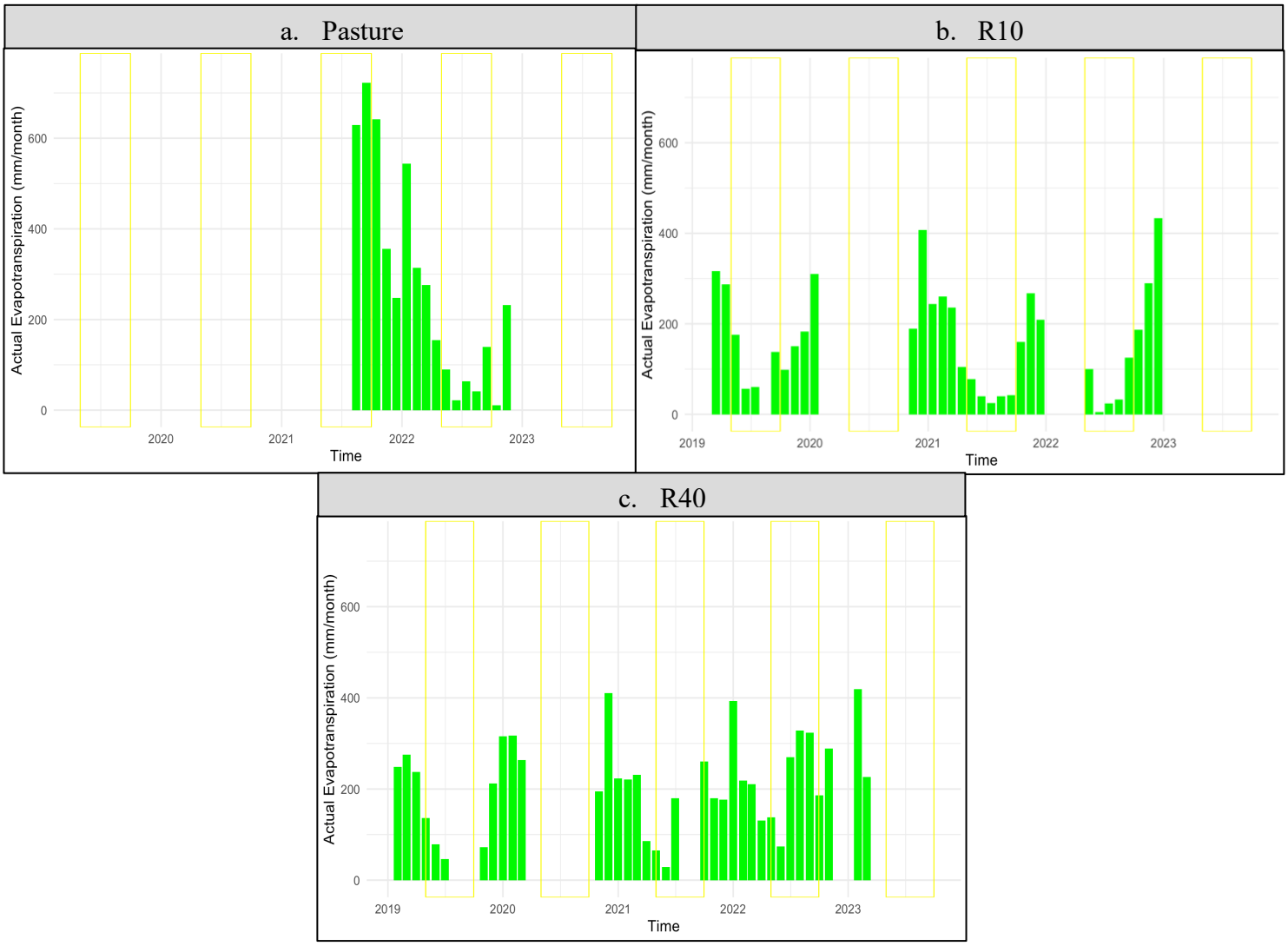

Figure 22: Monthly actual evapotranspiration assessed from the water balance for a. Pasture (P), b. The young forest of 10 years (R10) and c. The old forest of 40 years (R40). The dry seasons are represented by the yellow rectangles.

5.3.2 MODIS

The results obtained via the MODIS method are inconclusive. Indeed, due to the low resolution of 500m, the results obtained are two pixels of 500m^2 each. The first pixel contains the R40 area while the second pixel contains the R10, CA and P areas.

These results are difficult to exploit because the evapotranspiration obtained corresponds to the sum of the 500m^2 pixel evapotranspiration over 8 days. However, given the size of each plot (Table 1), even pixel 1, which contains only plot R40 among the study plots, is covered by other types of soil cover that will influence the measured evapotranspiration value. In addition, three of the four study areas are on the same pixel, which does not allow to obtain evapotranspiration values specific to each area for comparison.

MODIS could have given more conclusive results, particularly if larger study areas were available to cover the entire 500m^2 pixel. A possibility was considered to find near the study area, areas of 500m^2 with soil cover similar to those studied such as a 40-year-old forest, a 10-year-old young forest or a pasture. However, the research was inconclusive, as these areas could not be too far from the study area to maintain the same climatic and field conditions. As the results of MODIS are not reliable, they will not be presented as results but are included in the appendix (Appendix 10). The relevance of using SEN-ET with a spatial resolution of 20m is justified.

5.3.3 SEN-ET

In total, from 2019 to 2023, 196 satellite images processed by SEN-ET were obtained. Of these images, 56 images yielded results for the study areas, 127 had clouds over the study areas that prevented the algorithm from working and 13 were completely unusable.

The 56 images were processed via the QGIS software and an average of the pixels defining each of the 4 areas was calculated to obtain the average evapotranspiration of each area. A standard deviation function was also used to calculate the standard deviation of the measured value. The averages and standard deviations are shown in Figure 23.

The seasonality of evapotranspiration also seems to be identical across the four areas, with higher evapotranspiration values during the theoretical wet seasons and lower values in the dry season. R40 and CA seem to follow a very similar behavior with very similar evapotranspiration values. As CA is an area with a rather peculiar ground cover with trees, bushes, and trees in the same area, it may be that SEN-ET has been somewhat disturbed by the ground cover. P and R10 have very low evapotranspiration values during the dry season, even zero for P on several occasions indicating a potential water stress and no evapotranspiration due to the closure of stomata to conserve water within plants.
In general, there are no significant differences between the four areas in the evapotranspiration measured by SEN-ET.

Figure 23: Evolution of daily evapotranspiration for each of the four-study areas P, CA, R10 and R40 measured based on SEN-ET. Evapotranspiration of the area has been measured based on a mean of the pixels and standard deviation has been assessed. P is in blue, CA is in red, R10 is in orange and R40 is in green. Dry seasons are represented by the yellow rectangles.

A distribution of the evapotranspiration values in the dry and wet seasons was also performed to better visualize the value ranges that the evapotranspiration follows according to the season (Figure 24)

Daily evapotranspiration values can be observed in the dry season ranging from 2 to 4 mm/day for R10, R40 and CA with a peak at 3mm/day while P seems to vary between 0 and 3 mm/day with a peak at 2mm/day, in the dry season.

In the wet season, the four areas follow the same dynamic and show two peaks of evapotranspiration. The evapotranspiration values in the wet season are mostly between 2 and 7 mm/day with a first peak at 3-4mm/day and a second peak at 5.5-6 mm/day.

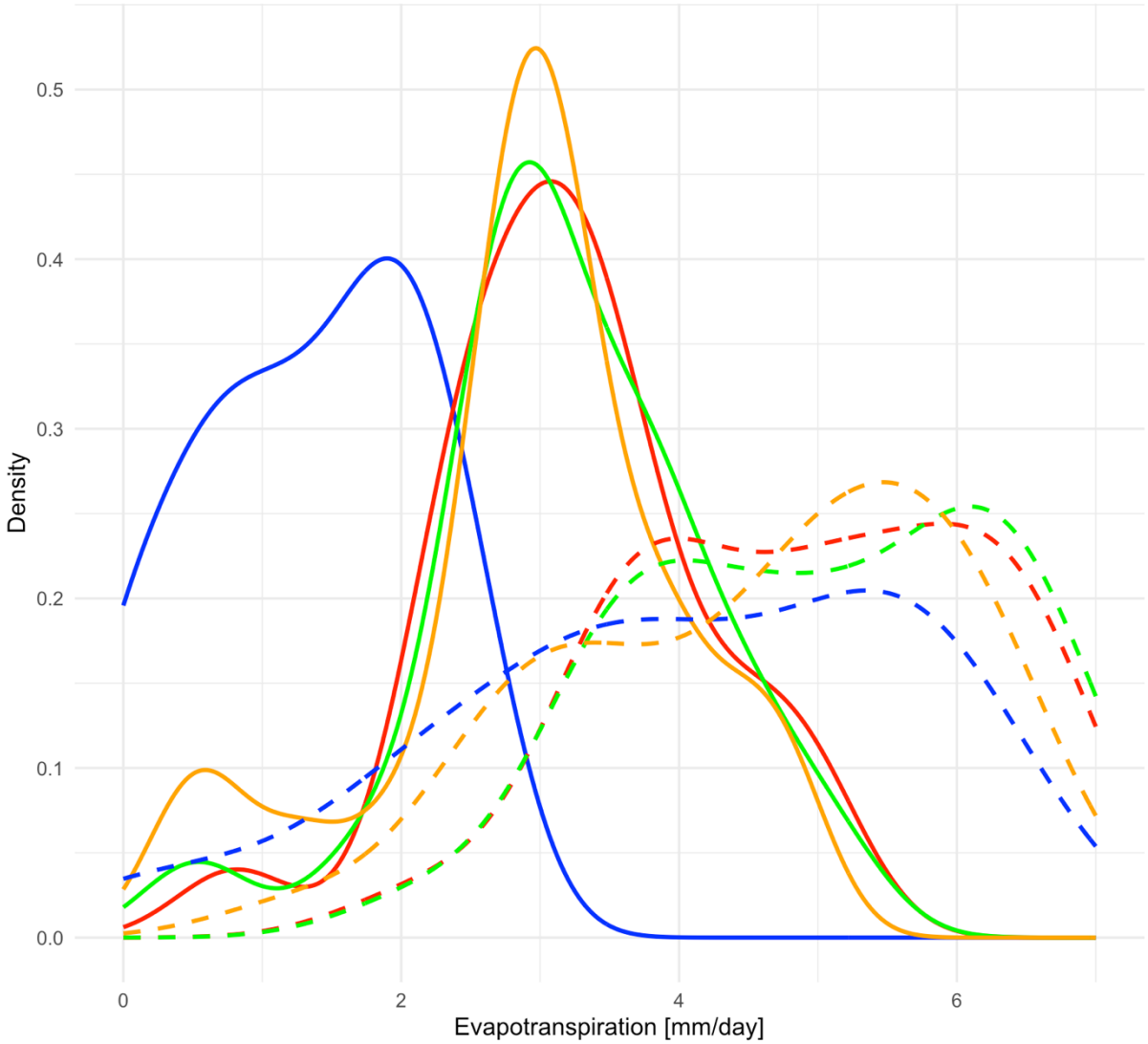

Figure 24: Density plot of the daily evapotranspiration for P(blue), CA (red), R10 (orange) and R40 (green) during the dry and the wet season. The dotted lines represent the distribution of evapotranspiration during the wet season while the continuous lines represent the distribution of evapotranspiration during the dry season.

The minimum and maximum values obtained for each area in the dry and wet seasons are presented in Table 16. The greatest difference observed is between the maximum evapotranspiration measured in P in the dry season and in the wet season with respectively 2.639 mm/day and 6.178 mm/day. The highest evapotranspiration value measured is during the wet season for the CA zone with 7.005 mm/day, followed by R10 with 6.960 mm/day and then R40 with 6.591 mm/day. The mean is also shown in Table 16. The higher mean during the wet season is both in CA and R40 (5.004 mm/day) while the higher in the dry season is in R40 (3.190 mm/day). The lower mean is for P either in the dry (0 mm/day) or the wet season (0.106 mm/day)

Table 16: Minimum, maximum, and mean daily evapotranspiration for P, CA, R10 and R40 during the dry and the wet season. The number of ET values from SEN-ET available and used for the calculation for each area is also indicated.

Area	Min/Max/Mean/Number of values used	Wet season [mm/day]	Dry season [mm/day]
P	Min	0.106	0.000
	Max	6.178	2.639
	Mean	3.976	1.349
	Number of values used	26 days	28 days
CA	Min	2.176	0.807
	Max	7.005	5.027
	Mean	5.004	3.115
	Number of values used	22 days	28 days
R10	Min	2.210	0.402
	Max	6.960	4.871
	Mean	4.576	2.958
	Number of values used	21 days	27 days
R40	Min	1.288	0.529
	Max	6.591	5.138
	Mean	5.004	3.190
	Number of values used	25 days	26 days

5.3.4 Comparison of the different methods used.

In general, the actual evapotranspiration values obtained by the water balance and SEN-ET respect the seasonality observed by reference evapotranspiration ET_0, with lower values of evapotranspiration in the dry season and higher values in the wet season. However, the results obtained for the four zones according to the two methods are contradictory.

Since the water balance is not trustable for CA due to the raw data, the comparison of actual evapotranspiration for this area between the two methods will not be possible.

According to the water balance it is P that transpire the most, whether in the dry or in the wet season, and this is justified by the very strong capillary rise visible in Figure 19. On the contrary, according to the results obtained by SEN-ET, P would be the area with less evapotranspiration zone in the dry and wet seasons. While R40 and CA are the areas with the more evapotranspiration in the wet season (maximum value recorded for CA) and R40 in the dry season (maximum value recorded for R40). According to SEN-ET, R40 and CA appear to follow similar values of ET, while R10, like P, sometimes reaches very low evapotranspiration values in the dry season, possibly indicating a lack of water. However, R10 is a riparian zone, close to the water table and should therefore have easy access to water, unless the water table is already exhausted?
This lower dry season evapotranspiration of R10, compared to R40, was also observed by the water balance. In the water balance however, strong capillary rise was noticed for R40 and even more uptake by the trees during the year 2022 than outtake by drainage, which can also in the long-term lead to water shortages.

Comparison between WB method, SEN-ET method, and reference ET_0 have been made in Figure 25Figure 26, Figure 27,Figure 28Figure 29Figure 30. Since the same number of values were not available each month, a daily mean by month has been calculated to allow better comparison based on the number of values available each month for each area.

Comparison of WB and SEN-ET methods to the reference evapotranspiration

The comparison of the ET from the WB to the reference ET_0 is represented in Figure 25 and Figure 26.

Figure 25 correspond to the values for the wet season and Figure 26 the dry season. The two figures show that ET from WB is higher than ET_0 as expected but some values seem to be much higher which could be link to an overestimation of the WB. Some of these high means are due to only one or two values available from the water balance for a month which are overestimated, and more high values are found in the dry season (Figure 26). By looking at R^2 based on the linear regression, the water balance ET during the wet season is higher than during the dry season. For the wet season (Figure 25), it is R10 that has the highest and in the dry season (Figure 26) it is R40. We can also see that nearly all the mean values assessed are above the black dotted line, passing through the 1:1 coordinate, which indicates that the K_c for the four areas is above 1. K_c can be assessed with the wet season because there is no risk of water stress normally in this period unlike during the dry season and that the difference between reference and actual evapotranspiration is only due to the soil cover. However, by looking at the value of K_c estimated through the slope of the linear regression, these are too high to be trustable and show one more time that WB method made overestimation of the ET values and is not precise enough in the fluxes measured. Normally, we could expected values a bit higher than 1. (Pereira et al., 2023)

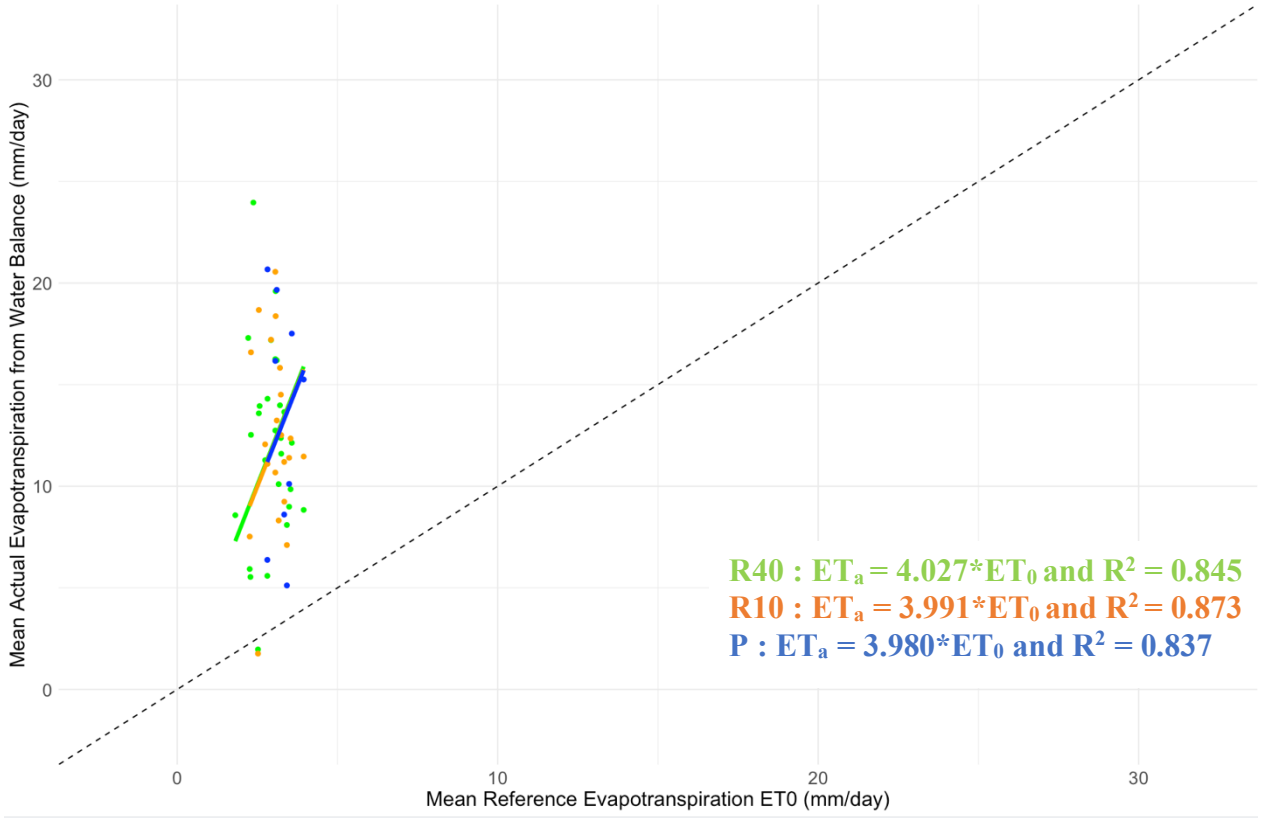

Figure 25: Comparison of the daily mean ET during the wet season based on the water balance method (Y axis) to the reference ET0 (X axis) assessed through Penman-Monteith equation for each month for Pasture (P), the young forest of 10 years (R10) and the old forest of 40 years (R40) P is in blue, R10 is in orange and R40 is in green. A linear regression and a R^2 linked to it have been assessed for each of the three areas and a line passing through 0:0 is represented by the black dotted line.

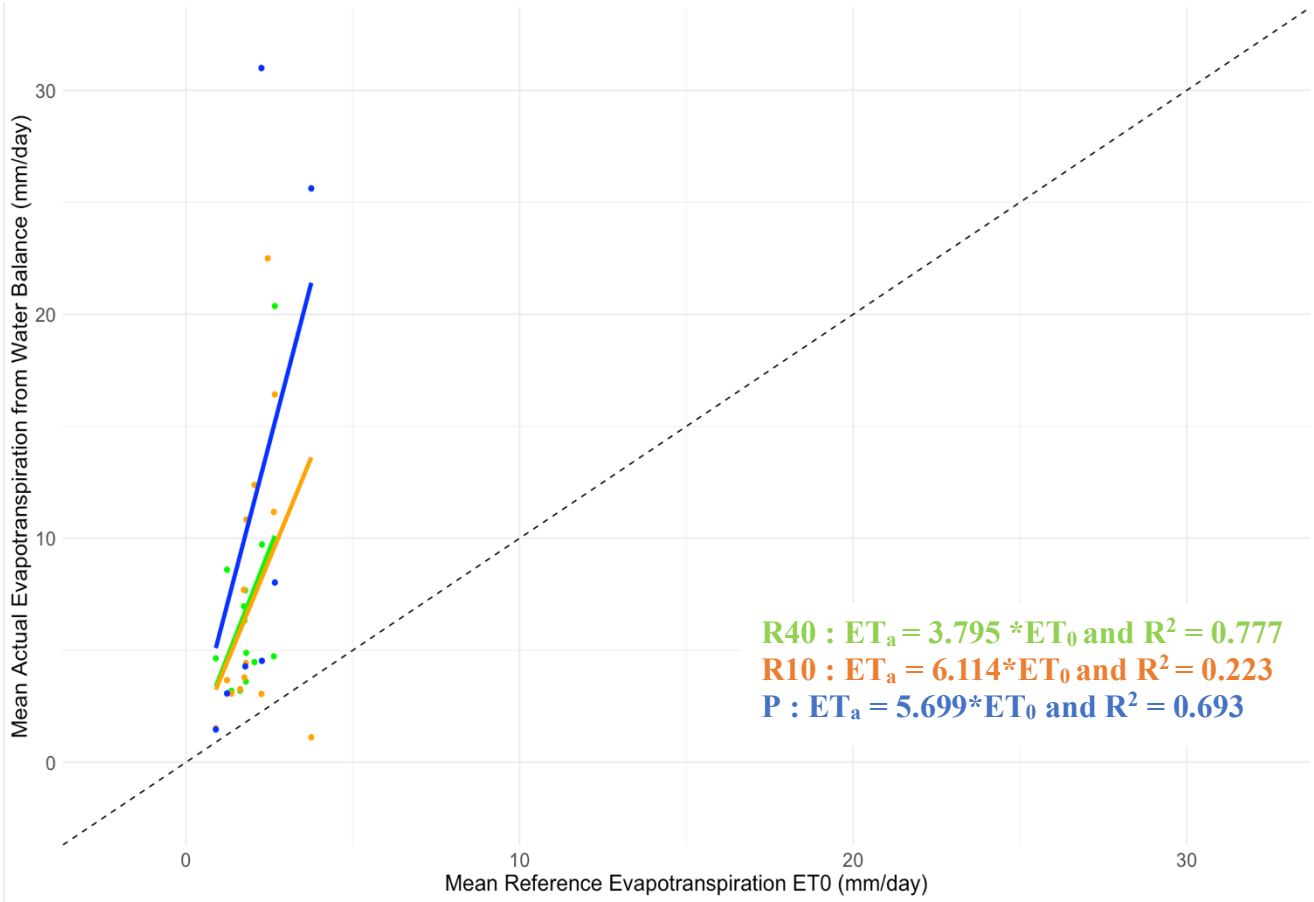

Figure 26: Comparison of the daily mean ET during the dry season based on the water balance method (Y axis) to the reference ET0 (X axis) assessed through Penman-Monteith equation for each month for Pasture (P), the young forest of 10 years (R10) and the old forest of 40 years (R40) P is in blue, R10 is in orange and R40 is in green. A linear regression and a R^2 linked to it have been assessed for each of the three areas and a line passing through 0:0 is represented by the black dotted line.

For SEN-ET (Figure 27Figure 28), the R^2 obtained are higher. They are nearly all above 0.9 except for P during the dry season (0.700). R10 has higher R2 during the wet season (Figure 27) as for WB method while CA has the higher for the dry season (Figure 28). By looking at the Kc values assessed based on the data for the wet season, all the Kc are between 1.2 and 1.7 which is more likely to be trustable based on Pereira et al. (2023). P has the lowest K_c and the highest is for CA and R40 which confirm that CA and R40 seems to be close to each other in term of soil cover and so ET. ET assessed through SEN-ET is nearly all the time higher than ET0 as expected but some values are below like for P most of the time.

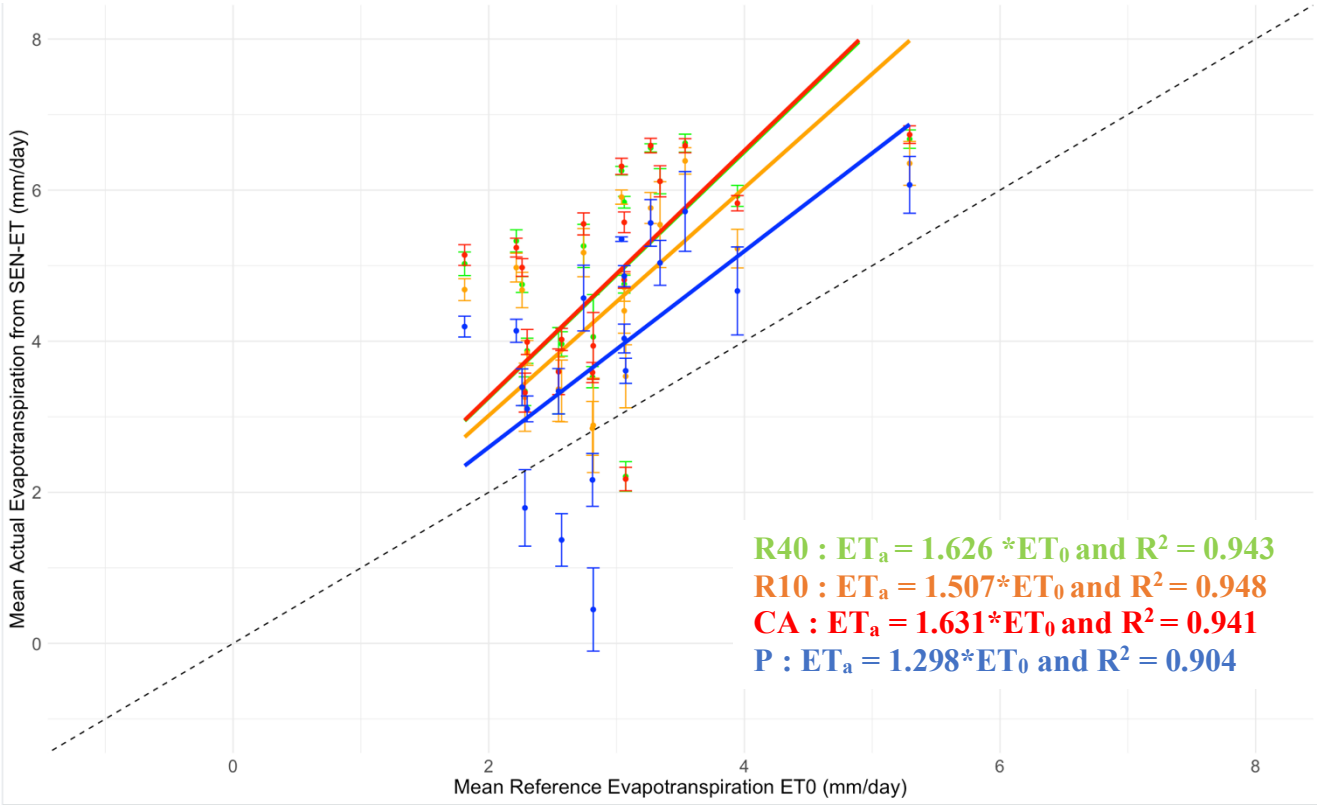

Figure 27: Comparison of the daily mean ET during the wet season based on the SEN-ET method (Y axis) to the reference ET0 (X axis) assessed through Penman-Monteith equation for each month for Pasture (P), Cleared area (CA), the young forest of 10 years (R10) and the old forest of 40 years (R40) P is in blue, CA is in red, R10 is in orange and R40 is in green. A linear regression and a R^2 linked to it have been assessed for each of the four area and a line passing through 0:0 is represented by the black dotted line. The standard deviation for the SEN-ET measurements is represented for each point for the four areas.

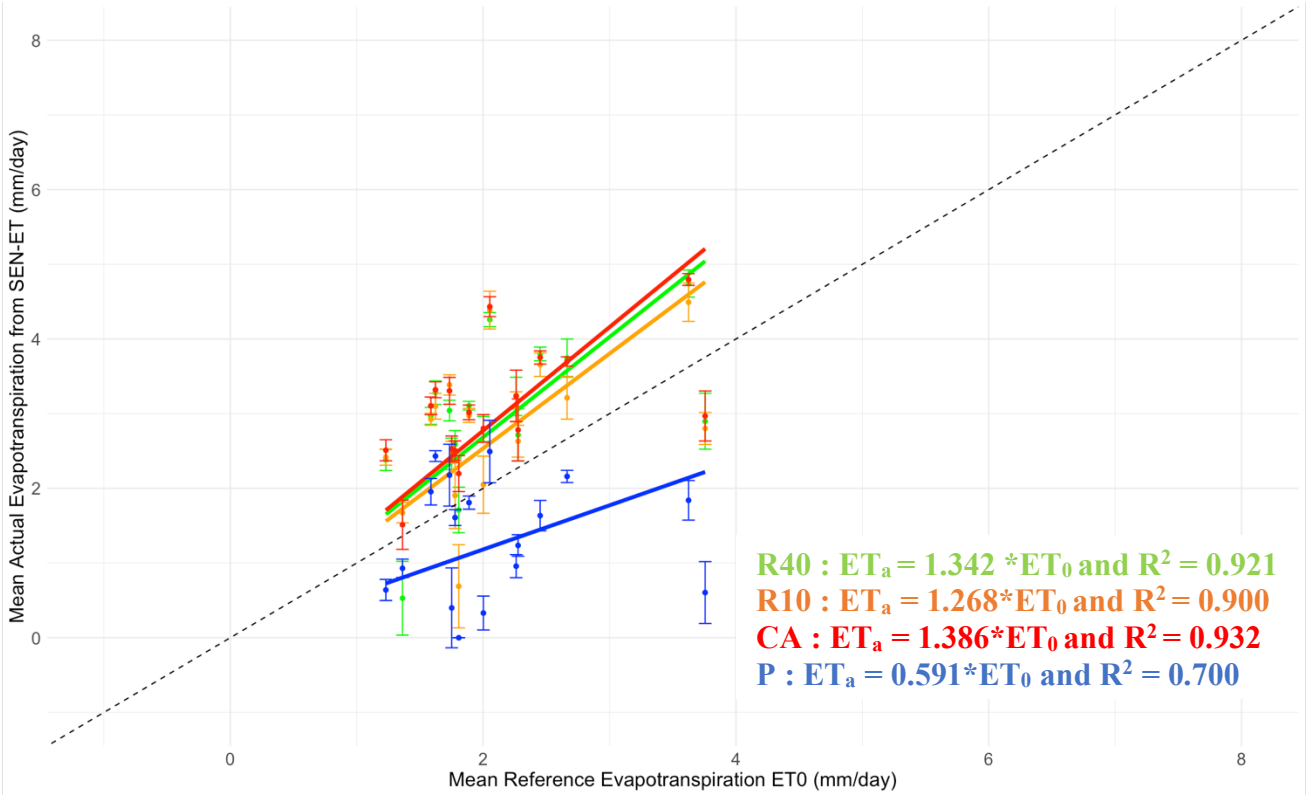

Figure 28: Comparison of the daily mean ET during the dry season based on the SEN-ET method (Y axis) to the reference ET0 (X axis) assessed through Penman-Monteith equation for each month for Pasture (P), Cleared area (CA), the young forest of 10 years (R10) and the old forest of 40 years (R40) P is in blue, CA is in red, R10 is in orange and R40 is in green. A linear regression and a R^2 linked to it have been assessed for each of the four area and a line passing through 0:0 is represented by the black dotted line. The standard deviation for the SEN-ET measurements is represented for each point for the four areas.

Comparison of WB and SEN-ET methods

Finally, the comparison of the water balance ET and the SEN-ET ET on Figure 29 andFigure 30 shows again the overestimations of the water balance but allows us to see which area have closer results between WB and SEN-ET like R10 for the wet season (R^2 = 0.822) and R40 for the dry season (R^2 = 0.745). The results between the two methods are closer for the wet season.

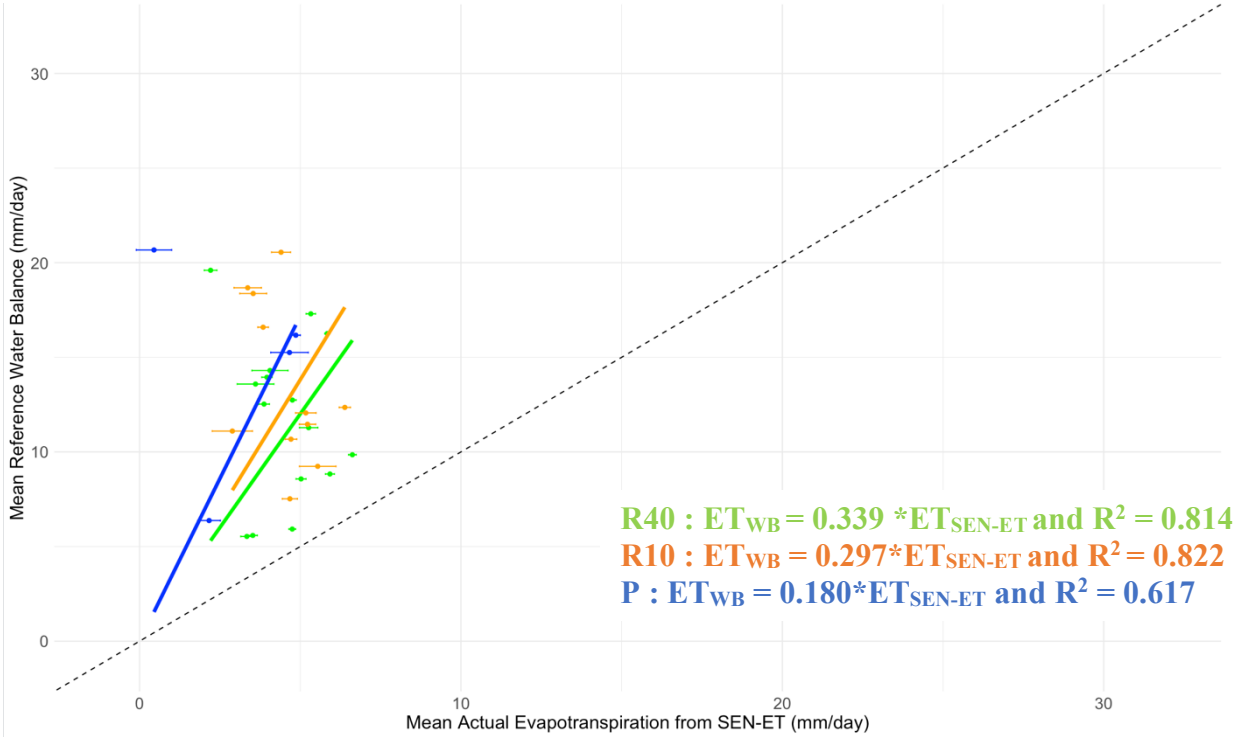

Figure 29: Comparison of the daily mean ET during the wet season based on the water balance method (Y axis) to the SEN-ET method (X axis) for each month for Pasture (P), the young forest of 10 years (R10) and the old forest of 40 years (R40) P is in blue, R10 is in orange and R40 is in green. A linear regression and a R^2 linked to it have been assessed for each of the four area and a line passing through 0:0 is represented by the black dotted line. The standard deviation for the SEN-ET measurements is represented for each point for the three areas.

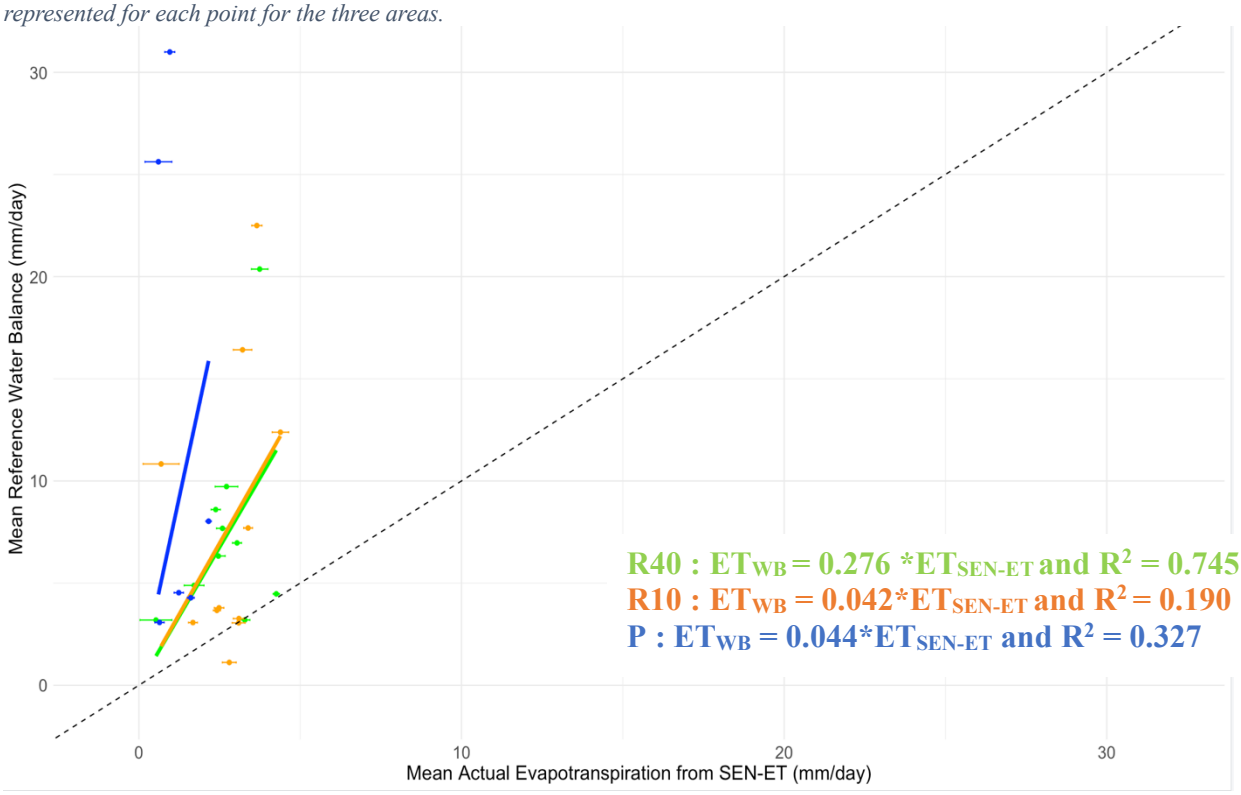

Figure 30: Comparison of the daily mean ET during the dry season based on the water balance method (Y axis) to the SEN-ET method (X axis) for each month for Pasture (P), the young forest of 10 years (R10) and the old forest of 40 years (R40) P is in blue, R10 is in orange and R40 is in green. A linear regression and a R^2 linked to it have been assessed for each of the four area and a line passing through 0:0 is represented by the black dotted line. The standard deviation for the SEN-ET measurements is represented for each point for the three areas.

To answer the main sub-question of this thesis which is: “Does a regenerate forest transpire more than an old forest? Could this have an impact on soil water resources?”. It would seem from the two methods carried out that both agree on the fact that the young forest (R10) does not transpire more than the old forest (R40) and that the latter two follow rather a rather similar pace. R10 even reaches lower evapotranspiration values in dry seasons. However, these lower values can be indirectly related to lower water availability even if R10 is a riparian zone.
However, given the difference in soil structure and texture of R10 and R40, it remains quite difficult to draw conclusions and answer this question correctly because different soil types reflect different behaviors in terms of water balance and available water. To answer this question correctly and with certainty, it would ideally have been necessary for R10 and R40 to have identical soil properties. The use of P and CA could have helped to better interpret these results, but WB and SEN-ET contradict each other for P and no comparison was possible for CA since the WB method has been supposed as not reliable due to the raw data. It is important to remember that the raw data for water potential used to assess drainage and capillary rise were also quite strange for P and that could induce wrong results for the drainage and the capillary rise since the sensors were not calibrated and were saturated at pF 2. Between the two methods, SEN-ET seems to be the most trustable and allows to give a K_c value quite close to what could be expected. These first trials in forest for SEN-ET seem to be quite conclusive.
However, various avenues for improvement could be considered in the continuation of this work and will be detailed in the next point (6).

6 Perspectives.

In the continuation of this thesis, various avenues for improvement could be considered to better quantify evapotranspiration.

INPE has installed sap flow sensors on several trees to measure direct transpiration. These sensors have already been installed on trees in plot R10 and were just installed in early January on plot R40. These data could not be analyzed this year because extensive data processing was necessary and would have been too much for this year in addition to the work already done. Moreover, not all study areas have sensors yet. It would therefore be wise to add sap flow sensors to the other plots and quantify this direct transpiration in the coming years using the dendrometer measurements. Another interesting avenue would be to better estimate the inflows and outflows of the water balance, especially the drainage and capillary rise. The main problem remains the uncertainties regarding the measurements of water potential sensors that saturate in too wet pF, preventing the interpretation and understanding of the dynamics of water potential for P and CA zones, which are saturated with water throughout the year. Sensors less sensible to water saturation could be used instead for example. Moreover, it could be interesting to continue the gap filling, especially for R10, for which the water stock is poor in data. For remote sensing, the use of MODIS could be considered by finding 500m2 pixels outside the study area and adjusting the results found, even though in all cases the accuracy of MODIS will remain significantly lower than that of SEN-ET. Finally, many uncertainties are present regarding the availability of water and the amount of water present in the aquifers. INPE already has sensors to measure the level of one of the aquifers, but not the others. By analyzing the level of groundwater, the water uptake by forests could be quantified as well as the seasonality of variations.

This thesis and the INPE project will continue in the future. More concretely, a master's thesis is already confirmed for next year and will aim to address the new issues raised by Charlotte Dermauw and myself in our respective master's theses, namely by trying to estimate ET based on the sap flow measurements and the dendrometer measurements. Direct measurements of ET will also be done using LAI (Leaf-Area-Index), and a water balance with these ET measurements will be conducted to assess drainage and capillary rise since it was one of the biggest uncertainties for this thesis.

7 Conclusion

The primary objective of this thesis was to quantify the impact of reforestation on evapotranspiration in the Atlantic Forest in Brazil with the aim to answer the following question: "Does a young, reforested forest transpire more than an old forest? Could this have an impact on soil water resources?"
To meet this objective, two different sub-objectives were defined corresponding to two different methods of estimating evapotranspiration. The first method of evapotranspiration based on the realization of a water balance. The second method is based on remote sensing with the use of SEN-ET, which has a resolution of 20m and is so far used only in agriculture.

This thesis was realized in collaboration with INPE through Laura Borma, co-promoter of this thesis, and was based on a study area divided into four study areas: a pasture (P), an area that was later deforested and converted to grassland before being now abandoned for nearly 40 years (CA), a 10-year regenerated forest (R10) and a 40-year-old forest (R40). Since February 2019, INPE has collected water potential and water content time series for plots R10 and R40, and since June 2021 for CA and P, which have been used to establish the water balance for this thesis. Data were filtered and gap filling procedures were tested. Yet, missing data could still be observed, especially for R10. The INPE also has meteorological data, including hourly precipitation data, which were used for the calculation of the water balance and for the estimation of the reference evapotranspiration.

The water balance and SEN-ET gave results that correspond to the seasonality of the ET observed with the reference evapotranspiration ET_0. Evapotranspiration was measured as lower in the dry season (May to September) and higher in the wet season (October to April). However, when comparing the results obtained for the four plots, differences were noted.

Due to poor estimates of the drainage values, CA ET could not be estimated with the mass balance approach. P had two contradictory results for WB and SEN-ET. According to WB, it is the area that have higher evapotranspiration while for SEN-ET, it is the area with less evapotranspiration, but some concerns are raised for the WB method based on the initial raw data and the sensors saturation at pF2. Regarding the comparison of the two types of forests, little significant difference was observed, thus not validating a higher evapotranspiration of R10, the regenerated forest: evapotranspiration in the dry season was even observed as lower. However, this lower evapotranspiration could be due to a lack of available water, although R10 is a riparian zone near a water table.
This same comparison between R10 and R40 was observed for SEN-ET. However, according to SEN-ET, P would be the area with less evapotranspiration in the dry and wet seasons.

This difference between the two validated methods may lie in the fact that many uncertainties are present in the calculation of drainage and capillary rise which was considered from 1.75m depth and calculated from water potential data that could not be measured at pF less than 2 due to saturation of the TEROS 21 sensors. This saturation of the sensors limits the understanding of the drainage and capillary rise process especially for the CA and P plots and have a significant impact on the evapotranspiration values obtained, justifying the major difference between the results of water balance and SEN-ET. However, the two methods agreed on the fact that a reforested young forest doesn't transpire more than an old one. SEN-ET which has only been tested in agricultural cases has been validated for forest after this master thesis and allowed to better assess the cultural coefficient for each of the four area.

In conclusion, although this thesis provided a better understanding of the dynamics of evapotranspiration and helped to partly address the problems and uncertainties encountered by Basile Delvoie last year, some areas for improvement, like the use of sap flow measurements already installed in some of the four area, could still be considered to better understand the impact of reforestation on evapotranspiration and soil water resources.

8 Bibliography

Allen, R. (s. d.). *PENMAN–MONTEITH EQUATION*.

Allen, R., Pereira, L., Raes, D., & Smith, M. (1998). FAO Irrigation and drainage paper No. 56. *Rome: Food and Agriculture Organization of the United Nations*, *56*, 26-40.

Barbosa, K. C., & Pizo, M. A. (2006). Seed Rain and Seed Limitation in a Planted Gallery Forest in Brazil. *Restoration Ecology*, *14*(4), 504-515. https://doi.org/10.1111/j.1526-100X.2006.00162.x

Bos, M. G., Molden, D. J., Kselik, R. A. L., & Allen, Richard G. (2009). *Water Requirements for Irrigation and the Environment*.

Brazil's Atlantic Forest (Mata Atlântica). (s. d.). WorldRainforests.com. Consulté 17 avril 2024, à l'adresse https://worldrainforests.com/mata-atlantica/

Brown, K. S., & Brown, G. G. (1992). Habitat alteration and species loss in Brazilian forests. *Tropical Deforestation and Species Extinction*, 119-142. Scopus.

Budowski, G. (1965). *Distribution of tropical American rain forest species in the light of successional processes.* CABI Databases. https://www.cabidigitallibrary.org/doi/full/10.5555/19650600379

CASELLES, V., SOBRINO, J. A., & COLL, C. (1992). On the use of satellite thermal data for determining evapotranspiration in partially vegetated areas. *International Journal of Remote Sensing*, *13*(14), 2669-2682. https://doi.org/10.1080/01431169208904071

Chen, G., Weil, R. R., & Hill, R. L. (2014). Effects of compaction and cover crops on soil least limiting water range and air permeability. *Soil and Tillage Research*, *136*, 61-69. https://doi.org/10.1016/j.still.2013.09.004

Corlett, R. T. (1999). Environmental forestry in Hong Kong : 1871–1997. *Forest Ecology and Management*, *116*(1), 93-105. https://doi.org/10.1016/S0378-1127(98)00443-5

Costa, M. H., Biajoli, M. C., Sanches, L., Malhado, A. C. M., Hutyra, L. R., da Rocha, H. R., Aguiar, R. G., & de Araújo, A. C. (2010). Atmospheric versus vegetation controls of Amazonian tropical rain forest evapotranspiration : Are the wet and seasonally dry rain forests any different? *Journal of Geophysical Research: Biogeosciences*, *115*(G4). https://doi.org/10.1029/2009JG001179

Damanesco, A. C. F. (2006). *Macrofauna edáfica, regeneração natural de espécies arbóreas, lianas e epífitas em...* https://www.teses.usp.br/teses/disponiveis/11/11150/tde-21052007-143659/en.php

Dean, W. (1995). *With broadax and firebrand : The destruction of the Brazilian Atlantic forest*. Berkeley : University of California Press. http://archive.org/details/withbroadaxfireb0000dean

Dean, W. (1997). *With Broadax and Firebrand : The Destruction of the Brazilian Atlantic*

Forest. University of California Press.

Delvoie, B. (2023). *Quel est l'impact de la reforestation sur l'équilibre des ressources en eau du sol ? Un cas d'étude dans la Forêt Atlantique Brésilienne, à São Francisco Xavier, État de São Paulo*.

Demetrio, W. C., Brown, G. G., Pupin, B., Dudas, R. T., Novo, R., Motta, A. C. V., Bartz, M. L. C., & Borma, L. S. (2024). Soil macrofauna and water-related functions in patches of regenerating Atlantic Forest in Brazil. *Pedobiologia*, *103*, 150944. https://doi.org/10.1016/j.pedobi.2024.150944

de Moraes, J. M., Schuler, A. E., Dunne, T., Figueiredo, R. de O., & Victoria, R. L. (2006). Water storage and runoff processes in plinthic soils under forest and pasture in eastern Amazonia. *Hydrological Processes*, *20*(12), 2509-2526. https://doi.org/10.1002/hyp.6213

de Oliveira, J. V., Ferreira, D. B. da S., Sahoo, P. K., Sodré, G. R. C., de Souza, E. B., & Queiroz, J. C. B. (2018). Differences in precipitation and evapotranspiration between forested and deforested areas in the Amazon rainforest using remote sensing data. *Environmental Earth Sciences*, *77*(6), 239. https://doi.org/10.1007/s12665-018-7411-9

de Souza, F. M., & Batista, J. L. F. (2004). Restoration of seasonal semideciduous forests in Brazil : Influence of age and restoration design on forest structure. *Forest Ecology and Management*, *191*(1), 185-200. https://doi.org/10.1016/j.foreco.2003.12.006

Destruction of Brazil's most imperiled rainforest continues. (2009, mai 31). Mongabay Environmental News. https://news.mongabay.com/2009/05/destruction-of-brazils-most-imperiled-rainforest-continues/

Dias, L. C. P., Macedo, M. N., Costa, M. H., Coe, M. T., & Neill, C. (2015). Effects of land cover change on evapotranspiration and streamflow of small catchments in the Upper Xingu River Basin, Central Brazil. *Journal of Hydrology: Regional Studies*, *4*, 108-122. https://doi.org/10.1016/j.ejrh.2015.05.010

El Maayar, M., & Chen, J. M. (2006). Spatial scaling of evapotranspiration as affected by heterogeneities in vegetation, topography, and soil texture. *Remote Sensing of Environment*, *102*(1), 33-51. https://doi.org/10.1016/j.rse.2006.01.017

Engel, V. L., & Parrotta, J. A. (2001). An evaluation of direct seeding for reforestation of degraded lands in central São Paulo state, Brazil. *Forest Ecology and Management*, *152*(1), 169-181. https://doi.org/10.1016/S0378-1127(00)00600-9

ESA. (2020). *SEN-ET user manual*.

Fan, Y., & Miguez-Macho, G. (2010). Potential groundwater contribution to Amazon evapotranspiration. *Hydrology and Earth System Sciences*, *14*(10), 2039-2056. https://doi.org/10.5194/hess-14-2039-2010

Farley, K. A., Jobbágy, E. G., & Jackson, R. B. (2005). Effects of afforestation on water yield : A global synthesis with implications for policy. *Global Change Biology*, *11*(10), 1565-1576. https://doi.org/10.1111/j.1365-2486.2005.01011.x

Foley, J. A., DeFries, R., Asner, G. P., Barford, C., Bonan, G., Carpenter, S. R., Chapin, F. S., Coe, M. T., Daily, G. C., Gibbs, H. K., Helkowski, J. H., Holloway, T., Howard, E. A., Kucharik, C. J., Monfreda, C., Patz, J. A., Prentice, I. C., Ramankutty, N., & Snyder, P. K. (2005). Global Consequences of Land Use. *Science*, *309*(5734), 570-574. https://doi.org/10.1126/science.1111772

Friedl, M. A., McIVer, D., Hodges, J., Zhang, X., Muchoney, D., Strahler, A. H., Woodcock, C., Gopal, S., Schneider, A., Cooper, A., Baccini, A., Gao, F., & Schaaf, C. (2002). Global land cover mapping from MODIS : Algorithms and early results. *Remote Sensing of Environment*, *83*, 287. https://doi.org/10.1016/S0034-4257(02)00078-0

Fritzsche, F., Abate, A., Fetene, M., Beck, E., Weise, S., & Guggenberger, G. (2006). Soil–plant hydrology of indigenous and exotic trees in an Ethiopian montane forest. *Tree Physiology*, *26*(8), 1043-1054. https://doi.org/10.1093/treephys/26.8.1043

Gaertner, B. A., Zegre, N., Warner, T., Fernandez, R., He, Y., & Merriam, E. R. (2019). Climate, forest growing season, and evapotranspiration changes in the central Appalachian Mountains, USA. *Science of The Total Environment*, *650*, 1371-1381. https://doi.org/10.1016/j.scitotenv.2018.09.129

Gentry, A. H., & Lopez-Parodi, J. (1980). Deforestation and Increased Flooding of the Upper Amazon. *Science*, *210*(4476), 1354-1356. https://doi.org/10.1126/science.210.4476.1354

Gholami, V. (2013). The influence of deforestation on runoff generation and soil erosion (Case study : Kasilian Watershed). *Journal of Forest Science*, *59*(7), 272-278. https://doi.org/10.17221/20/2013-JFS

Gholzom, E. H., & Gholami, V. (2012). A comparison between natural forests and reforested lands in terms of runoff generation potential and hydrologic response (case study : Kasilian Watershed). *Soil and Water Research*, *7*(4), 166-173. https://doi.org/10.17221/18/2012-SWR

Giambelluca, T. W. (2002). Hydrology of altered tropical forest. *Hydrological Processes*, *16*(8), 1665-1669. https://doi.org/10.1002/hyp.5021

Giambelluca, T. W., Scholz, F. G., Bucci, S. J., Meinzer, F. C., Goldstein, G., Hoffmann, W. A., Franco, A. C., & Buchert, M. P. (2009). Evapotranspiration and energy balance of Brazilian savannas with contrasting tree density. *Agricultural and Forest Meteorology*, *149*(8), 1365-1376. https://doi.org/10.1016/j.agrformet.2009.03.006

Gong, T., Lei, H., Yang, D., Jiao, Y., & Yang, H. (2017). Monitoring the variations of evapotranspiration due to land use/cover change in a semiarid shrubland. *Hydrology and Earth System Sciences*, *21*(2), 863-877. https://doi.org/10.5194/hess-21-863-2017

Goss, M. J., & Oliver, M. A. (2023). *Encyclopedia of Soils in the Environment—2nd Edition | Elsevier Shop*. https://shop.elsevier.com/books/encyclopedia-of-soils-in-the-environment/goss/978-0-12-822974-3

Gurgel Filho, O. A., de Moraes, J. L., & Morais, E. (1982). Caracteres silviculturais e competição entre espécies folhosas. *Silvicultura em São Paulo*, *16*(2). https://scholar.google.com/scholar?cluster=20885304463910791 33&hl=en&oi=scholarr

Harper, A., Baker, I. T., Denning, A. S., Randall, D. A., Dazlich, D., & Branson, M. (2014). Impact of Evapotranspiration on Dry Season Climate in the Amazon Forest. *Journal of Climate*, *27*(2), 574-591. https://doi.org/10.1175/JCLI-D-13-00074.1

Held, I. M., & Soden, B. J. (2006). Robust Responses of the Hydrological Cycle to Global Warming. *Journal of Climate*, *19*(21), 5686-5699. https://doi.org/10.1175/JCLI3990.1

Heo, J., Yu, J., Giardino, R., & Cho, H. (2015). Water Resources Response to Climate and Land-Cover Changes in a Semi-Arid Watershed, New Mexico, USA. *Terrestrial Atmospheric and Oceanic Sciences*, *26*. https://doi.org/10.3319/TAO.2015.03.24.01(Hy)

Hoang, N. T., & Kanemoto, K. (2021). Mapping the deforestation footprint of nations reveals growing threat to tropical forests. *Nature Ecology & Evolution*, *5*(6), 845-853. https://doi.org/10.1038/s41559-021-01417-z

Hougthon, R. A. (1994). *Land Use, Land-Use Change and Forestry*. https://archive.ipcc.ch/ipccreports/sres/land_use/index.php?idp=33

Huntington, T. G. (2006). Evidence for intensification of the global water cycle : Review and synthesis. *Journal of Hydrology*, *319*(1), 83-95. https://doi.org/10.1016/j.jhydrol.2005.07.003

Hwang, T., Martin, K. L., Vose, J. M., Wear, D., Miles, B., Kim, Y., & Band, L. E. (2018). Nonstationary Hydrologic Behavior in Forested Watersheds Is Mediated by Climate-Induced Changes in Growing Season Length and Subsequent Vegetation Growth. *Water Resources Research*, *54*(8), 5359-5375. https://doi.org/10.1029/2017WR022279

Idso, S. B., Jackson, R. D., & Reginato, R. J. (1975). Detection of Soil Moisture by Remote Surveillance : Difficult problems limit immediate applications, but the potential social benefits call for serious attempts at their solution. *American Scientist*, *63*(5), 549-557.

Idso, S. B., Schmugge, T. J., Jackson, R. D., & Reginato, R. J. (1975). The utility of surface temperature measurements for the remote sensing of surface soil water status. *Journal of Geophysical Research (1896-1977)*, *80*(21), 3044-3049. https://doi.org/10.1029/JC080i021p03044

INMET :: Météo. (s. d.). Consulté 17 avril 2024, à l'adresse https://clima.inmet.gov.br/NormaisClimatologicas/1961-1990/precipitacao_acumulada_mensal_anual

Jackson, R. B., Jobbágy, E. G., Avissar, R., Roy, S. B., Barrett, D. J., Cook, C. W., Farley, K. A., le Maitre, D. C., McCarl, B. A., & Murray, B. C. (2005). Trading water for carbon with biological carbon sequestration. *Science (New York, N.Y.)*, *310*(5756), 1944-1947. https://doi.org/10.1126/science.1119282

Jackson, R. D. (1985). Evaluating evapotranspiration at local and regional scales. *Proceedings of the IEEE*, *73*(6), 1086-1096. https://doi.org/10.1109/PROC.1985.13239

J.c.b, N. (1977). Reflorestamento heterogeneo com essencias indigenas [Sao Paulo; Brasil]. *Boletim Tecnico - Instituto Florestal (Brazil). No. 24.* https://agris.fao.org/search/en/providers/123819/records/64735c162c1d629bc97c40f8

Joly, C. A., Spigolon, J. R., Lieberg, S. A., Salis, S. M., Aidar, M. P. M., Metzger, J.-P., Zickel, C. S., Lobo, P. C., Shimabukuro, M. T., Marques, M. C. M., & Salino, A. (2000). Projeto Jacaré-Pepira : O desenvolvimento de um modelo de recomposição da mata ciliar com base na florística regional. *Matas ciliares: conservação e recuperação*. https://repositorio.usp.br/item/002164759

Juárez, R. I. N., Hodnett, M. G., Fu, R., Goulden, M. L., & Randow, C. von. (2007). Control of Dry Season Evapotranspiration over the Amazonian Forest as Inferred from Observations at a Southern Amazon Forest Site. *Journal of Climate*, *20*(12), 2827-2839. https://doi.org/10.1175/JCLI4184.1

Justice, C. O., Townshend, J., Vermote, E., Ed, M., Wolfe, R., Saleous, N., Roy, D., & Morisette, J. (2002). An overview of MODIS Land data processing and product status. *Remote Sensing of Environment*, *83*, 3-15. https://doi.org/10.1016/S0034-4257(02)00084-6

KAGEYAMA, P. Y., & Castro, C. de A. (1989). Sucessão secundária, estrutura genética e plantações de espécies arbóreas nativas. *IPEF, Piracicaba*, *41*(42), 83-93.

KUSTAS, W. P., & NORMAN, J. M. (1996). Use of remote sensing for evapotranspiration monitoring over land surfaces. *Hydrological Sciences Journal*, *41*(4), 495-516. https://doi.org/10.1080/02626669609491522

Lathuillière, M. J., Johnson, M. S., & Donner, S. D. (2012). Water use by terrestrial ecosystems : Temporal variability in rainforest and agricultural contributions to evapotranspiration in Mato Grosso, Brazil. *Environmental Research Letters*, *7*(2), 024024. https://doi.org/10.1088/1748-9326/7/2/024024

Lesica, P., & Allendorf, F. W. (2002). *Ecological Genetics and the Restoration of Plant Communities : Mix or Match ? - Lesica—1999—Restoration Ecology—Wiley Online Library*. https://onlinelibrary.wiley.com/doi/abs/10.1046/j.1526-100X.1999.07105.x?casa_token=PNjDBkr89CkAAAAA:-5i1AlQYqD7eLBkG2uFAjv_HQdEn8hOZ9i7V-gvEdHe_K-CXXS5PlYtrWrbdDAkOnNzX9S-x9PfN9w

Li, Z., Liu, W., Zhang, X., & Zheng, F. (2009). Impacts of land use change and climate variability on hydrology in an agricultural catchment on the Loess Plateau of China. *Journal of Hydrology*, *377*(1), 35-42. https://doi.org/10.1016/j.jhydrol.2009.08.007

Li, Z.-L., Tang, R., Wan, Z., Bi, Y., Zhou, C., Tang, B., Yan, G., & Zhang, X. (2009). A Review of Current Methodologies for Regional Evapotranspiration Estimation from Remotely Sensed Data. *Sensors*, *9*(5), Article 5. https://doi.org/10.3390/s90503801

Los, S. O., Pollack, N. H., Parris, M. T., Collatz, G. J., Tucker, C. J., Sellers, P. J., Malmström, C. M., DeFries, R. S., Bounoua, L., & Dazlich, D. A. (2000). A Global 9-yr Biophysical Land Surface Dataset from NOAA AVHRR Data. *Journal of Hydrometeorology*, *1*(2), 183-199. https://doi.org/10.1175/1525-7541(2000)001<0183:AGYBLS>2.0.CO;2

Lu, J., Wang, G., Li, S., Feng, A., Zhan, M., Jiang, T., Su, B., & Wang, Y. (2021). Projected Land Evaporation and Its Response to Vegetation Greening Over China Under Multiple Scenarios in the CMIP6 Models. *Journal of Geophysical Research: Biogeosciences*, *126*(9),

e2021JG006327. https://doi.org/10.1029/2021JG006327

Malmer, A., & Grip, H. (1990). Soil disturbance and loss of infiltrability caused by mechanized and manual extraction of tropical rainforest in Sabah, Malaysia. *Forest Ecology and Management*, *38*(1), 1-12. https://doi.org/10.1016/0378-1127(90)90081-L

Martens, S., Breshears, D. D., & Meyer, C. W. (2000). *[PDF] Spatial distributions of understory light along the grassland/forest continuum : Effects of cover, height, and spatial pattern of tree canopies | Semantic Scholar*. https://www.semanticscholar.org/paper/Spatial-distributions-of-understory-light-along-the-Martens-Breshears/127dd67a17ae9f23bcc74486a3f7d107665952fe

Mathias, S. A., Skaggs, T. H., Quinn, S. A., Egan, S. N. C., Finch, L. E., & Oldham, C. D. (2015). A soil moisture accounting-procedure with a Richards' equation-based soil texture-dependent parameterization. *Water Resources Research*, *51*(1), 506-523. https://doi.org/10.1002/2014WR016144

Mátyás, C., & Sun, G. (2014). Forests in a water limited world under climate change. *Environmental Research Letters*, *9*(8), 085001. https://doi.org/10.1088/1748-9326/9/8/085001

McCabe, M. F., & Wood, E. F. (2006). Scale influences on the remote estimation of evapotranspiration using multiple satellite sensors. *Remote Sensing of Environment*, *105*(4), 271-285. https://doi.org/10.1016/j.rse.2006.07.006

McKay, J. K., Christian, C. E., Harrison, S., & Rice, K. J. (2005). "How Local Is Local?"—A Review of Practical and Conceptual Issues in the Genetics of Restoration. *Restoration Ecology*, *13*(3), 432-440. https://doi.org/10.1111/j.1526-100X.2005.00058.x

Ming-yuan, W. (2002). Soil Moisture Regimen and Application for Plants in Maowusu Transition Zone From Sand Land to Desert. *Journal of Arid Land Resources and Environment*. https://www.semanticscholar.org/paper/Soil-Moisture-Regimen-and-Application-for-Plants-in-Ming-yuan/f895f0fd2b6e9943ff6cfda6c781b9966ede9aa4

Monteiro, M. J. (2023). *Ecohydrological implications of Pleroma pulchrum dominance in forest regeneration : Local ranchers' perceptions and implications for restoration in southern Brazil.*

Moran, M. S., Jackson, R. D., Raymond, L. H., Gay, L. W., & Slater, P. N. (1989). Mapping surface energy balance components by combining landsat thematic mapper and ground-based meteorological data. *Remote Sensing of Environment*, *30*(1), 77-87. https://doi.org/10.1016/0034-4257(89)90049-7

Moreira, M. Z., Sternberg, L. da S. L., & Nepstad, D. C. (2000). Vertical patterns of soil water uptake by plants in a primary forest and an abandoned pasture in the eastern Amazon : An isotopic approach. *Plant and Soil*, *222*(1), 95-107. https://doi.org/10.1023/A:1004773217189

Mu, Q., Heinsch, F. A., Zhao, M., & Running, S. W. (2007). Development of a global evapotranspiration algorithm based on MODIS and global meteorology data. *Remote Sensing of Environment*, *111*(4), 519-536. https://doi.org/10.1016/j.rse.2007.04.015

Mu, Q., Zhao, M., & Running, S. W. (2011). Improvements to a MODIS global terrestrial evapotranspiration algorithm. *Remote Sensing of Environment*, *115*(8), 1781-1800. https://doi.org/10.1016/j.rse.2011.02.019

Neuman, S. P. (1977). Theoretical derivation of Darcy's law. *Acta Mechanica*, *25*(3), 153-170. https://doi.org/10.1007/BF01376989

Nobre, C. A., Sellers, P. J., & Shukla, J. (1991). Amazonian Deforestation and Regional Climate Change. *Journal of Climate*, *4*(10), 957-988. https://doi.org/10.1175/1520-0442(1991)004<0957:ADARCC>2.0.CO;2

Obrist, D., Verburg, P. S. J., Young, M. H., Coleman, J. S., Schorran, D. E., & Arnone, J. A. (2003). Quantifying the effects of phenology on ecosystem evapotranspiration in planted grassland mesocosms using EcoCELL technology. *Agricultural and Forest Meteorology*, *118*(3), 173-183. https://doi.org/10.1016/S0168-1923(03)00111-4

Oliveira, Bezerra, L., Davidson, E. A., Pinto, F., Klink, C. A., Nepstad, D. C., & Moreira, A. (2005). Deep root function in soil water dynamics in cerrado savannas of central Brazil. *Functional Ecology*, *19*(4), 574-581. https://doi.org/10.1111/j.1365-2435.2005.01003.x

Oliveira, P. T. S., Nearing, M. A., Moran, M. S., Goodrich, D. C., Wendland, E., & Gupta, H. V. (2014). Trends in water balance components across the Brazilian Cerrado. *Water Resources Research*, *50*(9), 7100-7114. https://doi.org/10.1002/2013WR015202

Panferov, O., Knyazikhin, Y., Myneni, R. B., Szarzynski, J., Engwald, S., Schnitzler, K. G., & Gravenhorst, G. (2001). The role of canopy structure in the spectral variation of transmission and absorption of solar radiation in vegetation canopies. *IEEE Transactions on Geoscience and Remote Sensing*, *39*(2), 241-253. https://doi.org/10.1109/36.905232

Peng, H., Tague, C., & Jia, Y. (2016). Evaluating the eco-hydrologic impacts of reforestation in the Loess Plateau, China, using an eco-hydrologic model. *Ecohydrology*, *9*(3), 498-513. https://doi.org/10.1002/eco.1652

Pereira, L. S., Paredes, P., Espírito-Santo, D., & Salman, M. (2023). Actual and standard crop coefficients for semi-natural and planted grasslands and grasses : A review aimed at supporting water management to improve production and ecosystem services. *Irrigation Science*, 1-32. https://doi.org/10.1007/s00271-023-00867-6

Pickett, S. T. A., Cadenasso, M. L., & Meiners, S. J. (2013). Vegetation Dynamics. In *Vegetation Ecology* (p. 107-140). John Wiley & Sons, Ltd. https://doi.org/10.1002/9781118452592.ch4

Pickett, S. T. A., Collins, S. L., & Armesto, J. J. (1987). Models, mechanisms and pathways of succession. *The Botanical Review*, *53*(3), 335-371. https://doi.org/10.1007/BF02858321

Priante-Filho, N., Vourlitis, G. L., Hayashi, M. M. S., Nogueira, J. D. S., Campelo Jr., J. H., Nunes, P. C., Souza, L. S. E., Couto, E. G., Hoeger, W., Raiter, F., Trienweiler, J. L., Miranda, E. J., Priante, P. C., Fritzen, C. L., Lacerda, M., Pereira, L. C., Biudes, M. S., Suli, G. S., Shiraiwa, S., … Silveira, M. (2004). Comparison of the mass and energy exchange of a pasture and a mature transitional tropical forest of the southern Amazon Basin during a

seasonal transition. *Global Change Biology*, *10*(5), 863-876. https://doi.org/10.1111/j.1529-8817.2003.00775.x

Priesack, E., & Durner, W. (2006). Closed-Form Expression for the Multi-Modal Unsaturated Conductivity Function. *Vadose Zone Journal*, *5*(1), 121-124. https://doi.org/10.2136/vzj2005.0066

Qiu, G. Y., Xie, F., Feng, Y. C., & Tian, F. (2011). Experimental studies on the effects of the "Conversion of Cropland to Grassland Program" on the water budget and evapotranspiration in a semi-arid steppe in Inner Mongolia, China. *Journal of Hydrology*, *411*(1), 120-129. https://doi.org/10.1016/j.jhydrol.2011.09.040

Ranasinghe, R., Ruane, A. C., Vautard, R., Arnell, N., Coppola, E., Cruz, F. A., Dessai, S., Islam, A. S., Rahimi, M., Ruiz Carrascal, D., Sillmann, J., Sylla, M. B., Tebaldi, C., Wang, W., & Zaaboul, R. (2021). Climate change information for regional impact and for risk assessment. In V. Masson-Delmotte, P. Zhai, A. Pirani, S. L. Connors, C. Péan, S. Berger, N. Caud, Y. Chen, L. Goldfarb, M. I. Gomis, M. Huang, K. Leitzell, E. Lonnoy, J. B. R. Matthews, T. K. Maycock, T. Waterfield, Ö. Yelekçi, R. Yu, & B. Zhou (Éds.), *Climate Change 2021 : The Physical Science Basis. Contribution of Working Group I to the Sixth Assessment Report of the Intergovernmental Panel on Climate Change* (p. 1767-1926). Cambridge University Press. https://doi.org/10.1017/9781009157896.001

RANGO, A. (1994). Application of remote sensing methods to hydrology and water resources. *Hydrological Sciences Journal*, *39*(4), 309-320. https://doi.org/10.1080/02626669409492752

Reis, A. L., & Xavier, I. de M. (2003). Mulher e AIDS : Rompendo o silêncio de adesão. *Revista Brasileira de Enfermagem*, *56*, 28-34. https://doi.org/10.1590/S0034-71672003000100006

Roca, R., Bergès, J.-C., Brogniez, H., Capderou, M., Chambon, P., Chomette, O., Cloché, S., Fiolleau, T., Jobard, I., Lémond, J., Ly, M., Picon, L., Raberanto, P., Szantai, A., & Viollier, M. (2010). On the water and energy cycles in the Tropics. *Comptes Rendus Geoscience*, *342*(4), 390-402. https://doi.org/10.1016/j.crte.2010.01.003

Rodrigues, R. R. (2007a). *High Diversity Forest Restoration in Degraded Areas : Methods and Projects in Brazil*. Nova Publishers.

Rodrigues, R. R. (2007b). *High Diversity Forest Restoration in Degraded Areas : Methods and Projects in Brazil*. Nova Publishers.

Rodrigues, R. R., & Gandolfi, S. (2000). Conceitos, tendências e ações para a recuperação de florestas ciliares. *Matas ciliares: conservação e recuperação*. https://repositorio.usp.br/item/001104033

Rodrigues, R. R., Lima, R. A. F., Gandolfi, S., & Nave, A. G. (2009). On the restoration of high diversity forests : 30 years of experience in the Brazilian Atlantic Forest. *Biological Conservation*, *142*(6), 1242-1251. https://doi.org/10.1016/j.biocon.2008.12.008

Roy, J., Mooney, H. A., & Saugier, B. (2001). *Terrestrial Global Productivity*. Elsevier.

Santos, W., & Augustin, C. (2015). Water and sediment loss through runoff in areas of forest and pasture cover in southwestern Amazonia – Acre – Brazil. *Zeitschrift für Geomorphologie*, *59*. https://doi.org/10.1127/zfg_suppl/2015/S-59203

Saxton, K. E., & Rawls, W. J. (2006). Soil Water Characteristic Estimates by Texture and Organic Matter for Hydrologic Solutions. *Soil Science Society of America Journal*, *70*(5), 1569-1578. https://doi.org/10.2136/sssaj2005.0117

Saxton, K. E., Rawls, W. J., Romberger, J. S., & Papendick, R. I. (1986). Estimating Generalized Soil-water Characteristics from Texture. *Soil Science Society of America Journal*, *50*(4), 1031-1036. https://doi.org/10.2136/sssaj1986.03615995005000040039x

Sertel, E., Imamoglu, M., Cuceloglu, G., & Erturk, A. (2019). Impacts of Land Cover/Use Changes on Hydrological Processes in a Rapidly Urbanizing Mid-latitude Water Supply Catchment. *Water*, *11*, 1075. https://doi.org/10.3390/w11051075

Shukla, J., & Mintz, Y. (1982). Influence of Land-Surface Evapotranspiration on the Earth's Climate. *Science*, *215*(4539), 1498-1501. https://doi.org/10.1126/science.215.4539.1498

Shukla, J., Nobre, C., & Sellers, P. (1990). Amazon Deforestation and Climate Change. *Science*, *247*(4948), 1322-1325. https://doi.org/10.1126/science.247.4948.1322

Skole, D., & Tucker, C. (1993). Tropical Deforestation and Habitat Fragmentation in the Amazon : Satellite Data from 1978 to 1988. *Science*, *260*(5116), 1905-1910. https://doi.org/10.1126/science.260.5116.1905

Sterling, S. M., Ducharne, A., & Polcher, J. (2013). The impact of global land-cover change on the terrestrial water cycle. *Nature Climate Change*, *3*(4), 385-390. https://doi.org/10.1038/nclimate1690

Sun, G., Zhou, G., Zhang, Z., Wei, X., McNulty, S. G., & Vose, J. M. (2006). Potential water yield reduction due to forestation across China. *Journal of Hydrology*, *328*(3), 548-558. https://doi.org/10.1016/j.jhydrol.2005.12.013

TEROS 10—Meter Group. (s. d.). Consulté 15 janvier 2024, à l'adresse https://new.metergroup.com/fr/des-produits/teros-10/

TEROS 21. (2021, juillet 28). METER. https://www.metergroup.com/en/meter-environment/products/teros-21-soil-water-potential-sensor

Tóth, T., Balog, K., Szabó, A., Pásztor, L., Jobbágy, E. G., Nosetto, M. D., & Gribovszki, Z. (2014). Influence of lowland forests on subsurface salt accumulation in shallow groundwater areas. *AoB PLANTS*, *6*, plu054. https://doi.org/10.1093/aobpla/plu054

Urbanska, K. M., Webb, N. R., & Edwards, P. J. (1997). *Restoration Ecology and Sustainable Development*. Cambridge University Press.

van Genuchten, M. Th. (1980). A Closed-form Equation for Predicting the Hydraulic Conductivity of Unsaturated Soils. *Soil Science Society of America Journal*, *44*(5), 892-898. https://doi.org/10.2136/sssaj1980.03615995004400050002x

Vieira, D. C. M., & Gandolfi, S. (2006). Chuva de sementes e regeneração natural sob três espécies arbóreas em uma floresta em processo de restauração. *Brazilian Journal of Botany*, *29*, 541-554. https://doi.org/10.1590/S0100-84042006000400004

Vourlitis, G. L., de Souza Nogueira, J., de Almeida Lobo, F., Sendall, K. M., de Paulo, S. R., Antunes Dias, C. A., Pinto Jr., O. B., & de Andrade, N. L. R. (2008). Energy balance and canopy conductance of a tropical semi-deciduous forest of the southern Amazon Basin. *Water Resources Research*, *44*(3). https://doi.org/10.1029/2006WR005526

Vourlitis, G. L., Filho, N. P., Hayashi, M. M. S., de S. Nogueira, J., Caseiro, F. T., & Campelo Jr., J. H. (2002). Seasonal variations in the evapotranspiration of a transitional tropical forest of Mato Grosso, Brazil. *Water Resources Research*, *38*(6), 30-1-30-11. https://doi.org/10.1029/2000WR000122

Wagner, F. H., Sanchez, A., Aidar, M. P. M., Rochelle, A. L. C., Tarabalka, Y., Fonseca, M. G., Phillips, O. L., Gloor, E., & Aragão, L. E. O. C. (2020). Mapping Atlantic rainforest degradation and regeneration history with indicator species using convolutional network. *PLOS ONE*, *15*(2), e0229448. https://doi.org/10.1371/journal.pone.0229448

Werth, D., & Avissar, R. (2002). *The local and global effects of Amazon deforestation—Werth—2002—Journal of Geophysical Research : Atmospheres—Wiley Online Library*. https://agupubs.onlinelibrary.wiley.com/doi/full/10.1029/2001JD000717

What is the Atlantic Forest and why do we need to save it? | Stories | WWF. (s. d.). World Wildlife Fund. Consulté 5 mai 2024, à l'adresse https://www.worldwildlife.org/stories/what-is-the-atlantic-forest-and-why-do-we-need-to-save-it

White, M. A., Running, S. W., & Thornton, P. E. (1999). The impact of growing-season length variability on carbon assimilation and evapotranspiration over 88 years in the eastern US deciduous forest. *International Journal of Biometeorology*, *42*(3), 139-145. https://doi.org/10.1007/s004840050097

Williams, M., Malhi, Y., Nobre, A. D., Rastetter, E. B., Grace, J., & Pereira, M. G. P. (1998). Seasonal variation in net carbon exchange and evapotranspiration in a Brazilian rain forest : A modelling analysis. *Plant, Cell & Environment*, *21*(10), 953-968. https://doi.org/10.1046/j.1365-3040.1998.00339.x

Woodwell, G. M., & Pecan, E. V. (1973). *Carbon and the biosphere*. https://cds.cern.ch/record/414705

Wu, G. Z. (2006). *Roots' Distribution Characteristics and Fine Root Dynamics of Sabina Vulgaris and Artemisia Ordosica in Mu Us Sandland—Master's thesis—Dissertation*. https://www.dissertationtopic.net/doc/939618

Yang, L., Wei, W., Chen, L., Chen, W., & Wang, J. (2014). Response of temporal variation of soil moisture to vegetation restoration in semi-arid Loess Plateau, China. *CATENA*, *115*, 123-133. https://doi.org/10.1016/j.catena.2013.12.005

Yang, Y., Zhang, S., Roderick, M. L., McVicar, T. R., Yang, D., Liu, W., & Li, X. (2020). Comparing Palmer Drought Severity Index drought assessments using the traditional offline

approach with direct climate model outputs. *Hydrology and Earth System Sciences*, *24*(6), 2921-2930. https://doi.org/10.5194/hess-24-2921-2020

Young, A. M., Friedl, M. A., Novick, K., Scott, R. L., Moon, M., Frolking, S., Li, X., Carrillo, C. M., & Richardson, A. D. (2022). Disentangling the Relative Drivers of Seasonal Evapotranspiration Across a Continental-Scale Aridity Gradient. *Journal of Geophysical Research: Biogeosciences*, *127*(8), e2022JG006916. https://doi.org/10.1029/2022JG006916

Zeng, N., & Yoon, J. (2009). Expansion of the world's deserts due to vegetation-albedo feedback under global warming. *Geophysical Research Letters*, *36*(17). https://doi.org/10.1029/2009GL039699

ZL6. (2021, juillet 14). METER. https://www.metergroup.com/en/meter-environment/products/zl6-data-logger

9 Appendices

Appendix 1: Normal distributions of θ and h for each parcel at each depth.

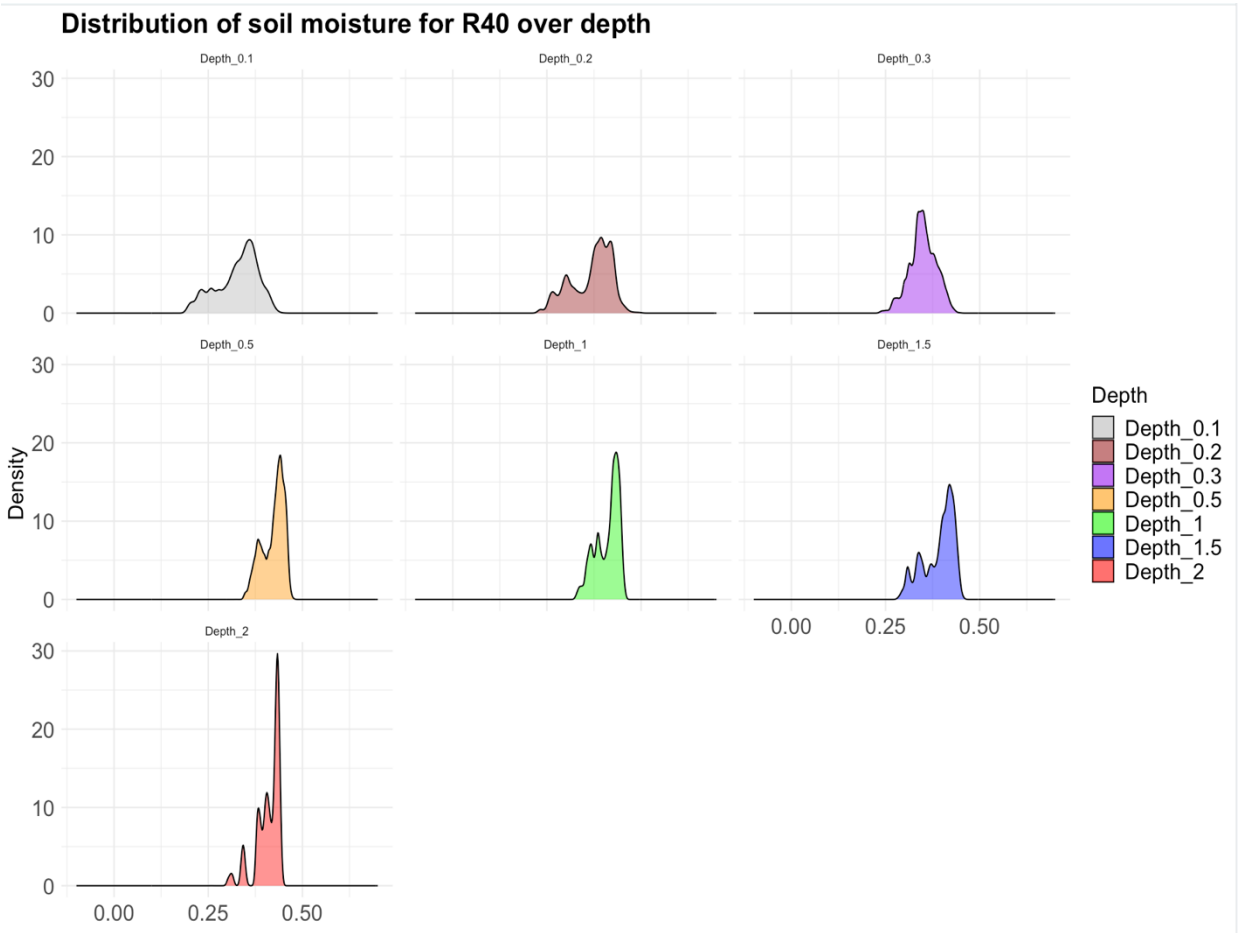

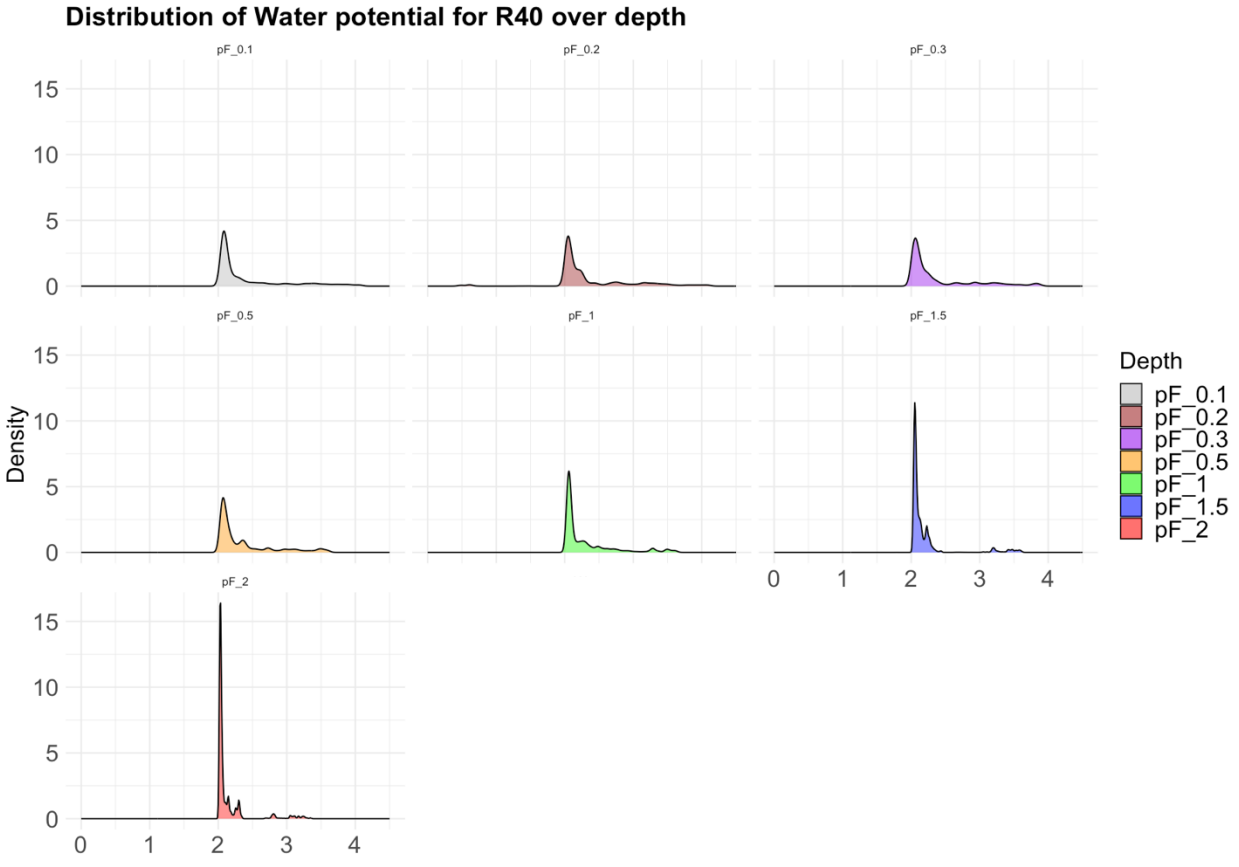

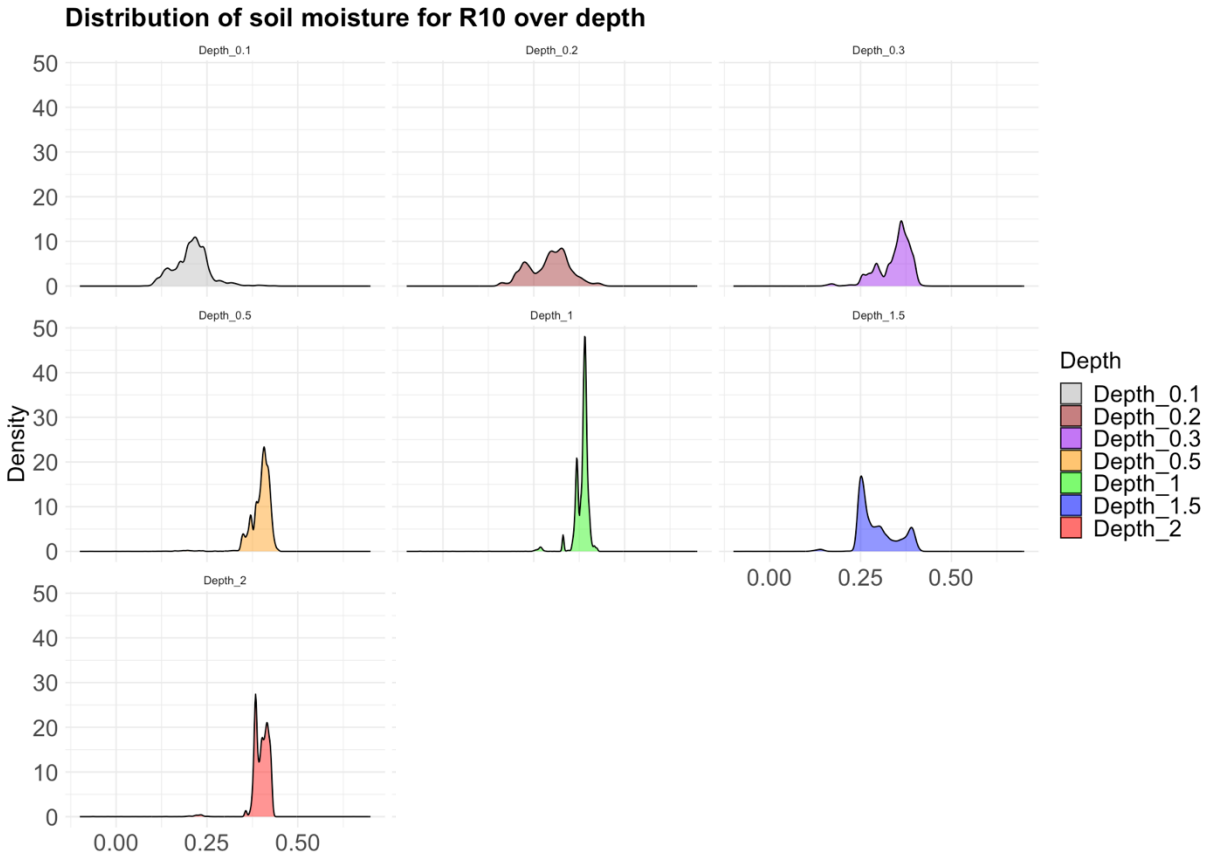
Distribution of soil moisture for R10 over depth
Depth_0.1
Depth_0.2
Depth_0.3
Depth_0.5
Depth_1
Depth_1.5
Depth_2
Density
0
10
20
30
40
50
0.00
0.25
0.50
Depth
Depth_0.1
Depth_0.2
Depth_0.3
Depth_0.5
Depth_1
Depth_1.5
Depth_2

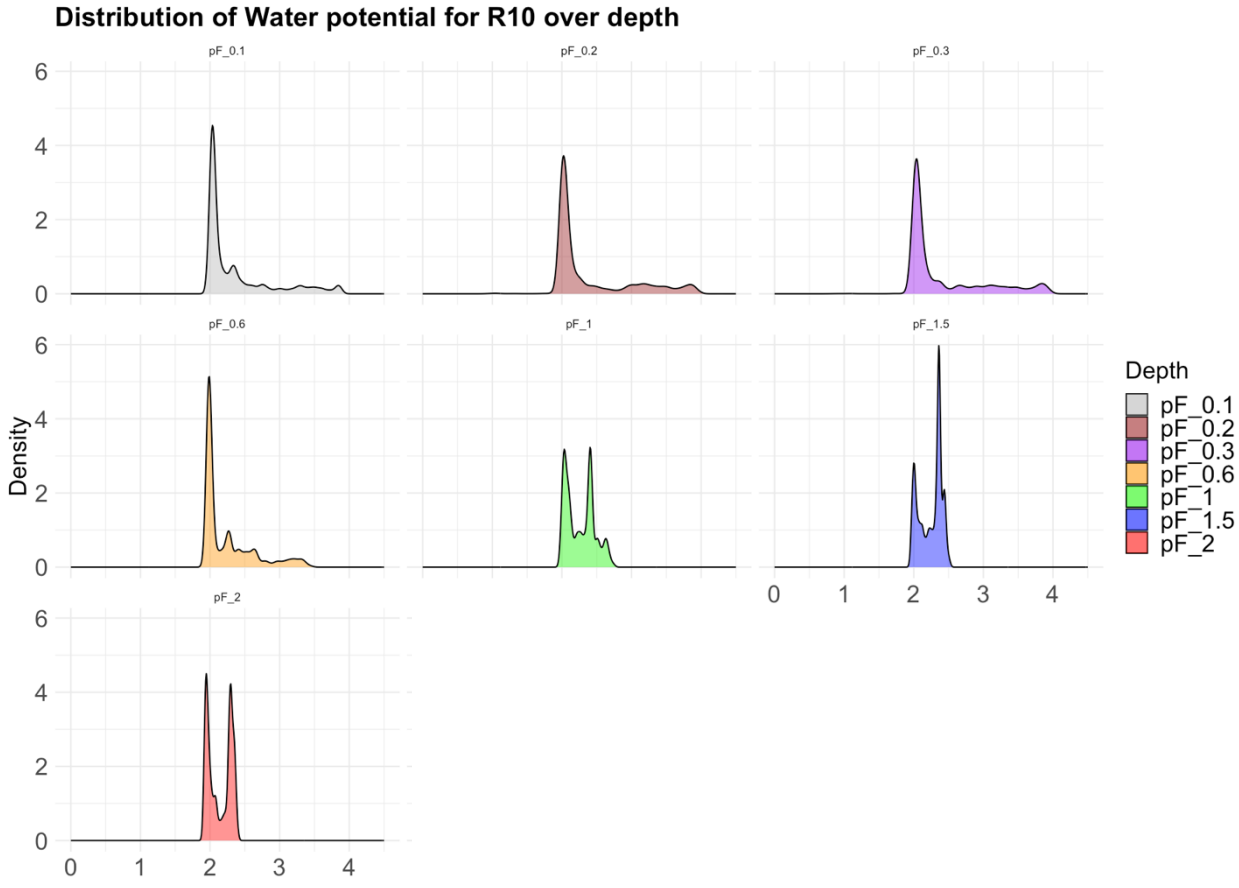
Distribution of Water potential for R10 over depth
pF_0.1
pF_0.2
pF_0.3
pF_0.6
pF_1
pF_1.5
pF_2
Density
0
2
4
6
0
1
2
3
4
Depth
pF_0.1
pF_0.2
pF_0.3
pF_0.6
pF_1
pF_1.5
pF_2

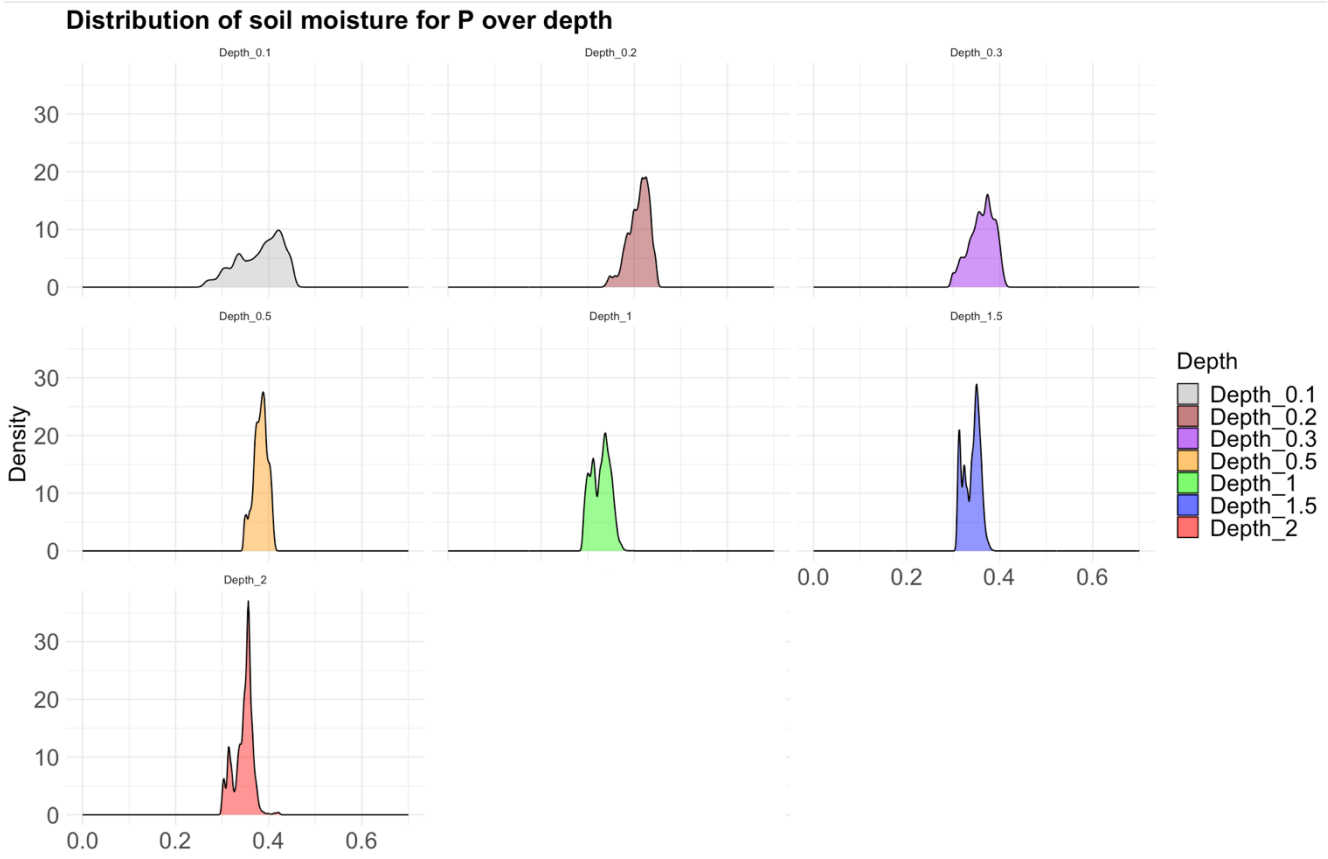
Distribution of soil moisture for P over depth
Depth_0.1
Depth_0.2
Depth_0.3
Depth_0.5
Depth_1
Depth_1.5
Depth_2
Density
Depth
Depth_0.1
Depth_0.2
Depth_0.3
Depth_0.5
Depth_1
Depth_1.5
Depth_2

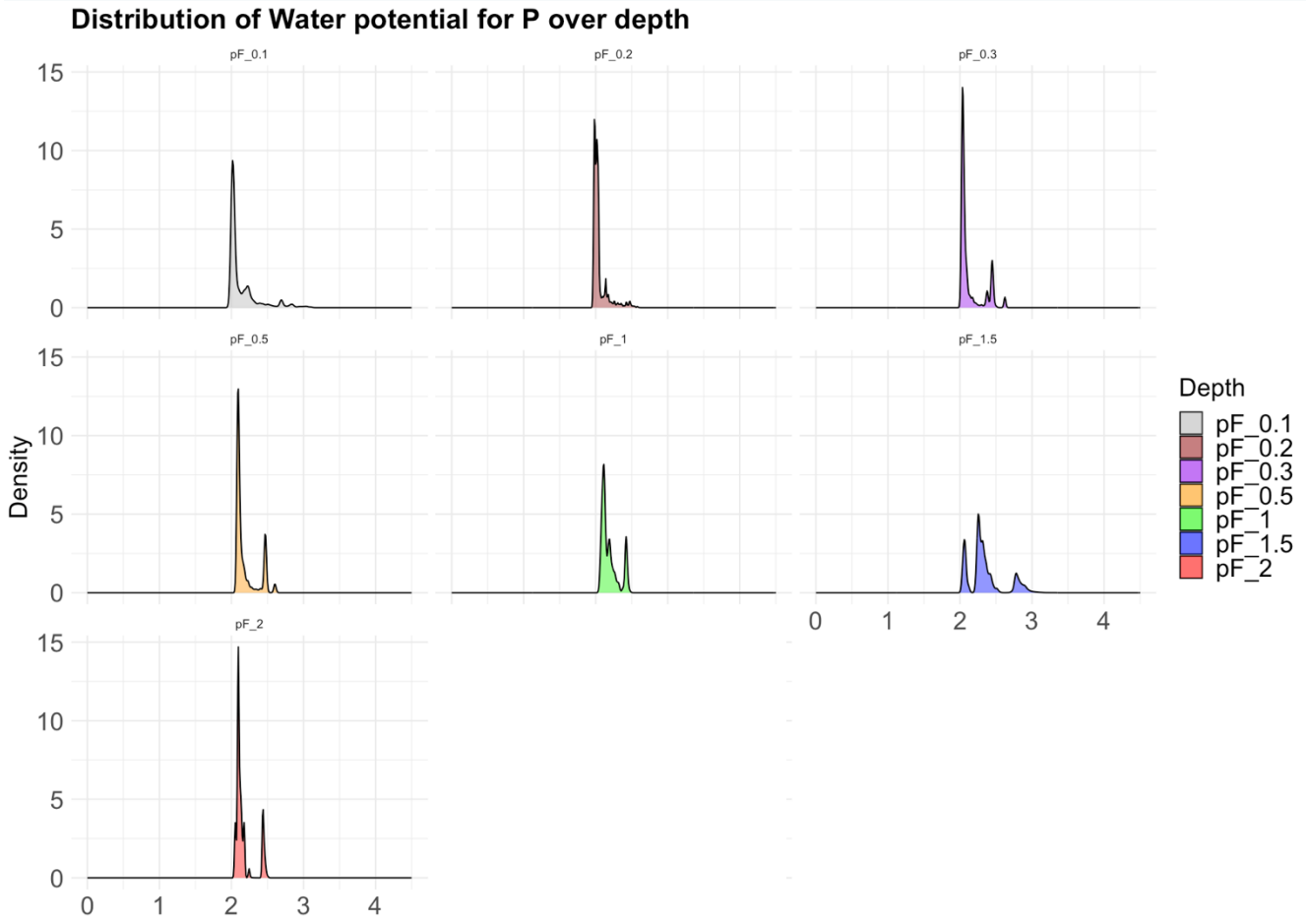
Distribution of Water potential for P over depth
pF_0.1
pF_0.2
pF_0.3
pF_0.5
pF_1
pF_1.5
pF_2
Density
Depth
pF_0.1
pF_0.2
pF_0.3
pF_0.5
pF_1
pF_1.5
pF_2

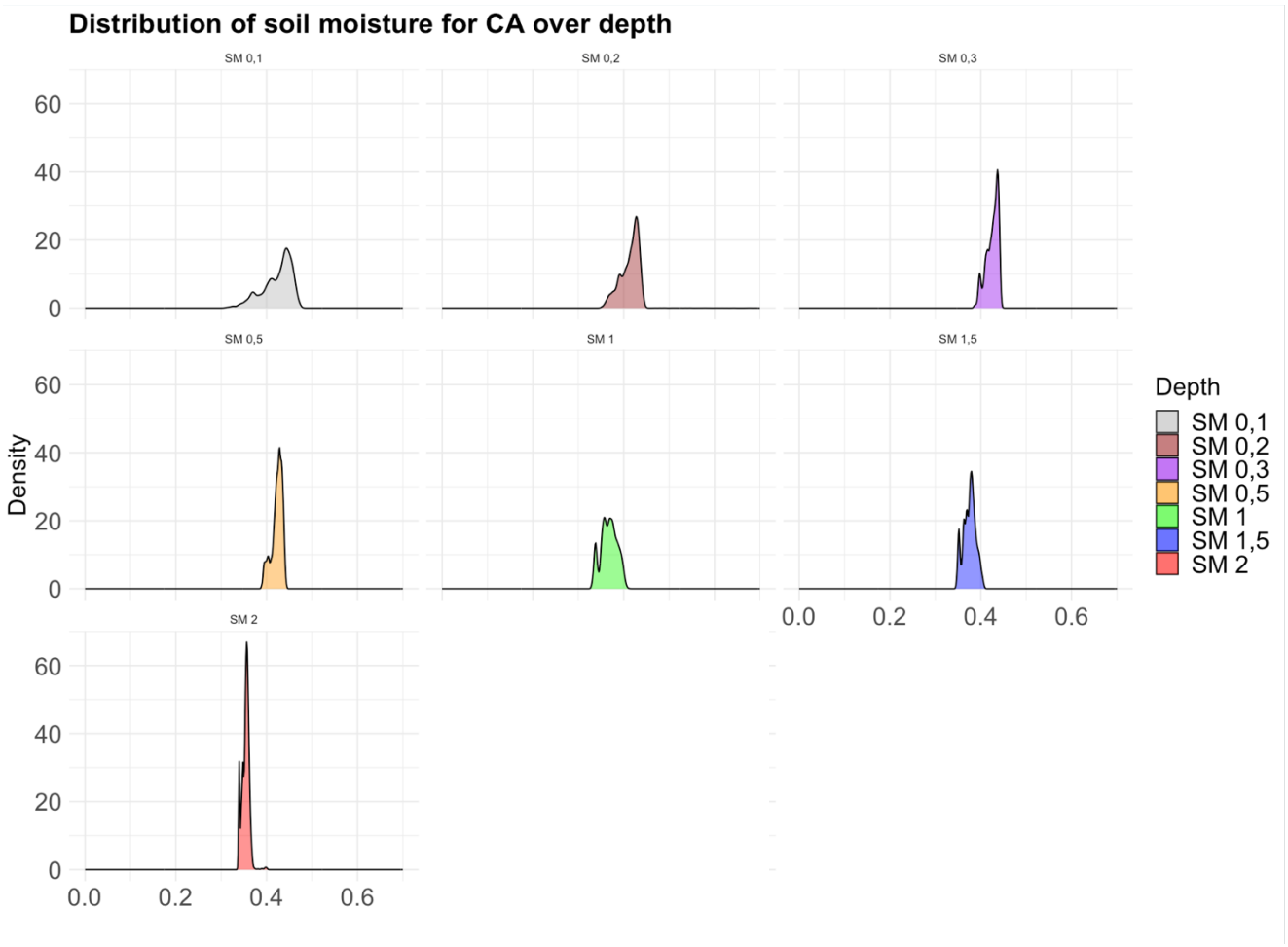
Distribution of soil moisture for CA over depth
SM 0,1
SM 0,2
SM 0,3
SM 0,5
SM 1
SM 1,5
SM 2
Density
Depth
SM 0,1
SM 0,2
SM 0,3
SM 0,5
SM 1
SM 1,5
SM 2

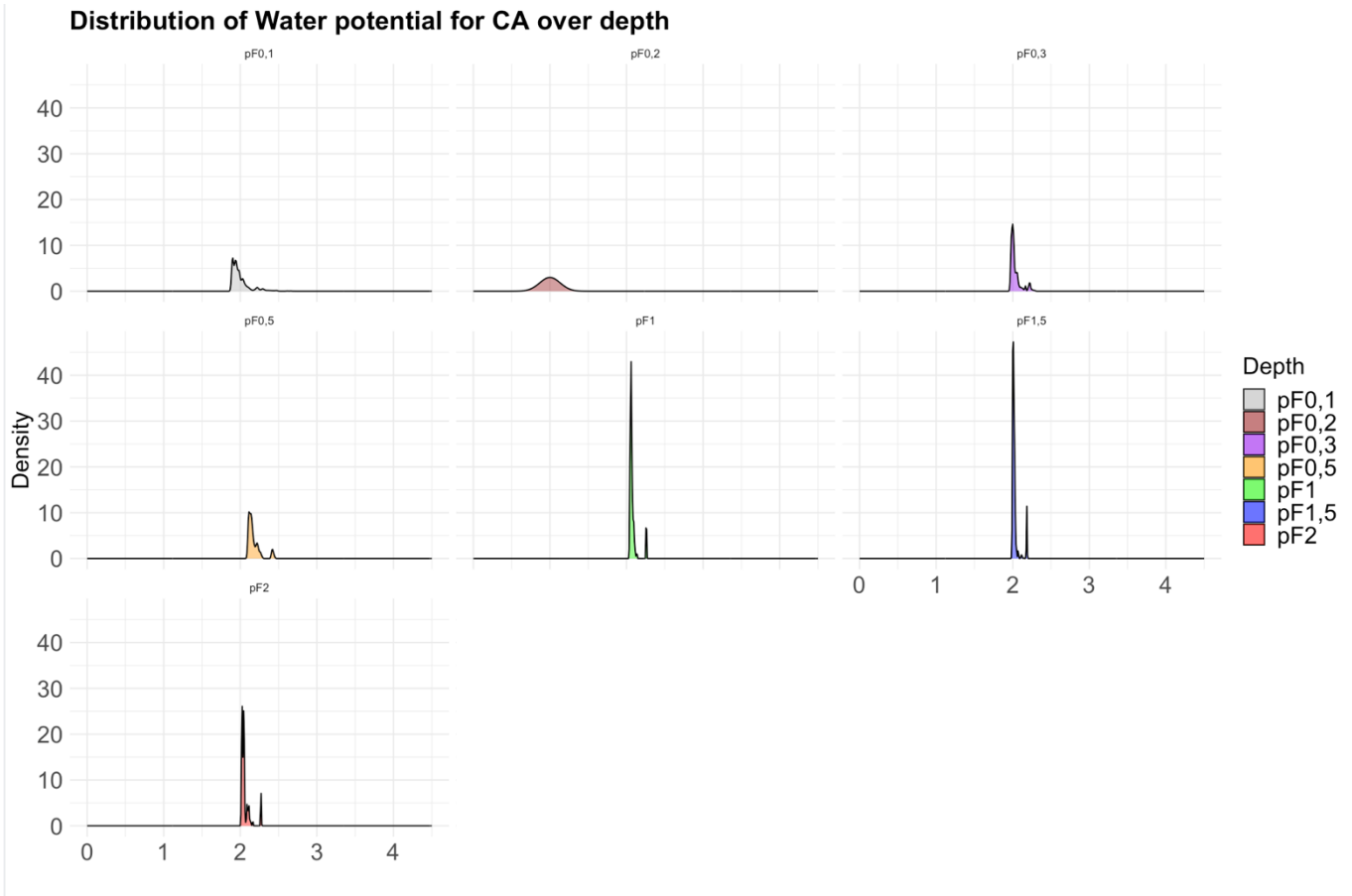
Distribution of Water potential for CA over depth
pF0,1
pF0,2
pF0,3
pF0,5
pF1
pF1,5
pF2
Density
Depth
pF0,1
pF0,2
pF0,3
pF0,5
pF1
pF1,5
pF2

Appendix 2: Soil moisture & Water potential data available for each area after filtering

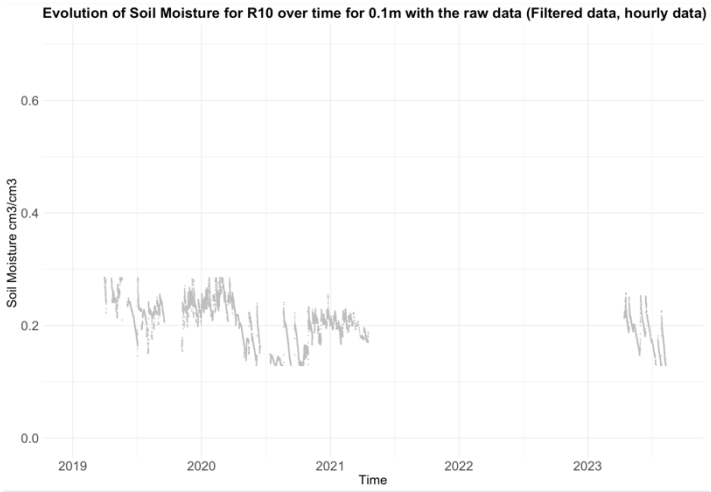

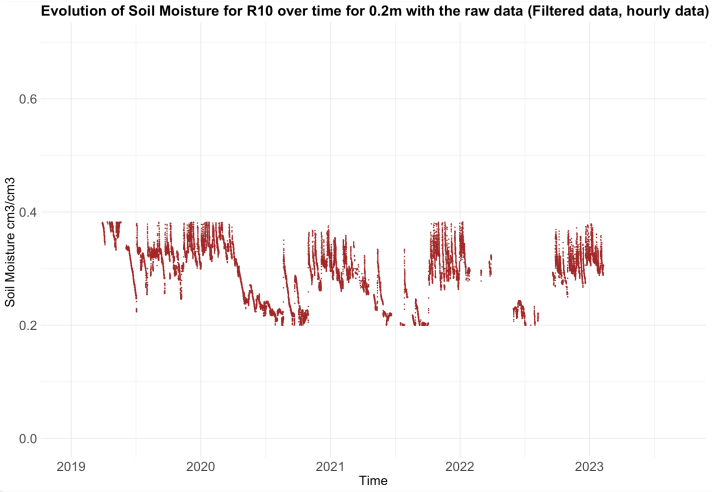

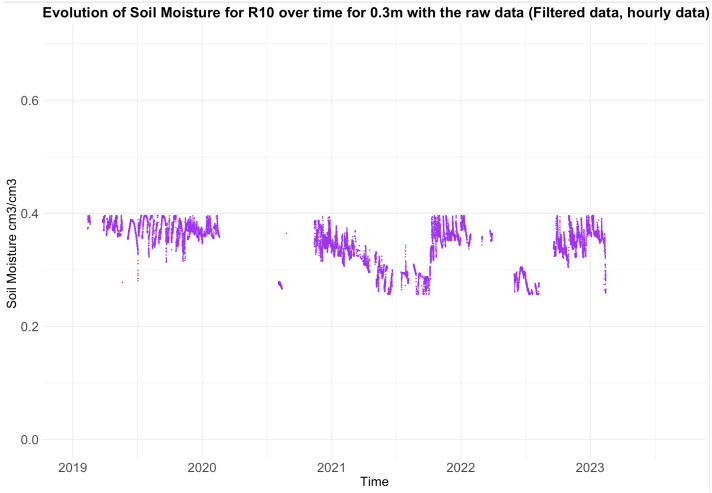

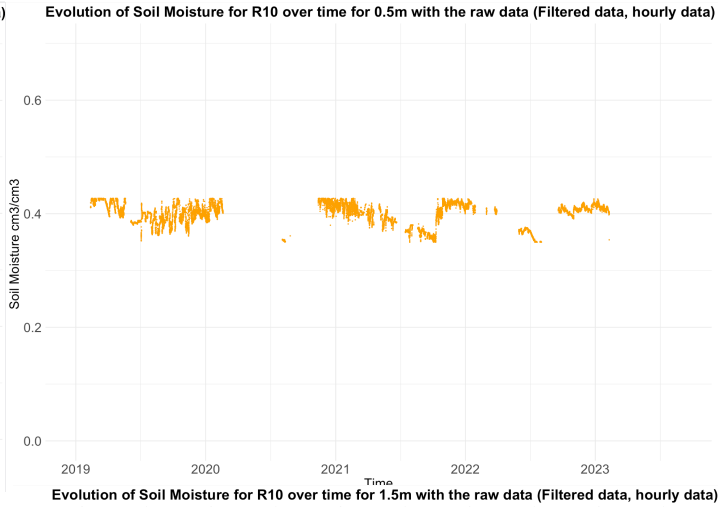

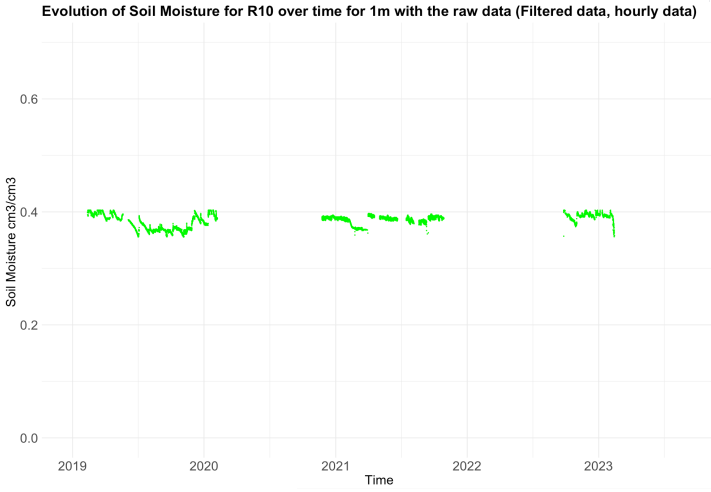

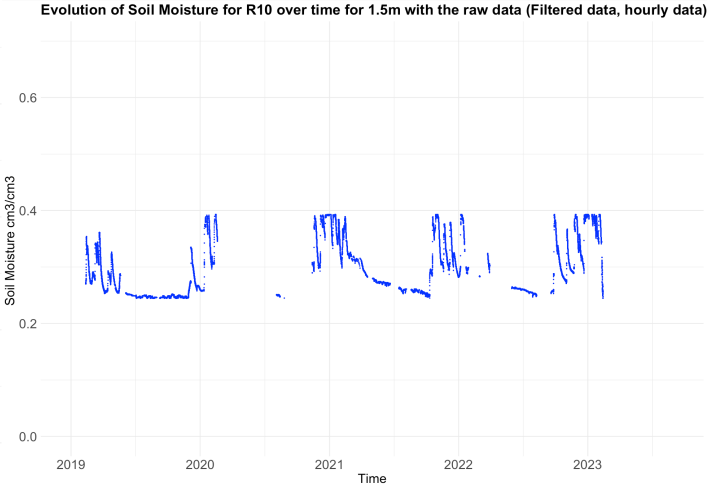

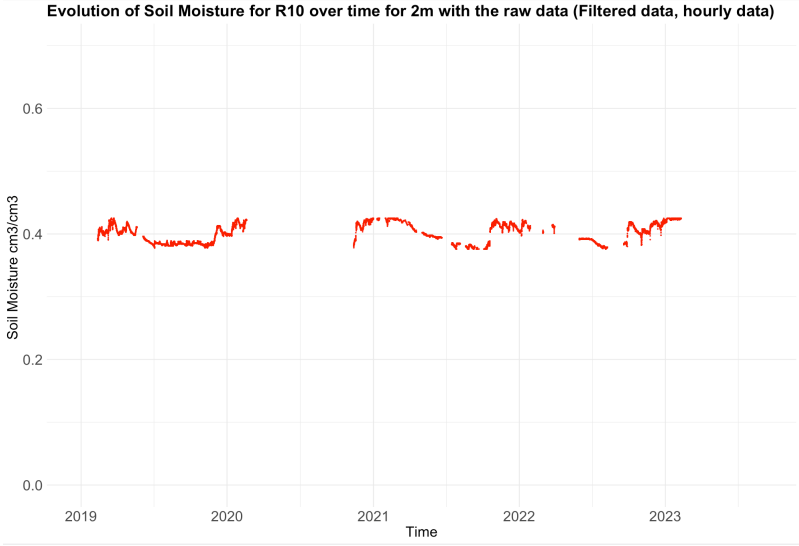

Evolution of Water potential over time for R10 at 0.1m with the raw data (Filtered data, hourly data)

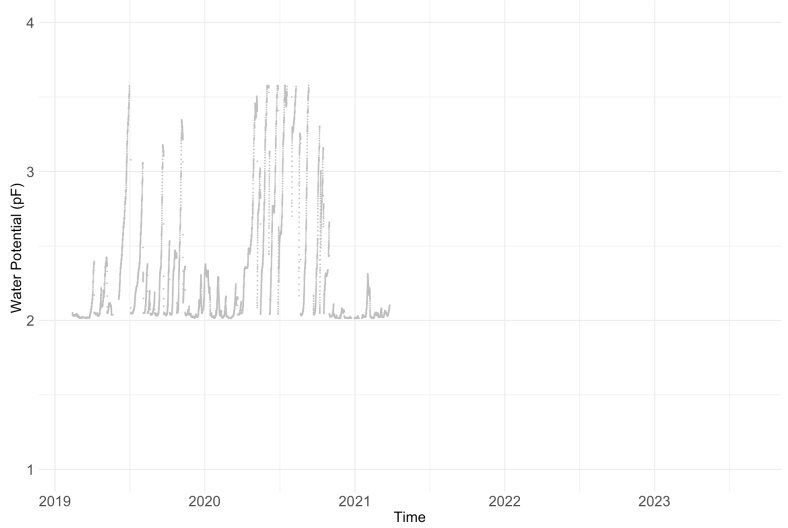

Evolution of Water potential over time for R10 at 0.2m with the raw data (Filtered data, hourly data)

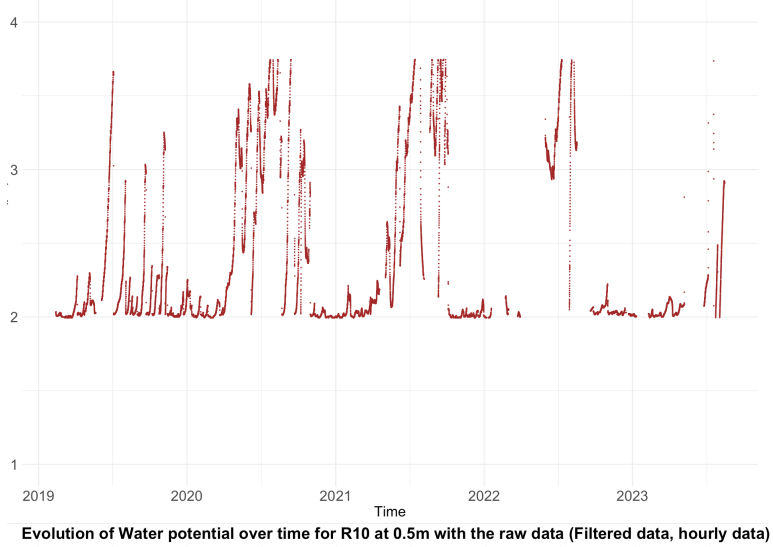

Evolution of Water potential over time for R10 at 0.3m with the raw data (Filtered data, hourly data)

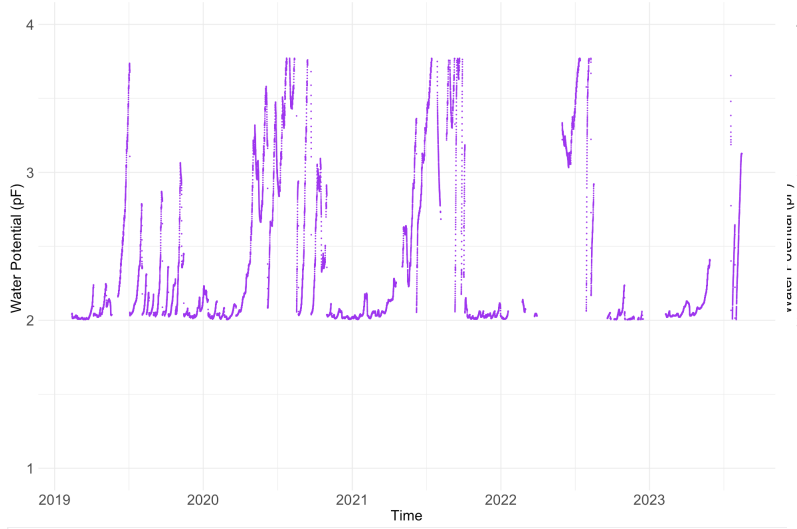

Evolution of Water potential over time for R10 at 0.5m with the raw data (Filtered data, hourly data)

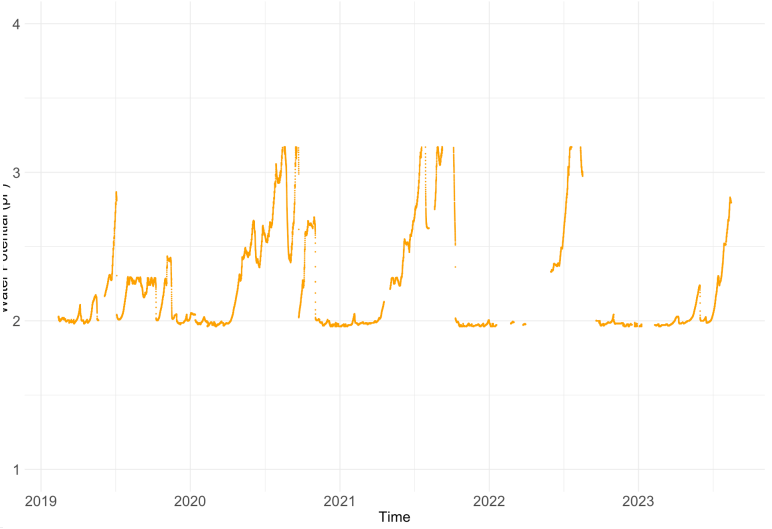

Evolution of Water potential over time for R10 at 1m with the raw data (Filtered data, hourly data)

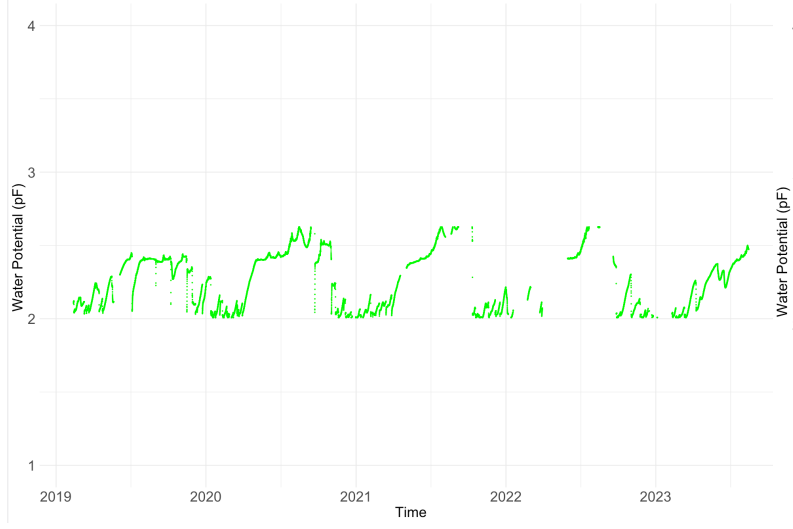

Evolution of Water potential over time for R10 at 1.5m with the raw data (Filtered data, hourly data)

Evolution of Water potential over time for R10 at 2m with the raw data (Filtered data, hourly data)

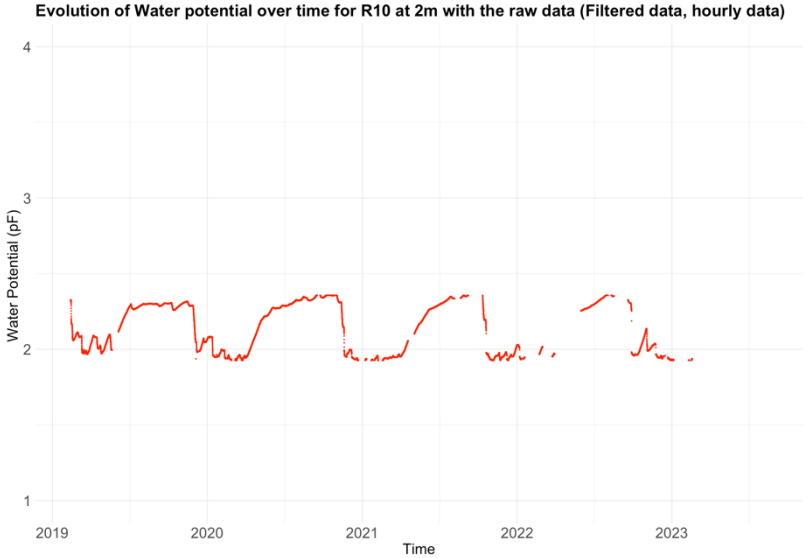

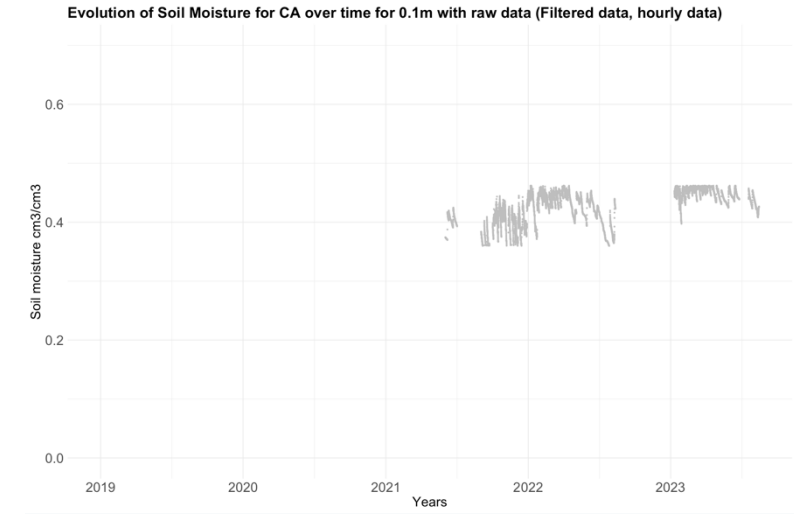
Evolution of Soil Moisture for CA over time for 0.1m with raw data (Filtered data, hourly data)
Soil moisture cm3/cm3
0.0
0.2
0.4
0.6
2019
2020
2021
2022
2023
Years

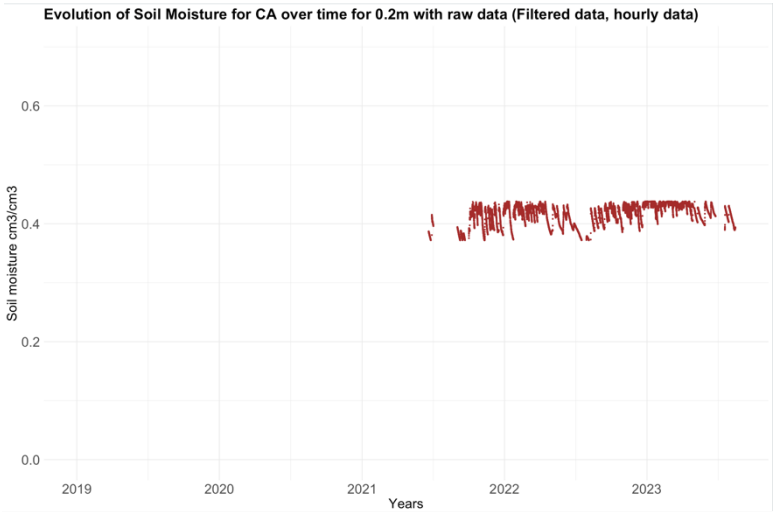
Evolution of Soil Moisture for CA over time for 0.2m with raw data (Filtered data, hourly data)
Soil moisture cm3/cm3
0.0
0.2
0.4
0.6
2019
2020
2021
2022
2023
Years

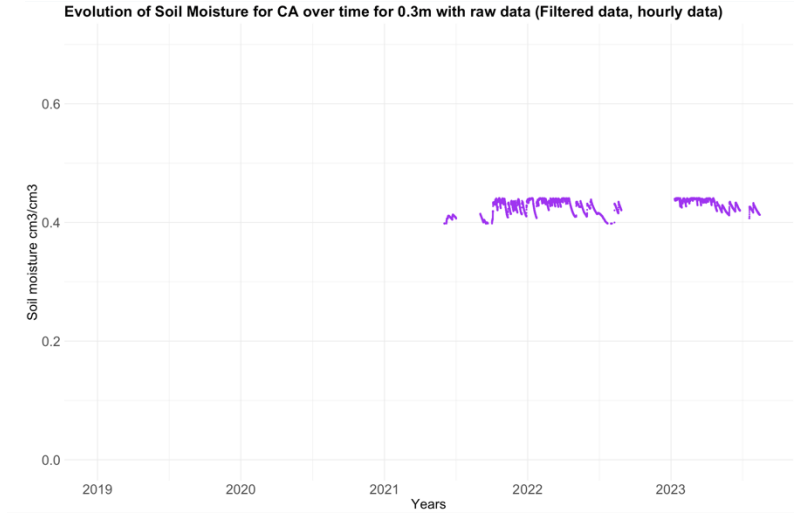
Evolution of Soil Moisture for CA over time for 0.3m with raw data (Filtered data, hourly data)
Soil moisture cm3/cm3
0.0
0.2
0.4
0.6
2019
2020
2021
2022
2023
Years

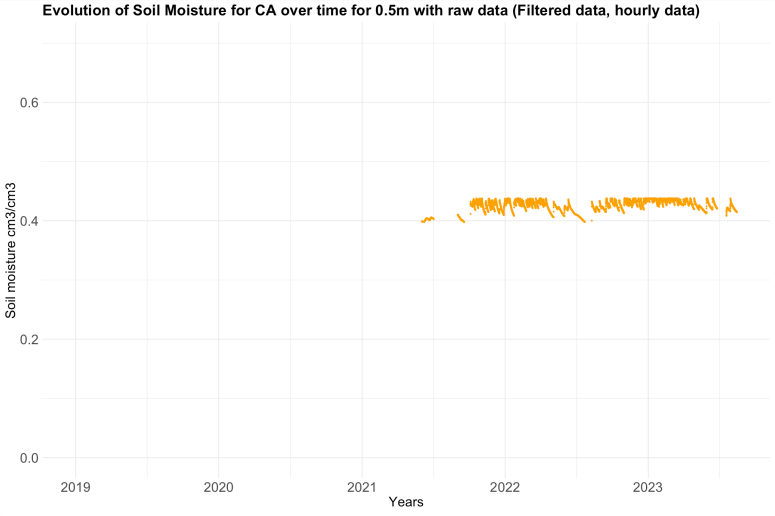
Evolution of Soil Moisture for CA over time for 0.5m with raw data (Filtered data, hourly data)
Soil moisture cm3/cm3
0.0
0.2
0.4
0.6
2019
2020
2021
2022
2023
Years

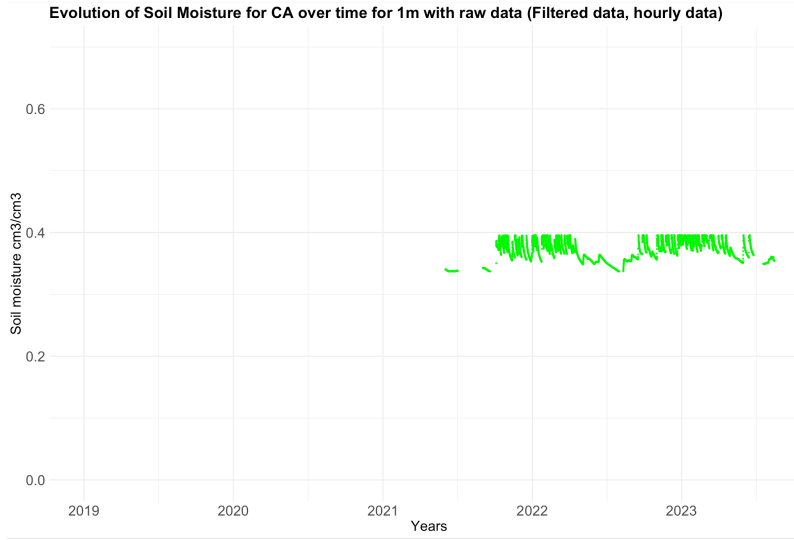
Evolution of Soil Moisture for CA over time for 1m with raw data (Filtered data, hourly data)
Soil moisture cm3/cm3
0.0
0.2
0.4
0.6
2019
2020
2021
2022
2023
Years

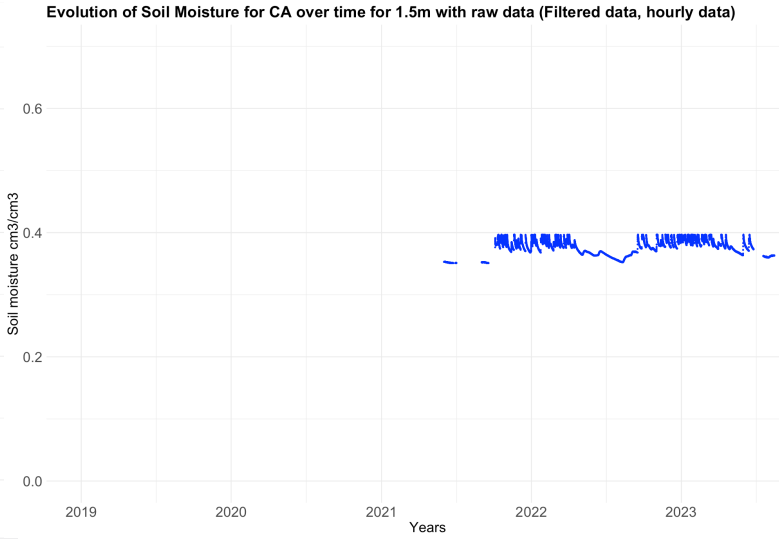
Evolution of Soil Moisture for CA over time for 1.5m with raw data (Filtered data, hourly data)
Soil moisture cm3/cm3
0.0
0.2
0.4
0.6
2019
2020
2021
2022
2023
Years

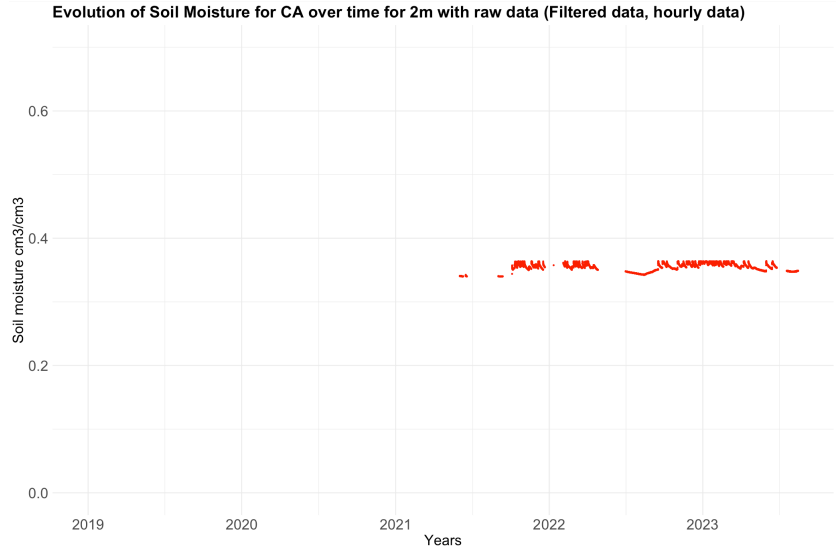
Evolution of Soil Moisture for CA over time for 2m with raw data (Filtered data, hourly data)
Soil moisture cm3/cm3
0.0
0.2
0.4
0.6
2019
2020
2021
2022
2023
Years

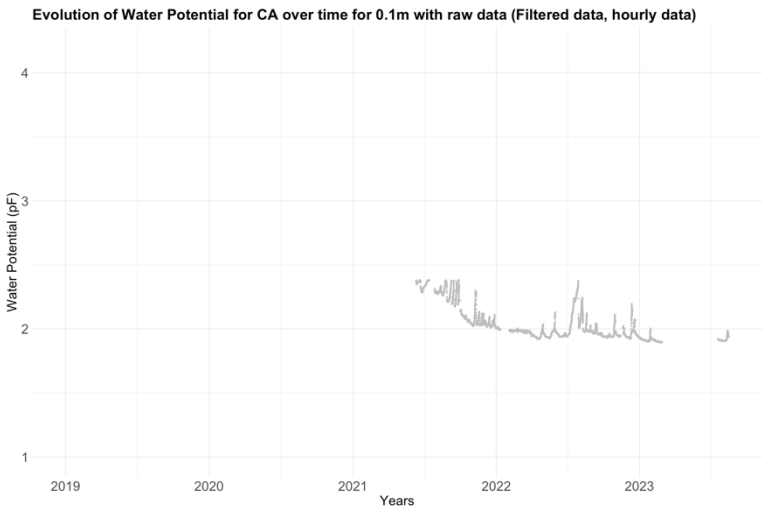
Evolution of Water Potential for CA over time for 0.1m with raw data (Filtered data, hourly data)
Water Potential (pF)
4
3
2
1
2019
2020
2021
2022
2023
Years

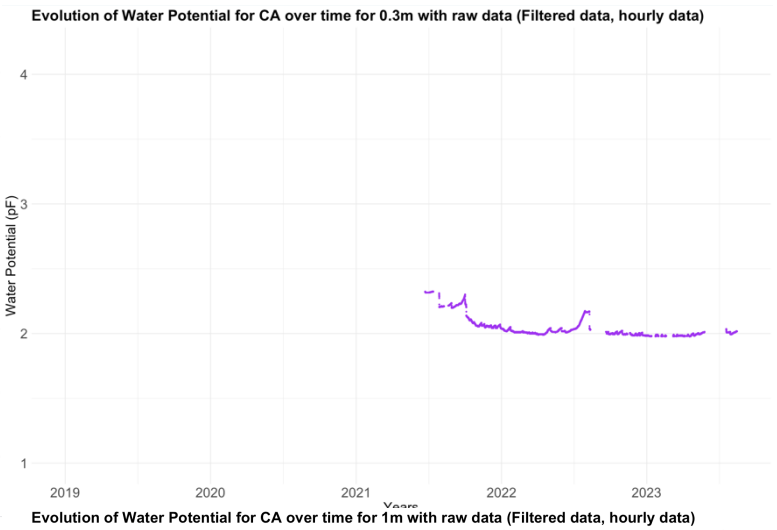
Evolution of Water Potential for CA over time for 0.3m with raw data (Filtered data, hourly data)
Water Potential (pF)
4
3
2
1
2019
2020
2021
2022
2023

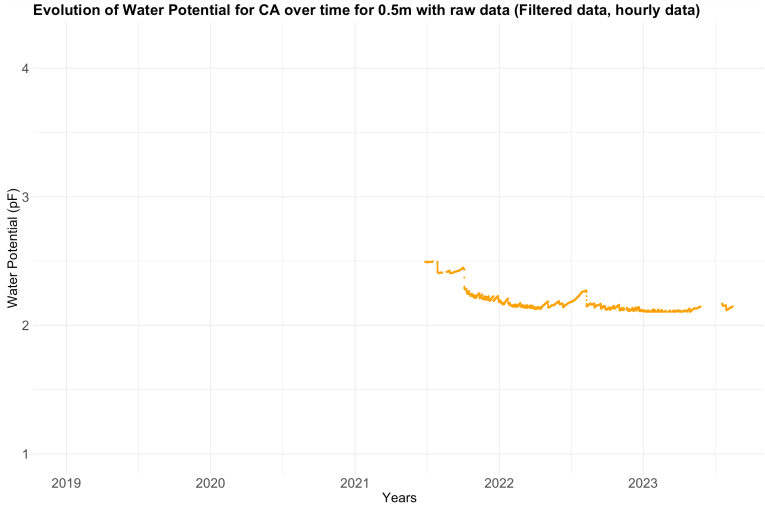
Evolution of Water Potential for CA over time for 0.5m with raw data (Filtered data, hourly data)
Water Potential (pF)
4
3
2
1
2019
2020
2021
2022
2023
Years

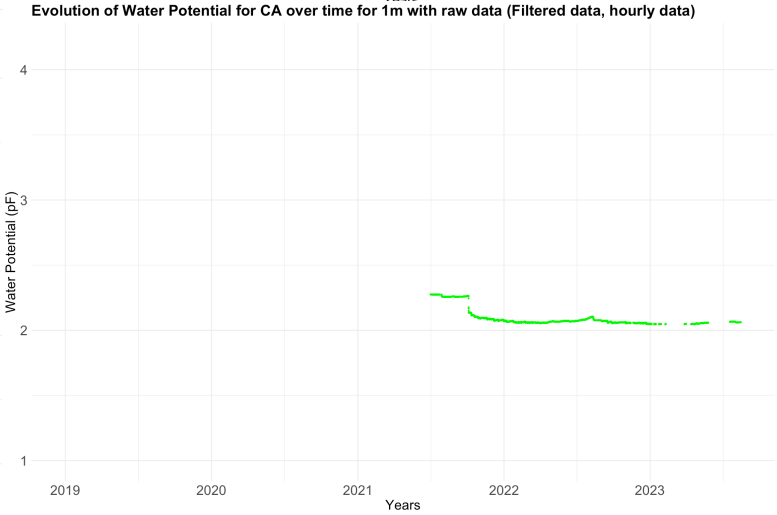
Evolution of Water Potential for CA over time for 1m with raw data (Filtered data, hourly data)
Water Potential (pF)
4
3
2
1
2019
2020
2021
2022
2023
Years

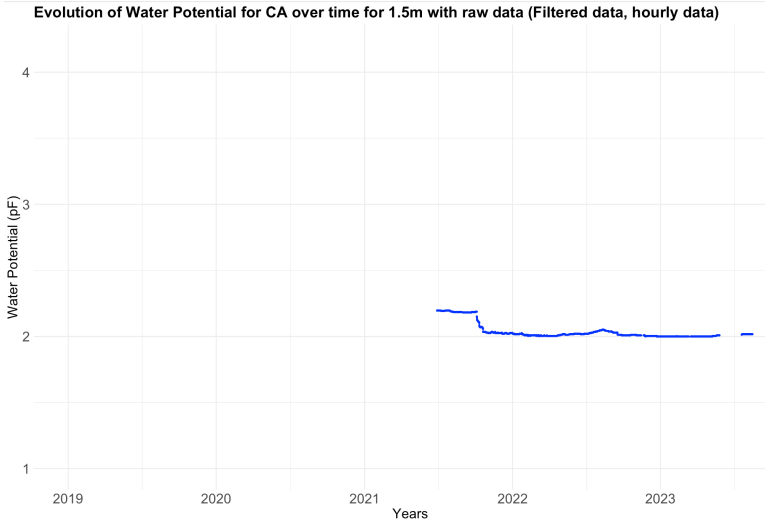
Evolution of Water Potential for CA over time for 1.5m with raw data (Filtered data, hourly data)
Water Potential (pF)
4
3
2
1
2019
2020
2021
2022
2023
Years

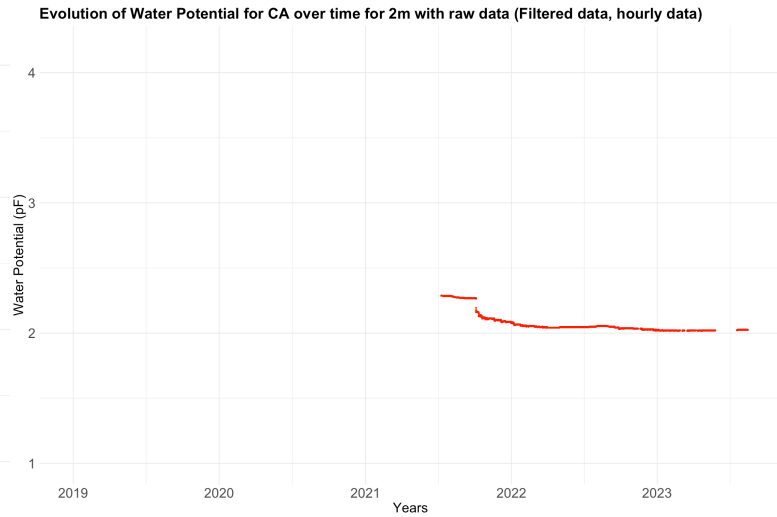
Evolution of Water Potential for CA over time for 2m with raw data (Filtered data, hourly data)
Water Potential (pF)
4
3
2
1
2019
2020
2021
2022
2023
Years

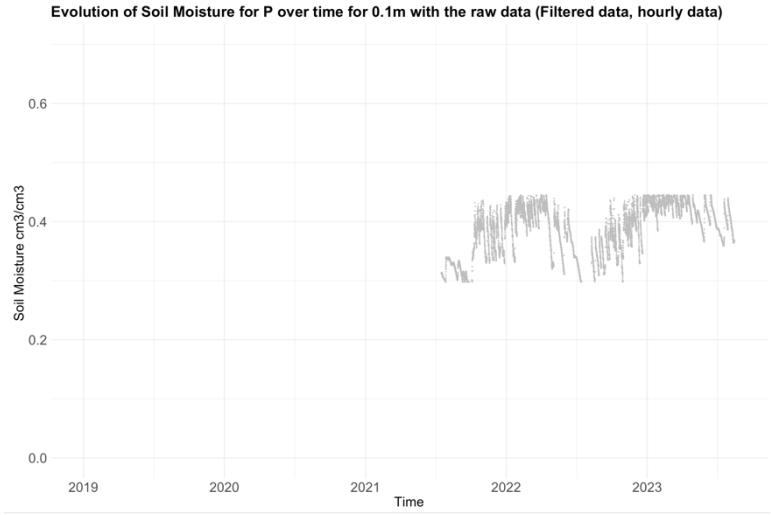
Evolution of Soil Moisture for P over time for 0.1m with the raw data (Filtered data, hourly data)
Soil Moisture cm3/cm3
0.0
0.2
0.4
0.6
2019
2020
2021
2022
2023
Time

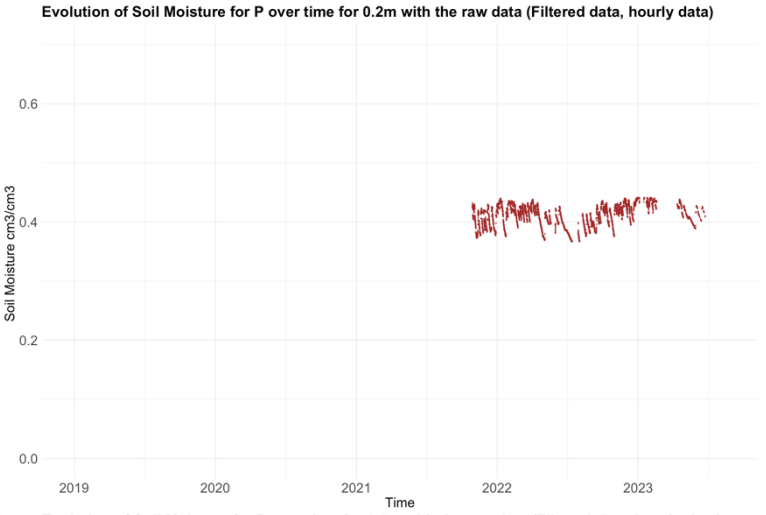
Evolution of Soil Moisture for P over time for 0.2m with the raw data (Filtered data, hourly data)
Soil Moisture cm3/cm3
0.0
0.2
0.4
0.6
2019
2020
2021
2022
2023
Time

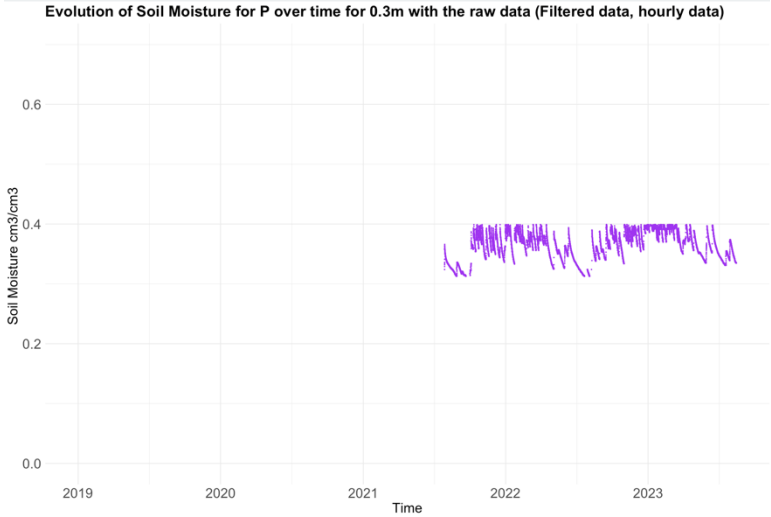
Evolution of Soil Moisture for P over time for 0.3m with the raw data (Filtered data, hourly data)
Soil Moisture cm3/cm3
0.0
0.2
0.4
0.6
2019
2020
2021
2022
2023
Time

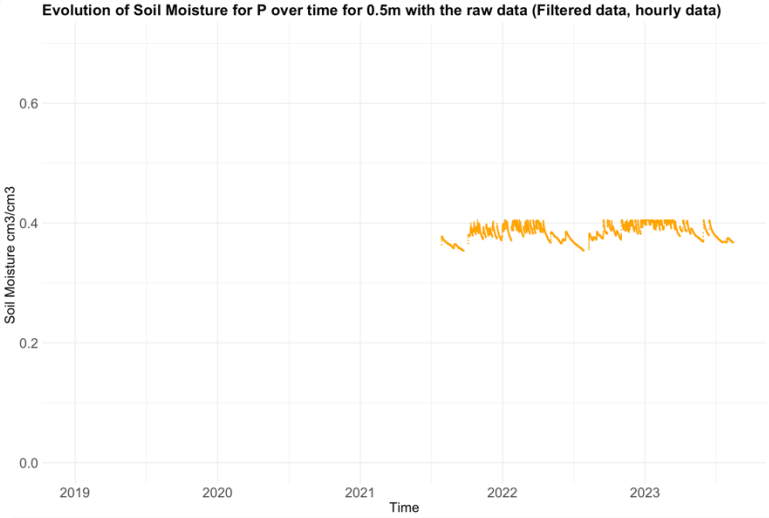
Evolution of Soil Moisture for P over time for 0.5m with the raw data (Filtered data, hourly data)
Soil Moisture cm3/cm3
0.0
0.2
0.4
0.6
2019
2020
2021
2022
2023
Time

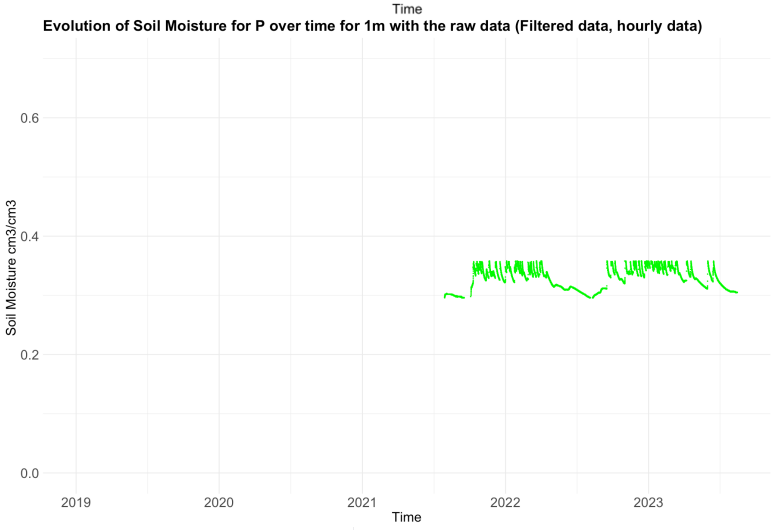
Evolution of Soil Moisture for P over time for 1m with the raw data (Filtered data, hourly data)
Soil Moisture cm3/cm3
0.0
0.2
0.4
0.6
2019
2020
2021
2022
2023
Time

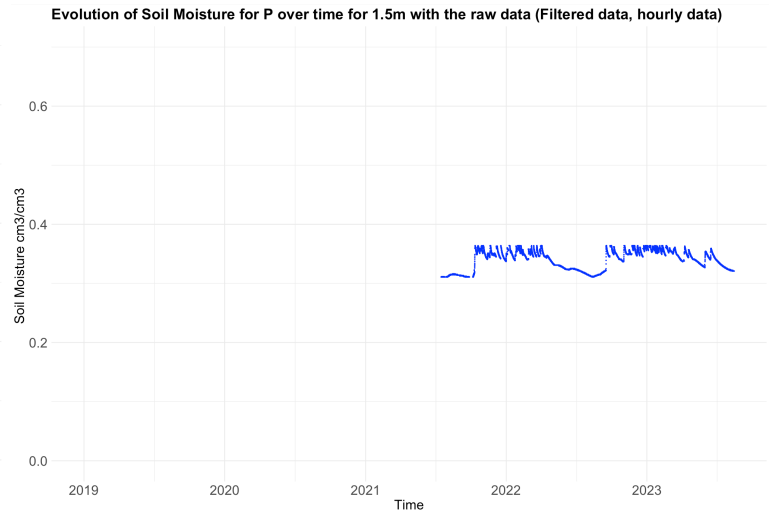
Evolution of Soil Moisture for P over time for 1.5m with the raw data (Filtered data, hourly data)
Soil Moisture cm3/cm3
0.0
0.2
0.4
0.6
2019
2020
2021
2022
2023
Time

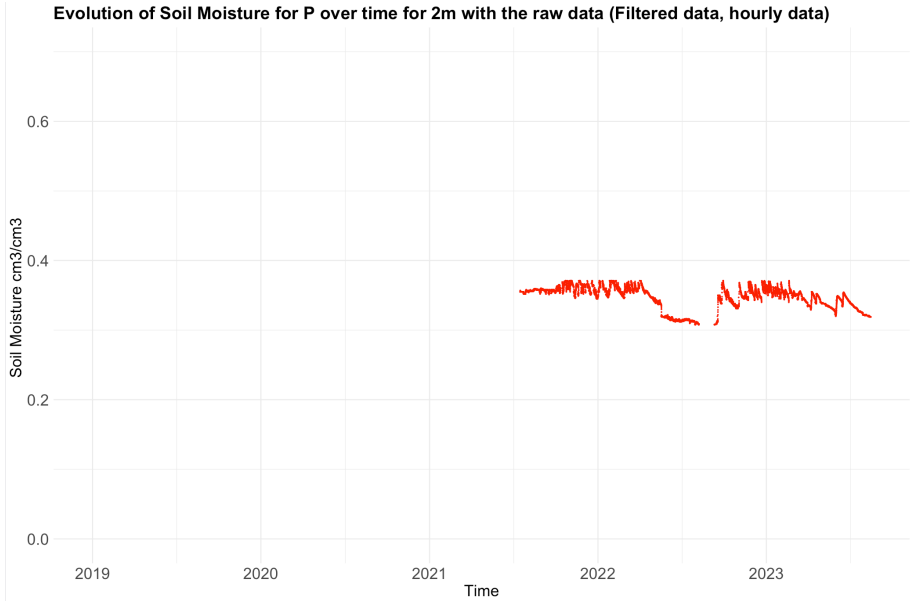
Evolution of Soil Moisture for P over time for 2m with the raw data (Filtered data, hourly data)
Soil Moisture cm3/cm3
0.0
0.2
0.4
0.6
2019
2020
2021
2022
2023
Time

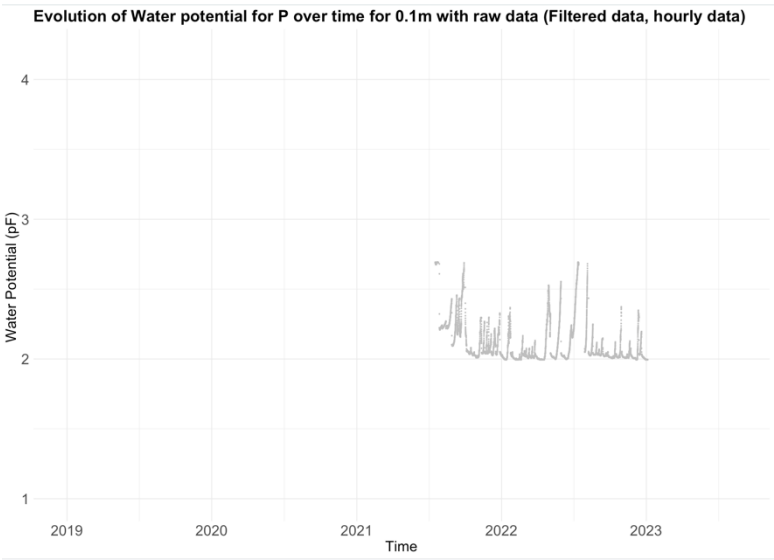
Evolution of Water potential for P over time for 0.1m with raw data (Filtered data, hourly data)
Water Potential (pF)
4
3
2
1
2019
2020
2021
2022
2023
Time

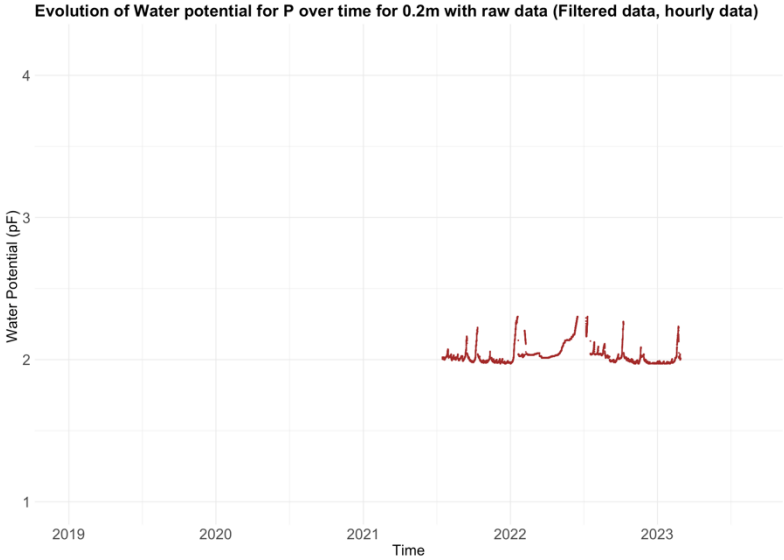
Evolution of Water potential for P over time for 0.2m with raw data (Filtered data, hourly data)
Water Potential (pF)
4
3
2
1
2019
2020
2021
2022
2023
Time

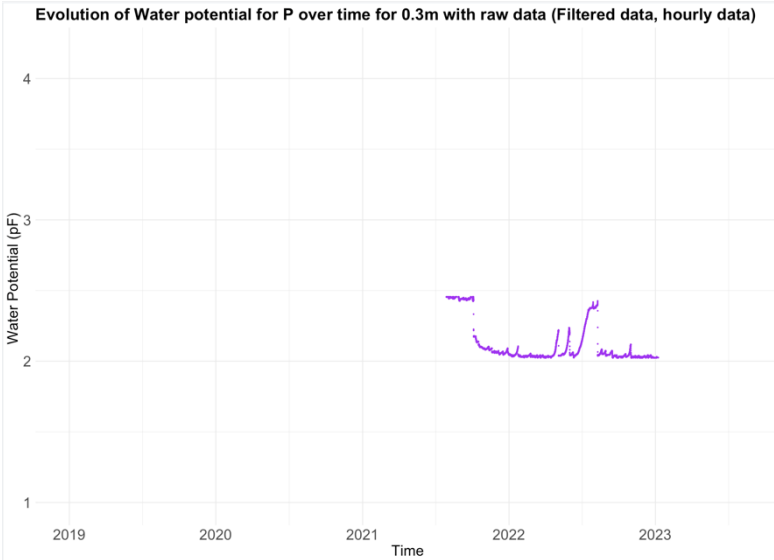
Evolution of Water potential for P over time for 0.3m with raw data (Filtered data, hourly data)
Water Potential (pF)
4
3
2
1
2019
2020
2021
2022
2023
Time

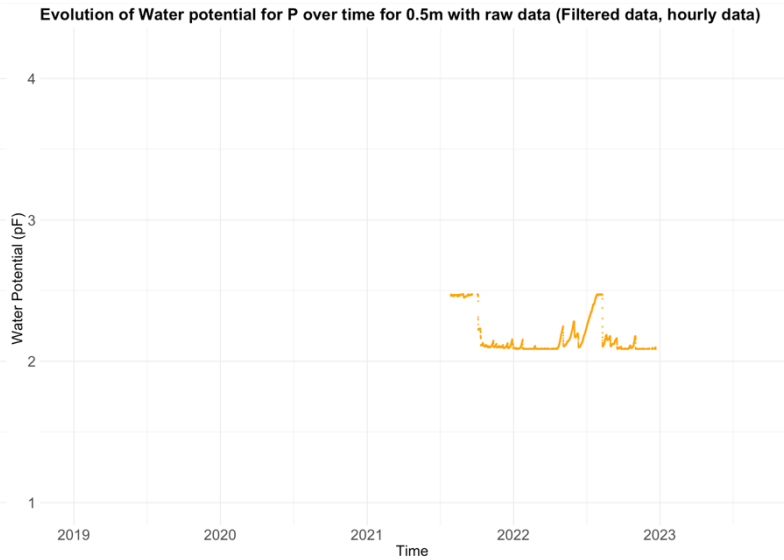
Evolution of Water potential for P over time for 0.5m with raw data (Filtered data, hourly data)
Water Potential (pF)
4
3
2
1
2019
2020
2021
2022
2023
Time

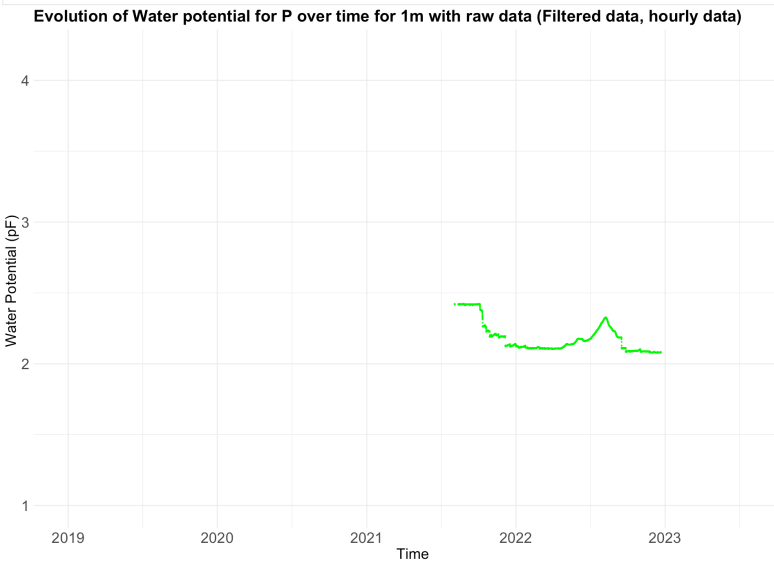
Evolution of Water potential for P over time for 1m with raw data (Filtered data, hourly data)
Water Potential (pF)
4
3
2
1
2019
2020
2021
2022
2023
Time

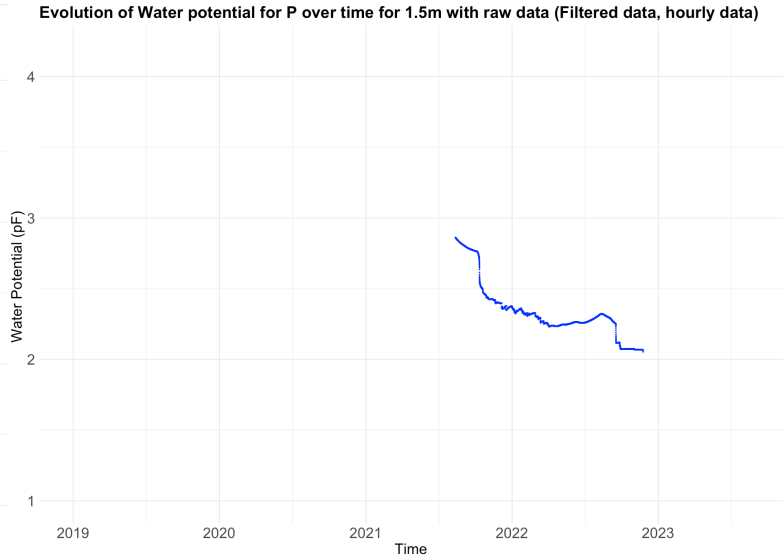
Evolution of Water potential for P over time for 1.5m with raw data (Filtered data, hourly data)
Water Potential (pF)
4
3
2
1
2019
2020
2021
2022
2023
Time

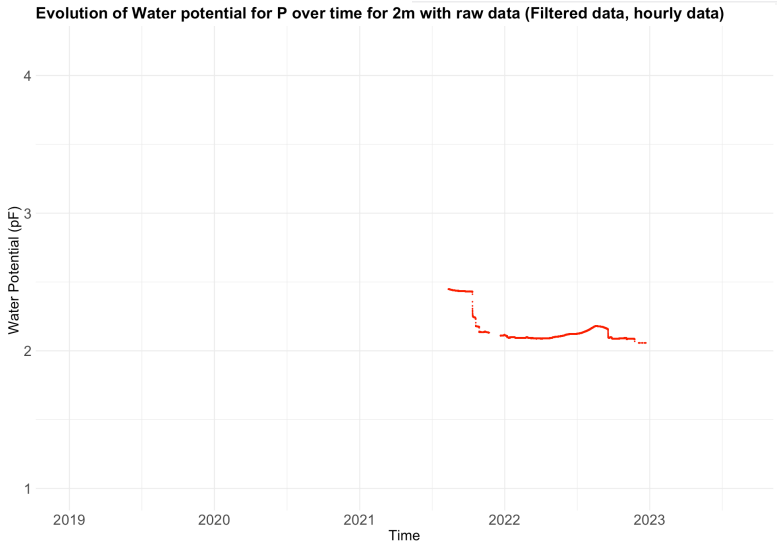
Evolution of Water potential for P over time for 2m with raw data (Filtered data, hourly data)
Water Potential (pF)
4
3
2
1
2019
2020
2021
2022
2023
Time

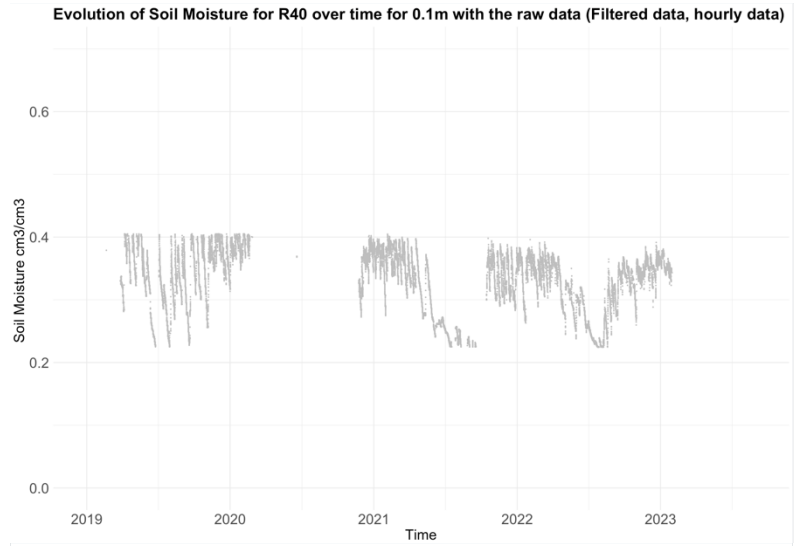
Evolution of Soil Moisture for R40 over time for 0.1m with the raw data (Filtered data, hourly data)
Soil Moisture cm3/cm3
0.0
0.2
0.4
0.6
2019
2020
2021
2022
2023
Time

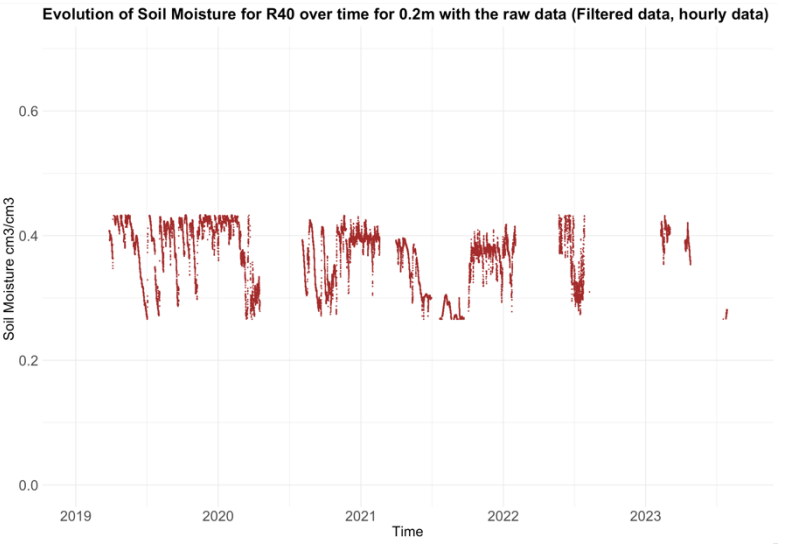
Evolution of Soil Moisture for R40 over time for 0.2m with the raw data (Filtered data, hourly data)
Soil Moisture cm3/cm3
0.0
0.2
0.4
0.6
2019
2020
2021
2022
2023
Time

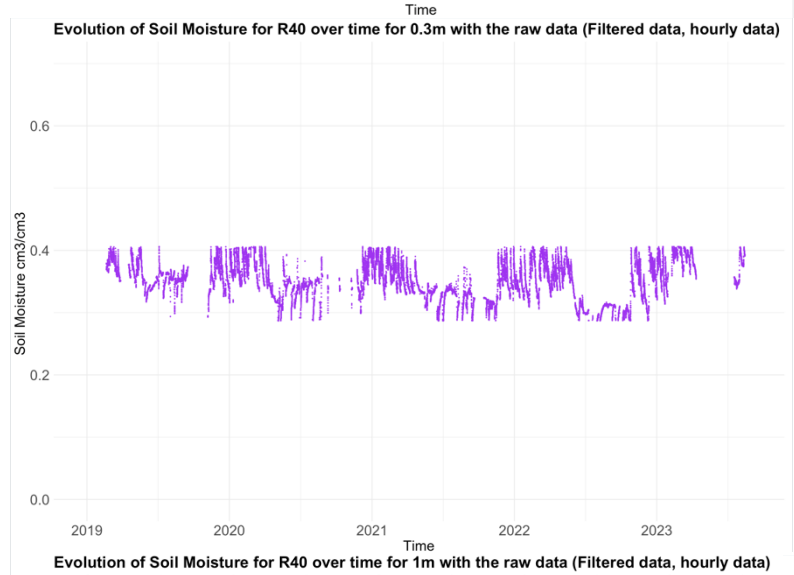
Evolution of Soil Moisture for R40 over time for 0.3m with the raw data (Filtered data, hourly data)
Soil Moisture cm3/cm3
0.0
0.2
0.4
0.6
2019
2020
2021
2022
2023
Time

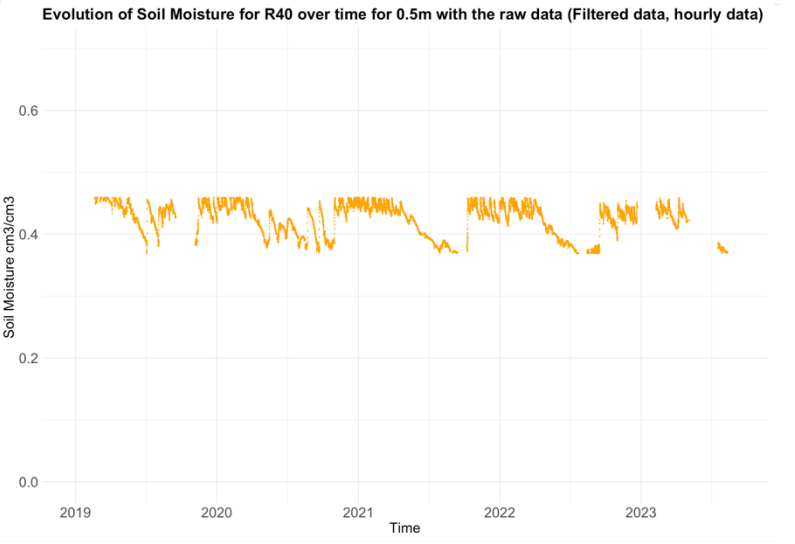
Evolution of Soil Moisture for R40 over time for 0.5m with the raw data (Filtered data, hourly data)
Soil Moisture cm3/cm3
0.0
0.2
0.4
0.6
2019
2020
2021
2022
2023
Time

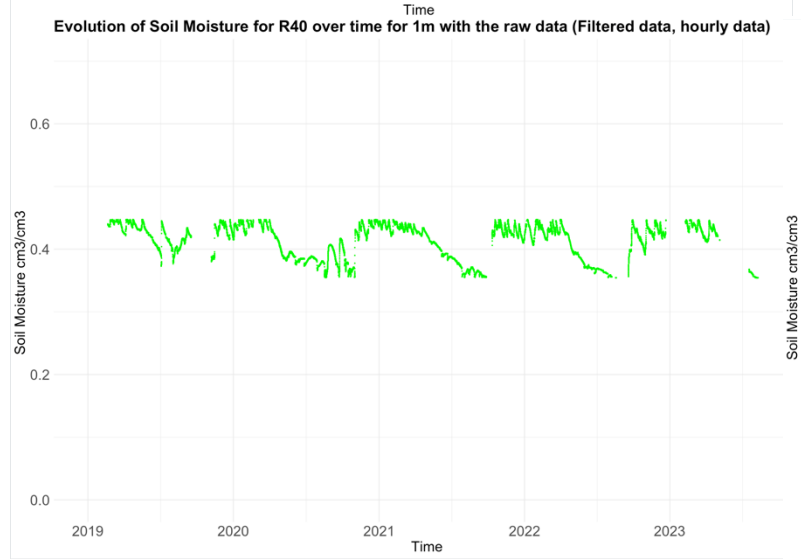
Evolution of Soil Moisture for R40 over time for 1m with the raw data (Filtered data, hourly data)
Soil Moisture cm3/cm3
0.0
0.2
0.4
0.6
2019
2020
2021
2022
2023
Time

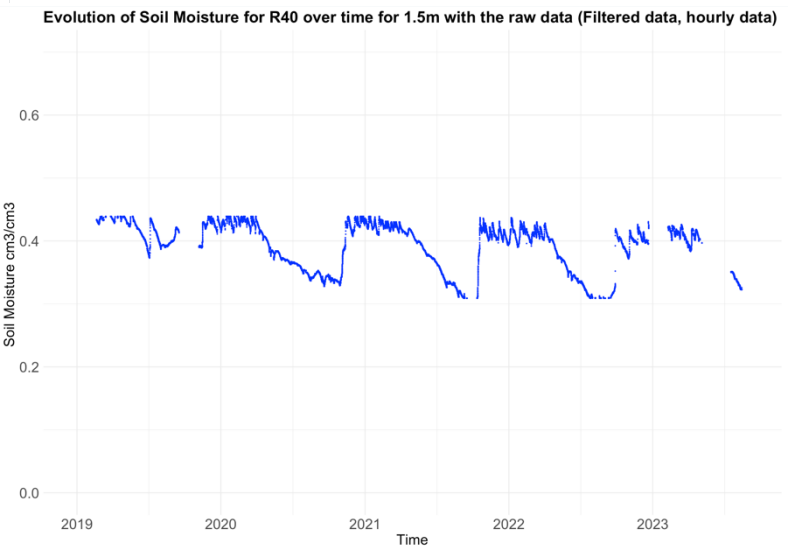
Evolution of Soil Moisture for R40 over time for 1.5m with the raw data (Filtered data, hourly data)
Soil Moisture cm3/cm3
0.0
0.2
0.4
0.6
2019
2020
2021
2022
2023
Time

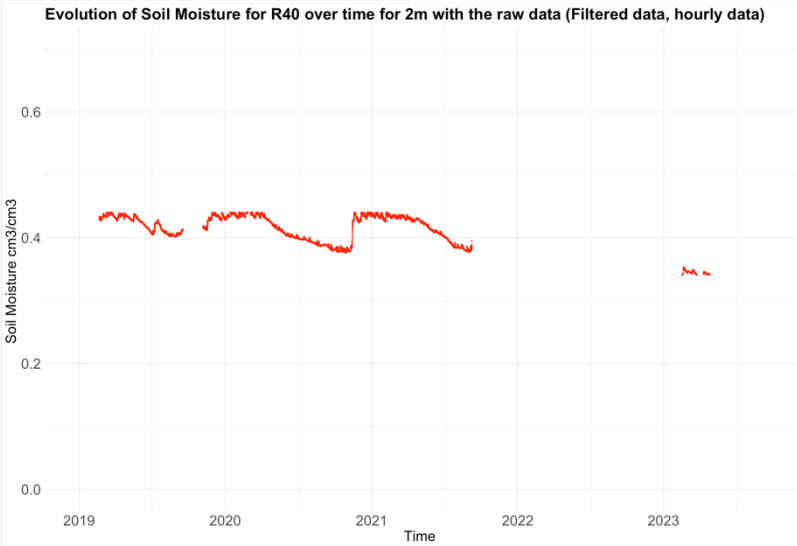
Evolution of Soil Moisture for R40 over time for 2m with the raw data (Filtered data, hourly data)
Soil Moisture cm3/cm3
0.0
0.2
0.4
0.6
2019
2020
2021
2022
2023
Time

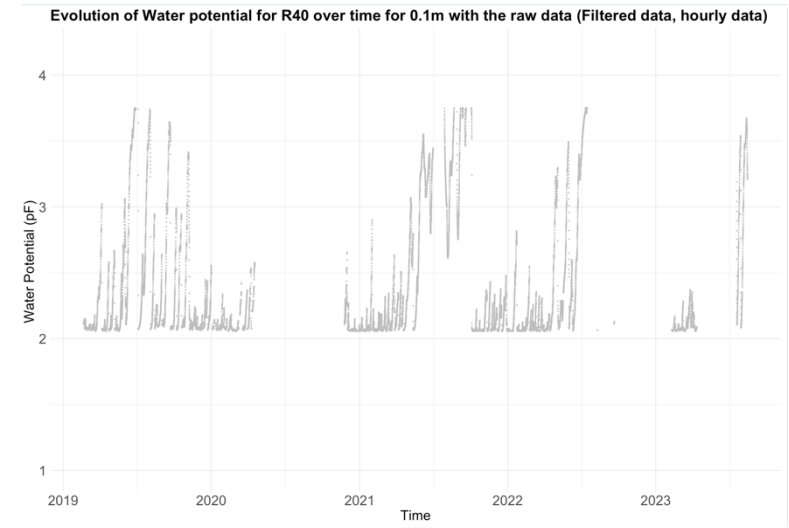
Evolution of Water potential for R40 over time for 0.1m with the raw data (Filtered data, hourly data)
Water Potential (pF)
Time
4
3
2
1
2019
2020
2021
2022
2023

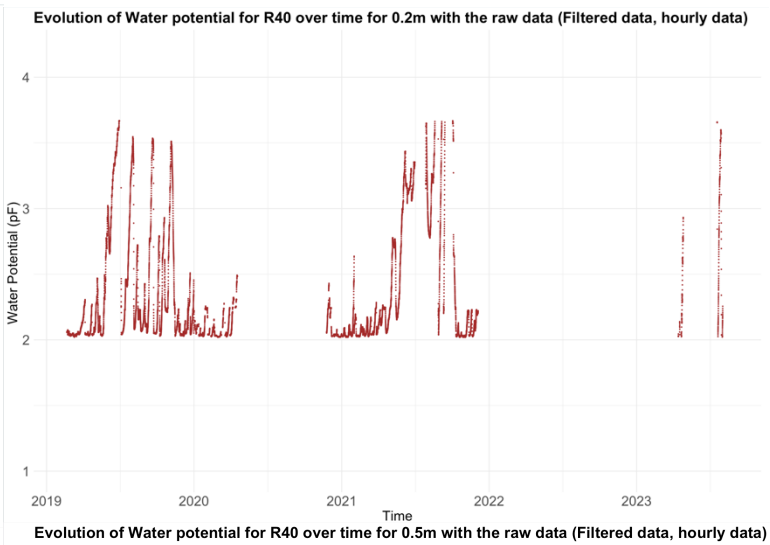
Evolution of Water potential for R40 over time for 0.2m with the raw data (Filtered data, hourly data)
Water Potential (pF)
Time
4
3
2
1
2019
2020
2021
2022
2023

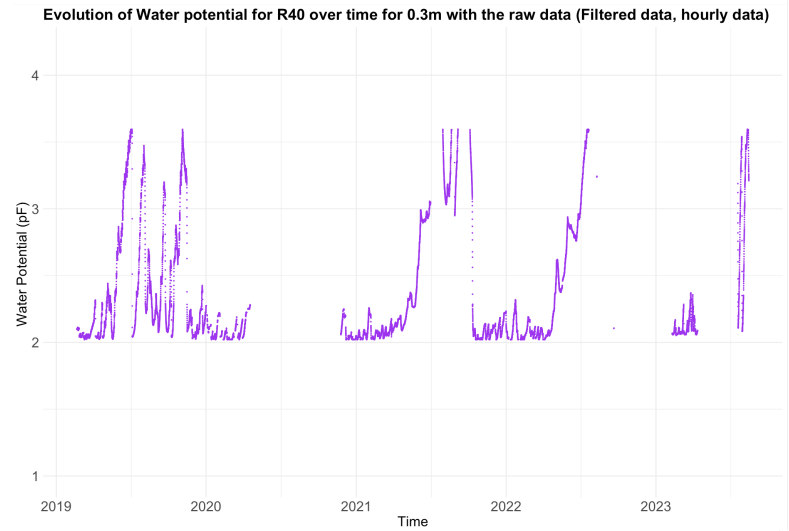
Evolution of Water potential for R40 over time for 0.3m with the raw data (Filtered data, hourly data)
Water Potential (pF)
Time
4
3
2
1
2019
2020
2021
2022
2023

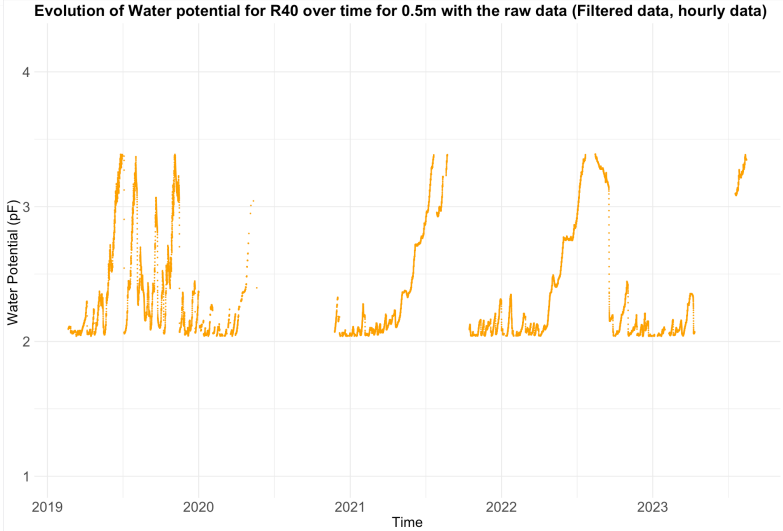
Evolution of Water potential for R40 over time for 0.5m with the raw data (Filtered data, hourly data)
Water Potential (pF)
Time
4
3
2
1
2019
2020
2021
2022
2023

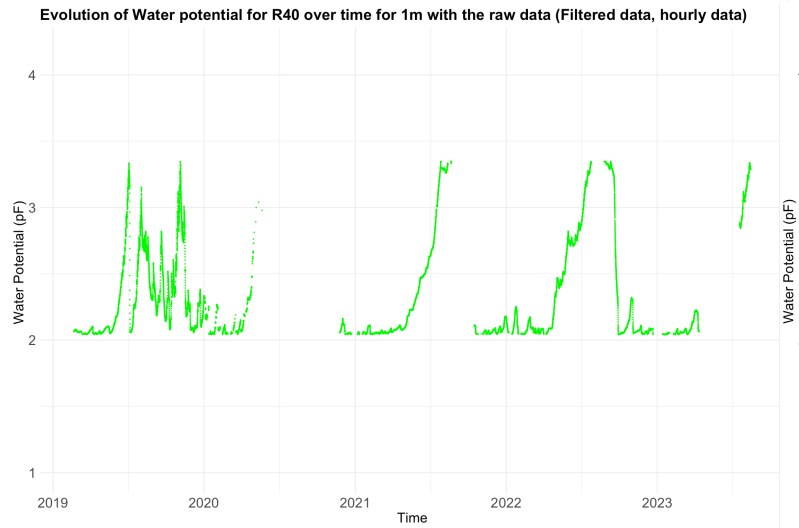
Evolution of Water potential for R40 over time for 1m with the raw data (Filtered data, hourly data)
Water Potential (pF)
Time
4
3
2
1
2019
2020
2021
2022
2023

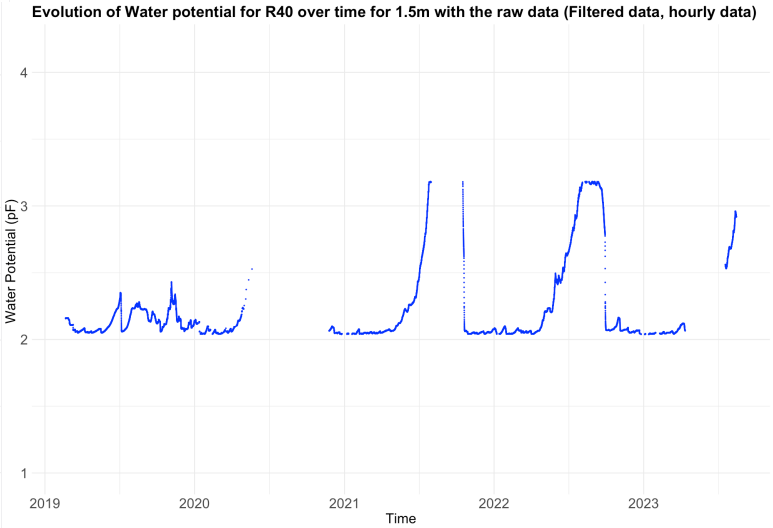
Evolution of Water potential for R40 over time for 1.5m with the raw data (Filtered data, hourly data)
Water Potential (pF)
Time
4
3
2
1
2019
2020
2021
2022
2023

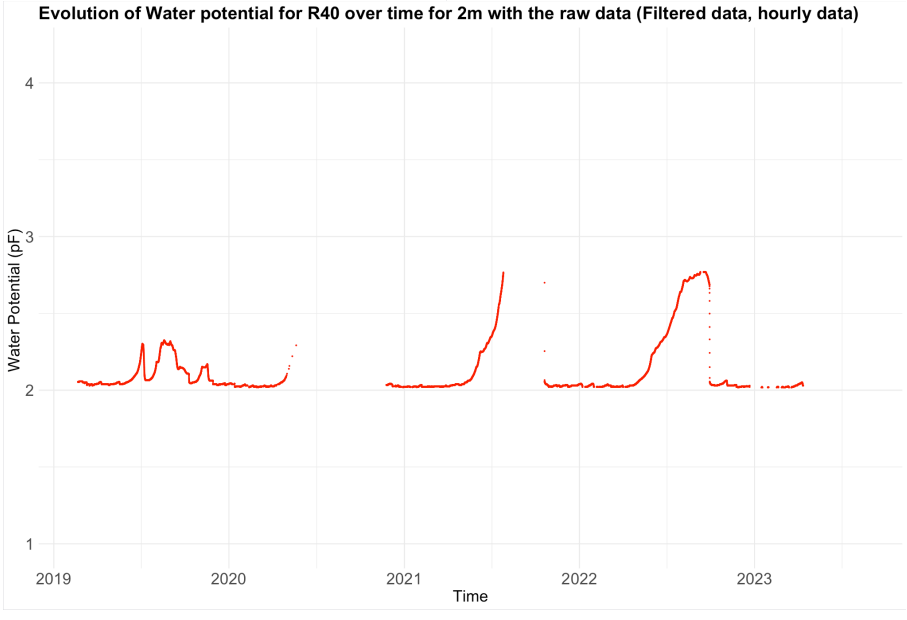
Evolution of Water potential for R40 over time for 2m with the raw data (Filtered data, hourly data)
Water Potential (pF)
Time
4
3
2
1
2019
2020
2021
2022
2023

Appendix 3: Retentions curves for each area and for each depth based on field data.

Retention curves for CA

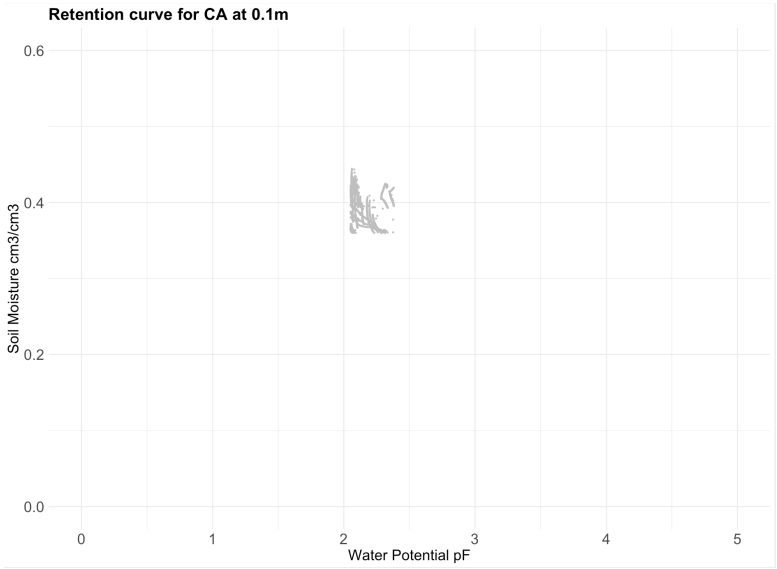

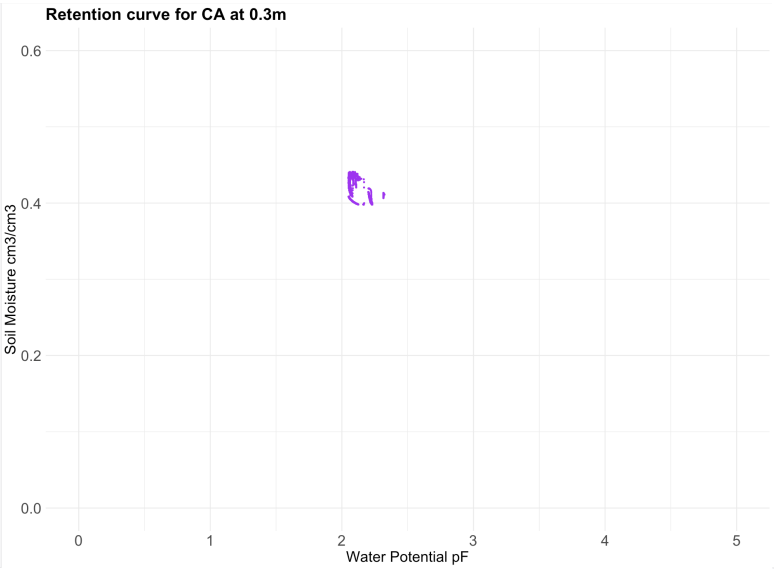

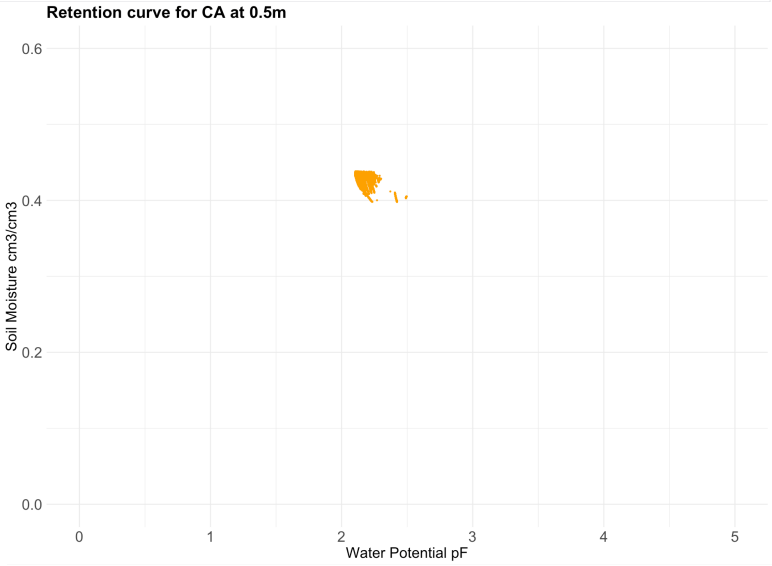

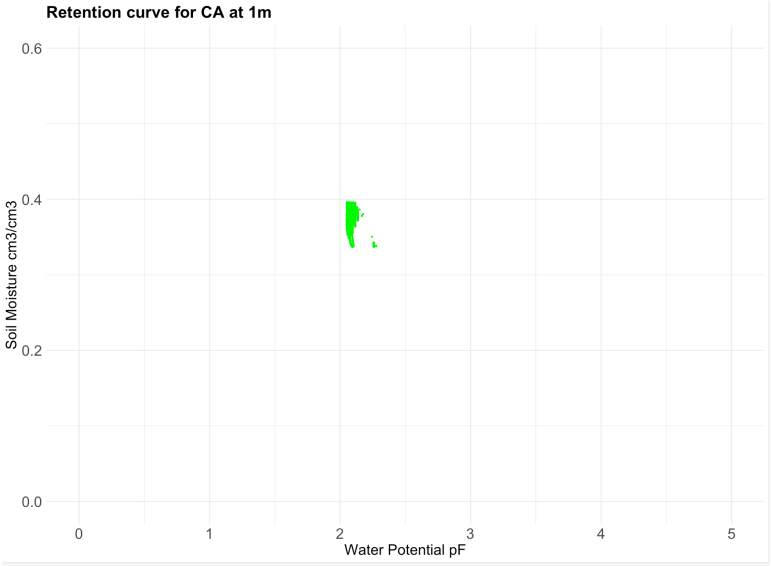

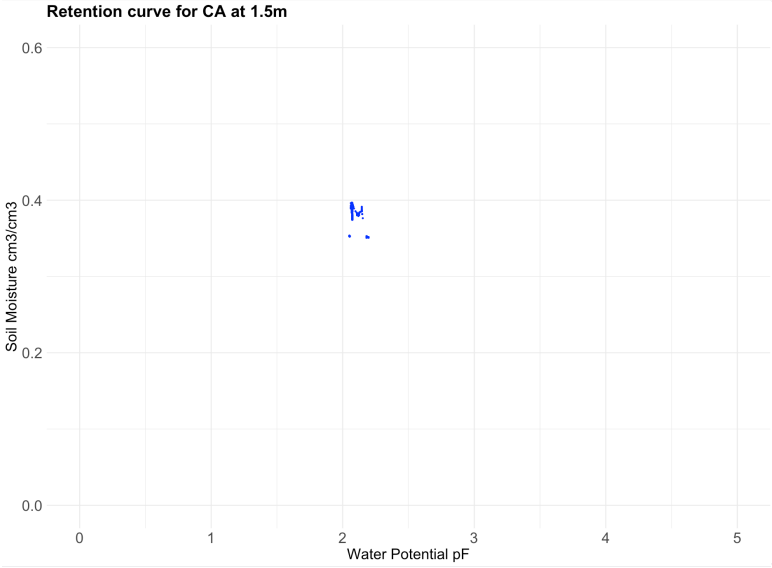

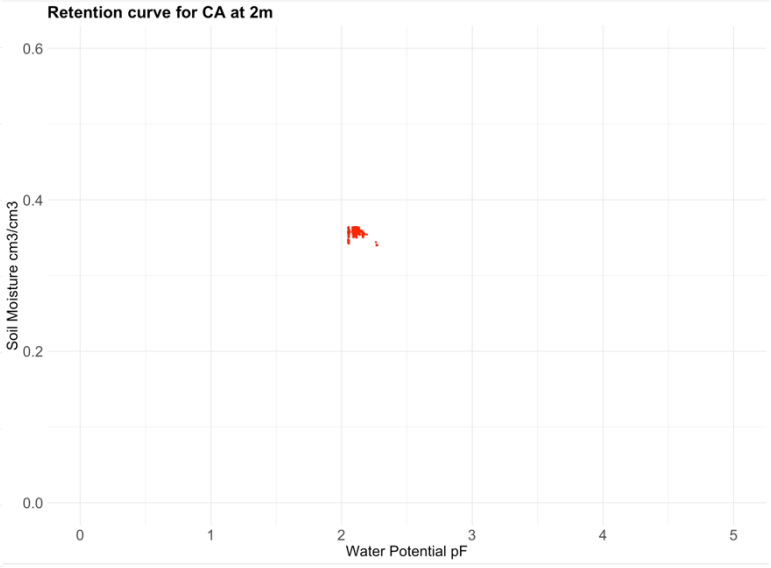

Retention curves for Pasture

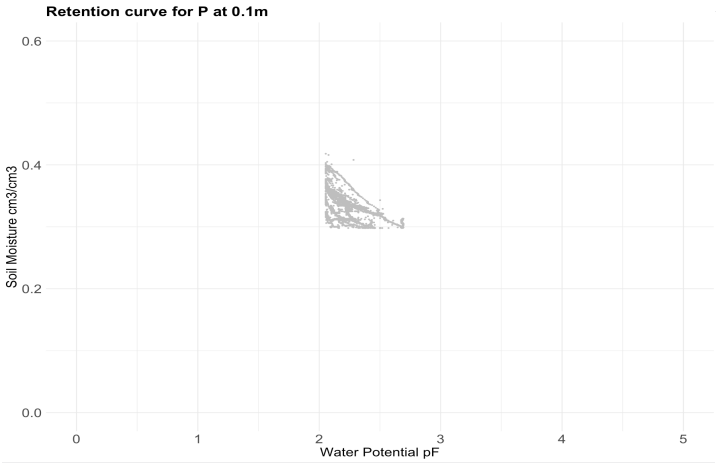

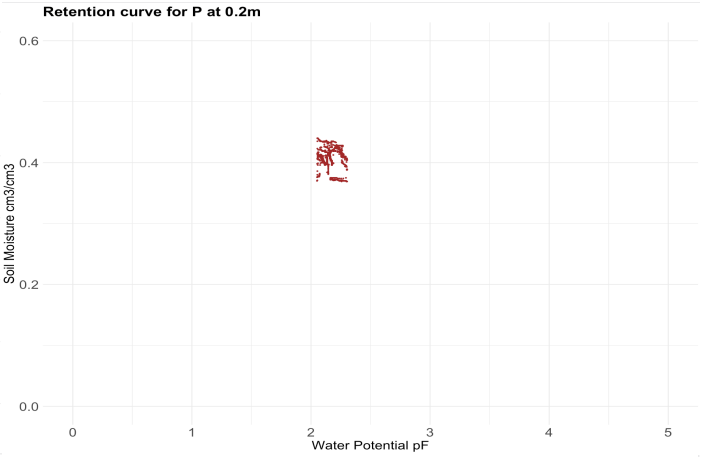

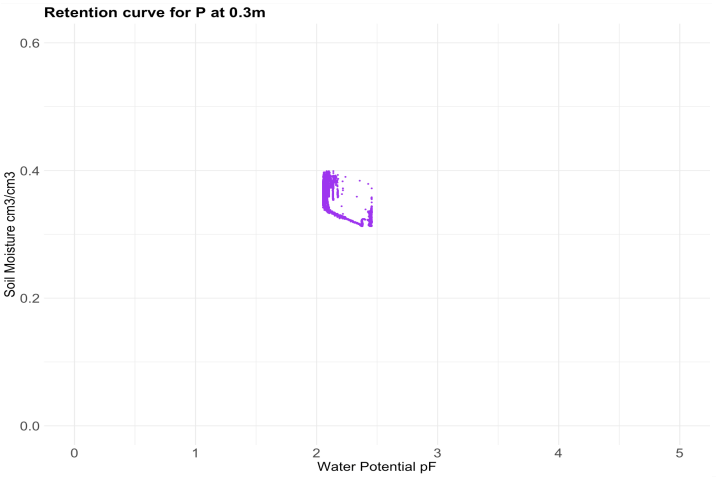

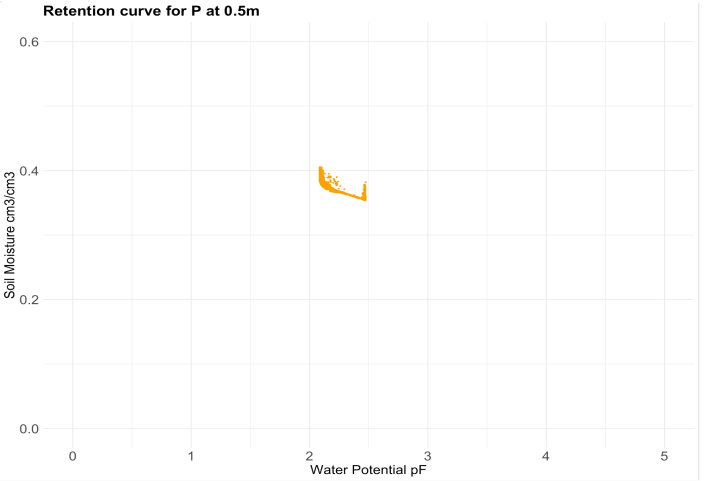

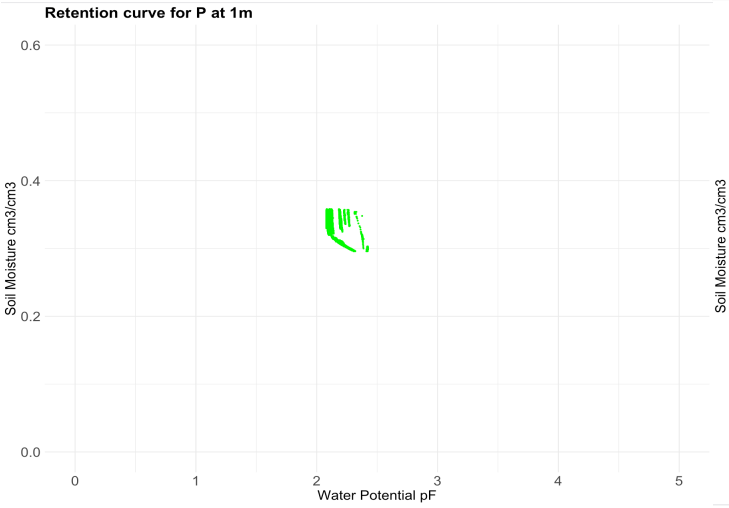

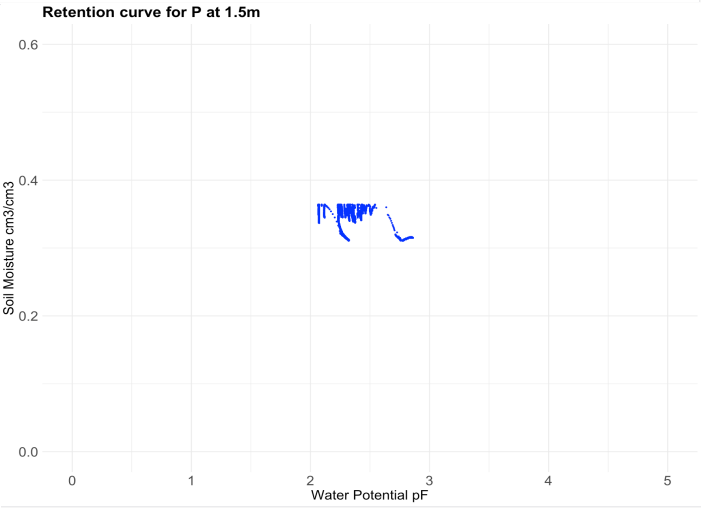

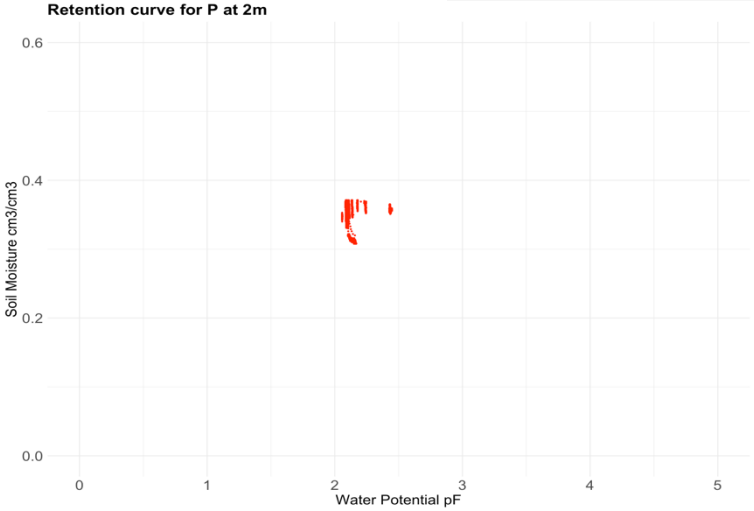

Retention curves for R10

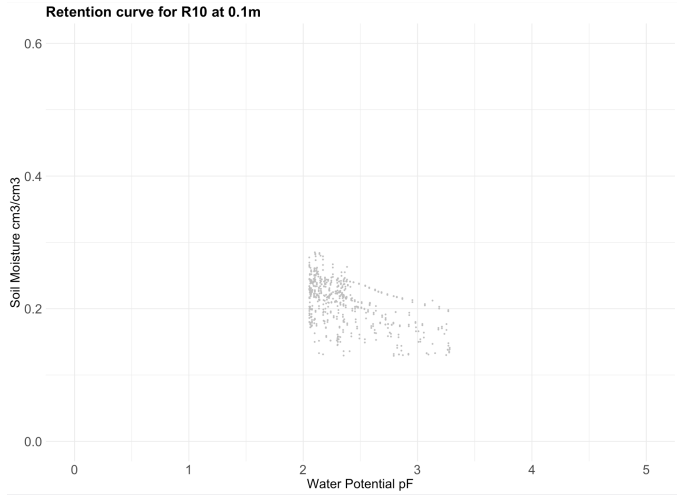

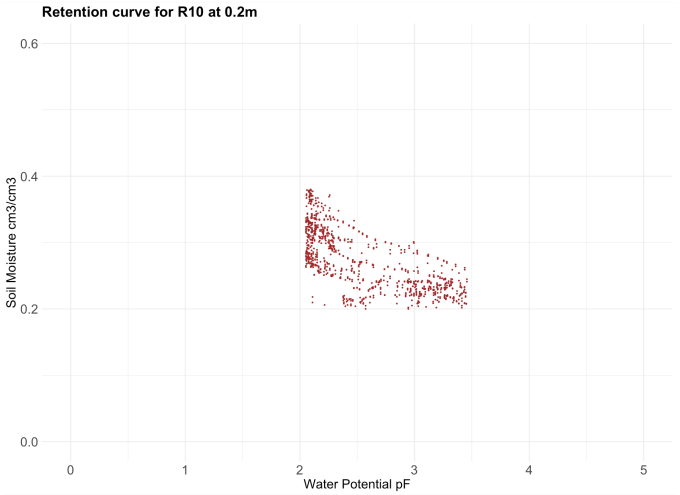

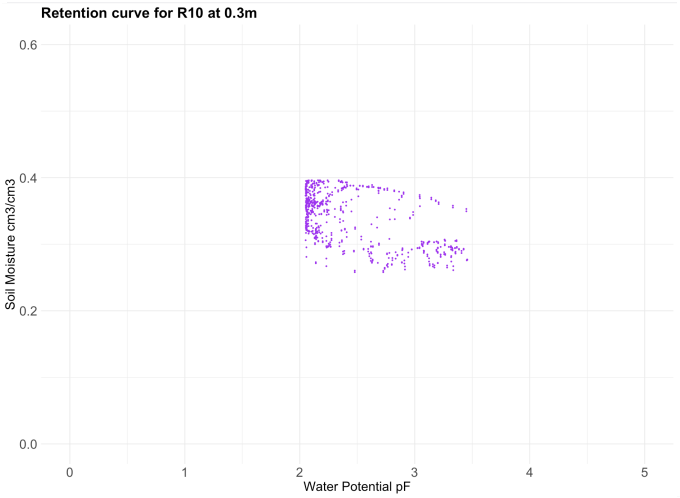

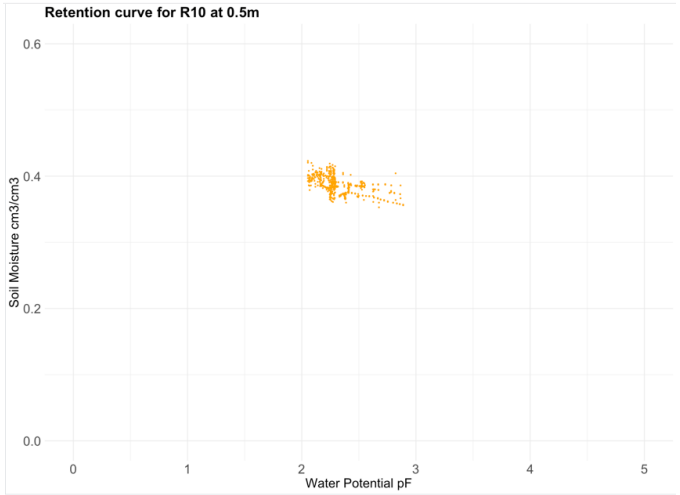

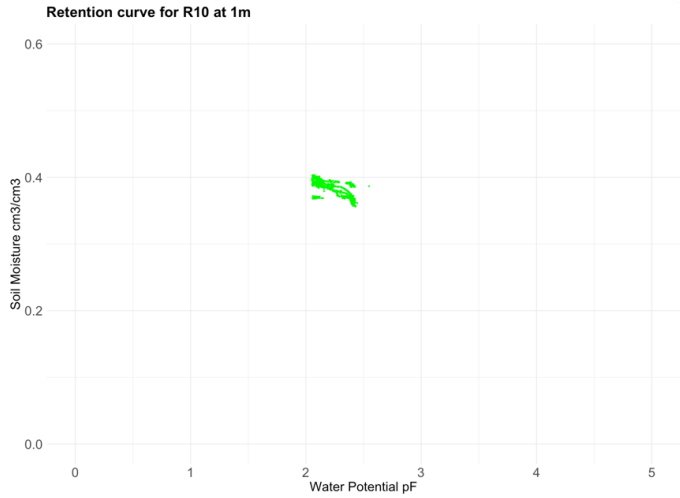

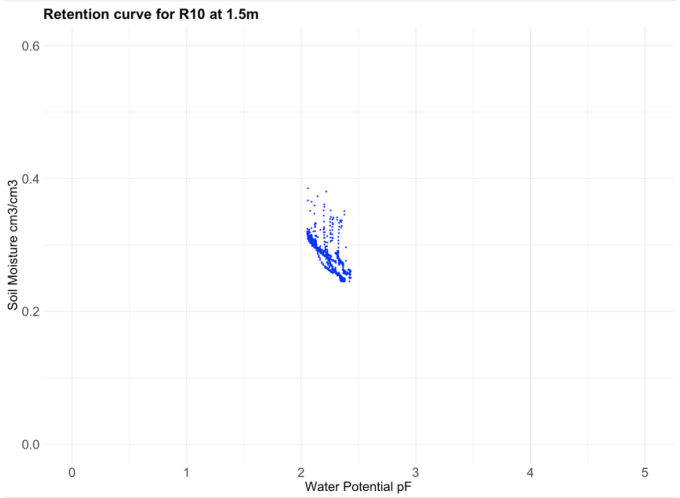

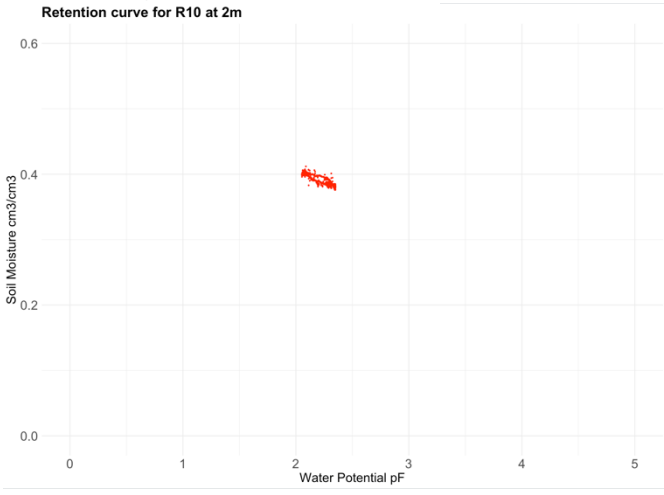

Retention curves for R40

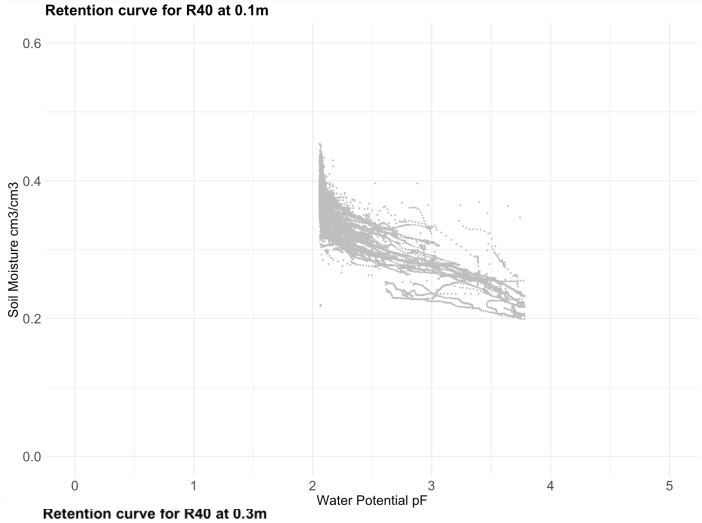

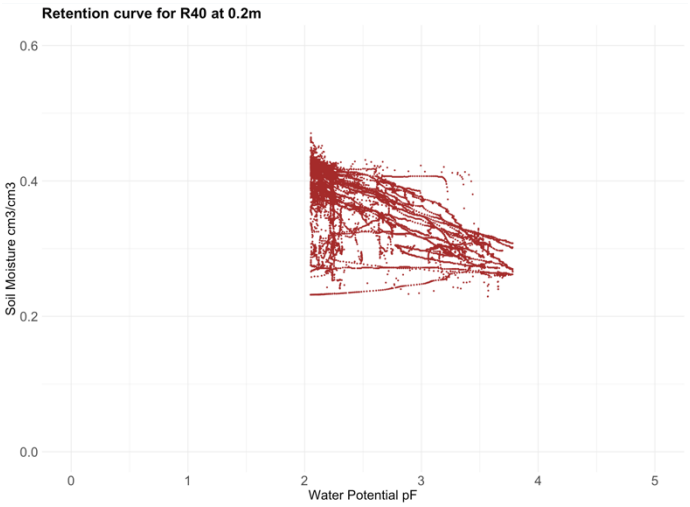

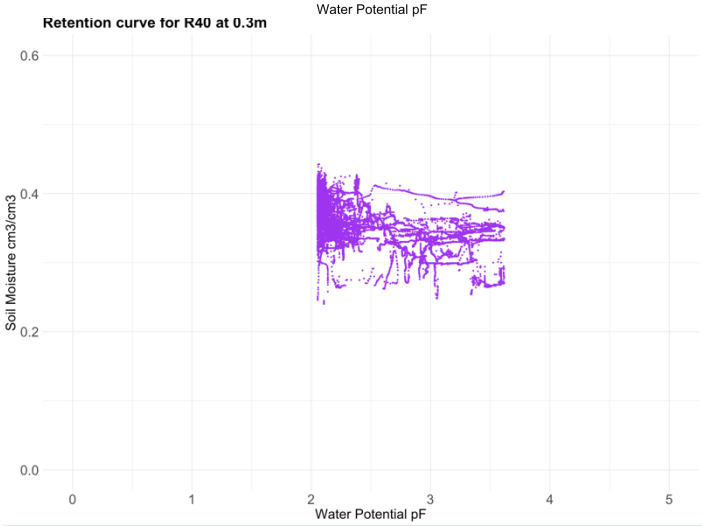

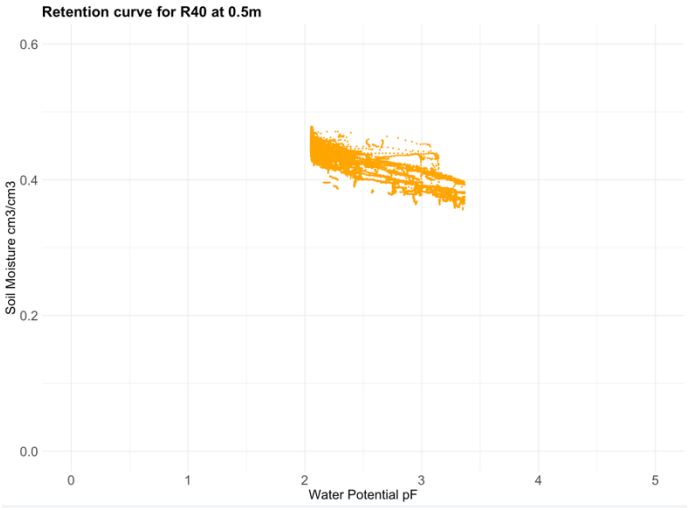

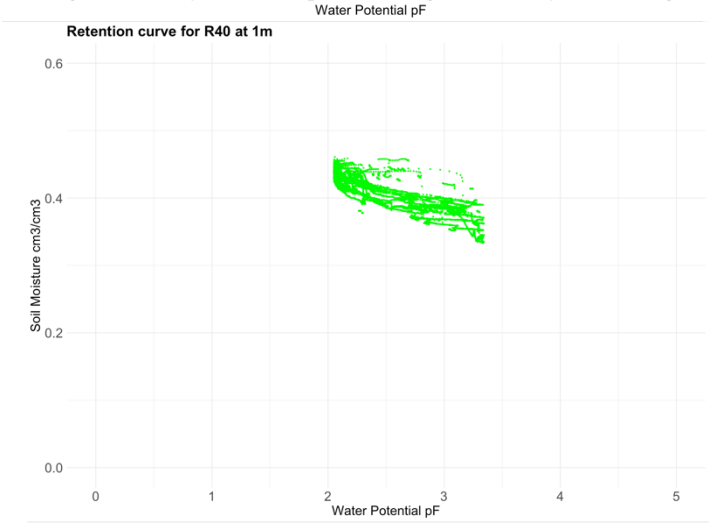

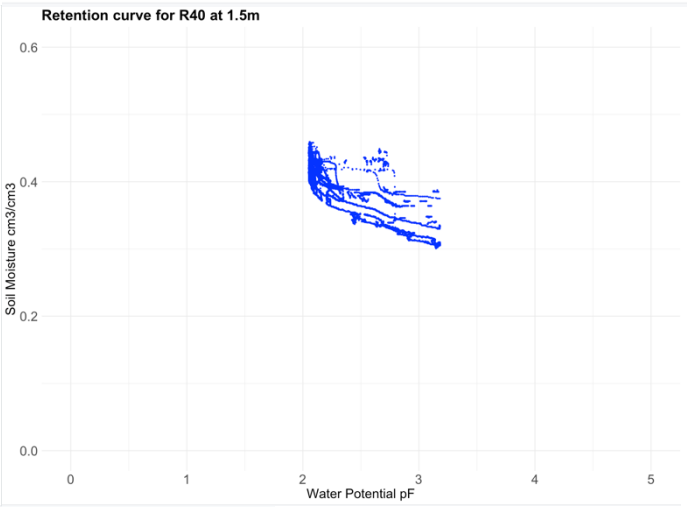

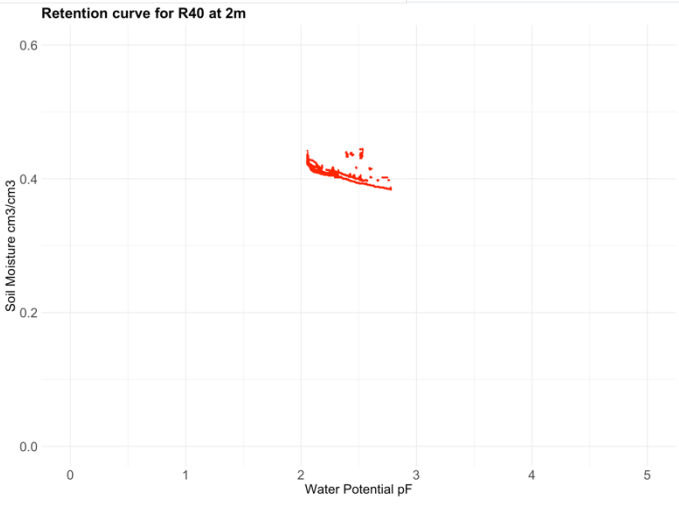

Appendix 4: Graphic of the gradient H for the four area under study

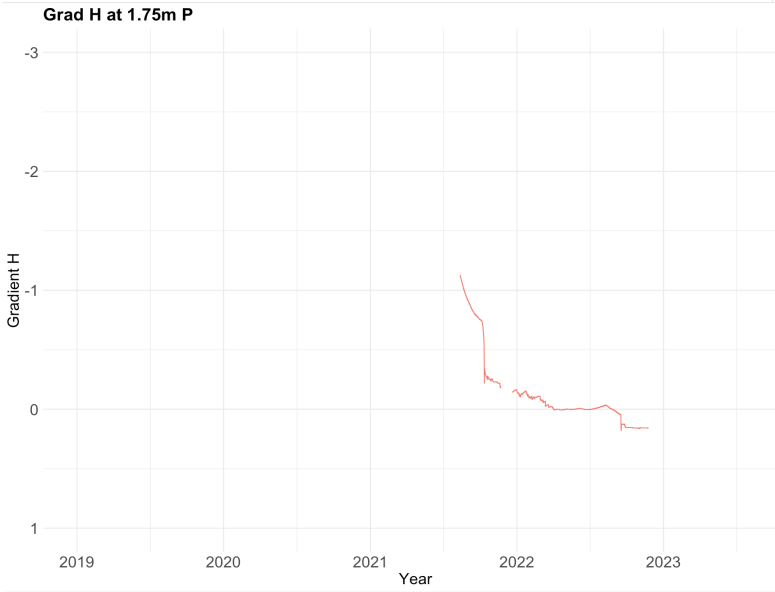

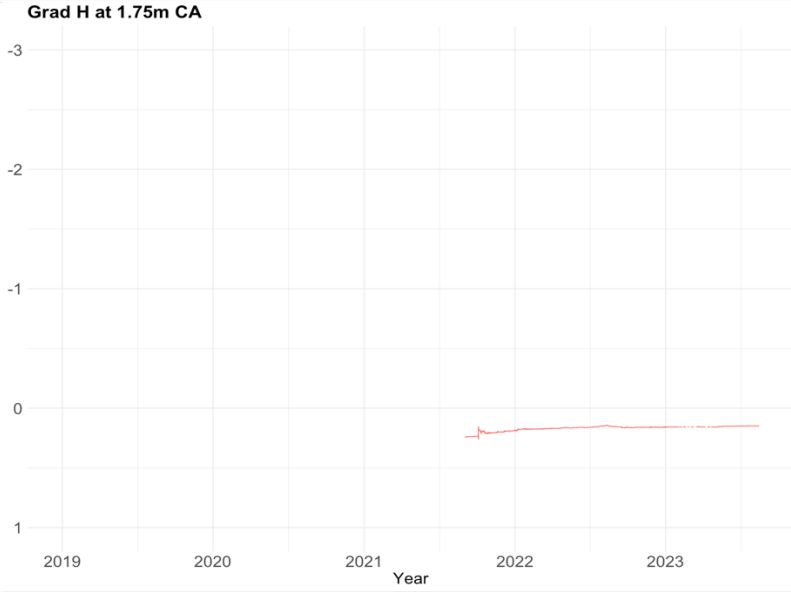

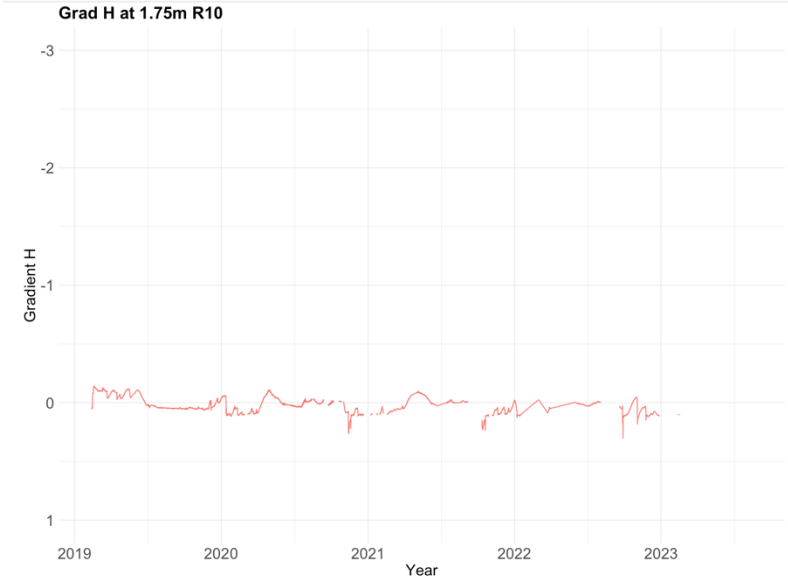

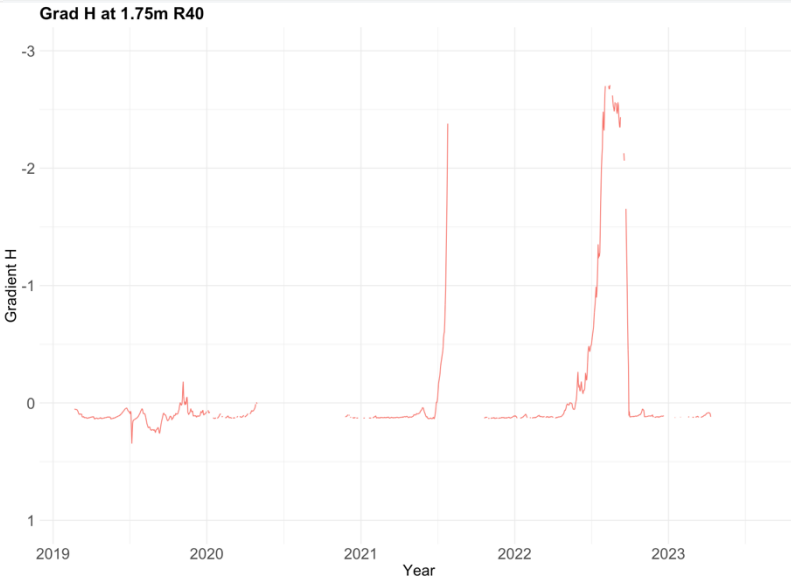

Appendix 5: Graphic of the conductivity for the four area under study

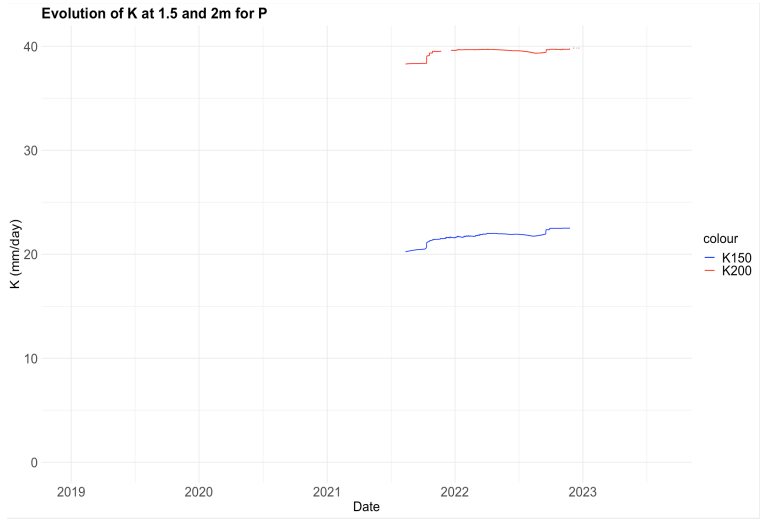

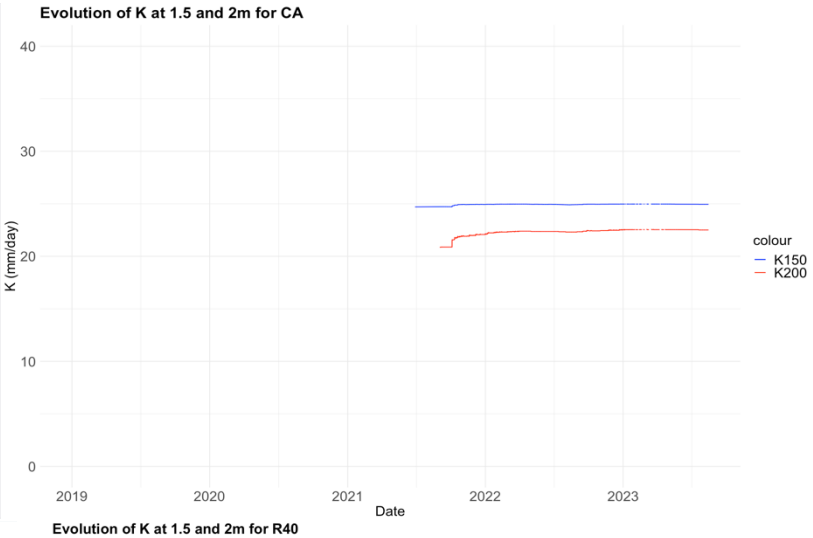

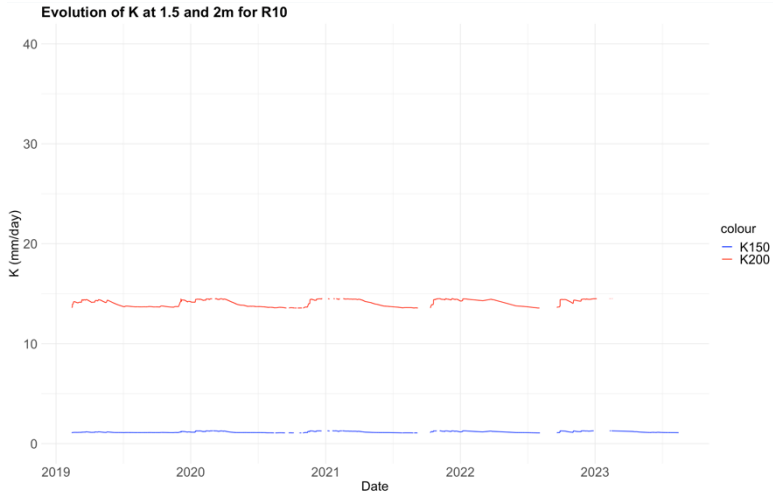

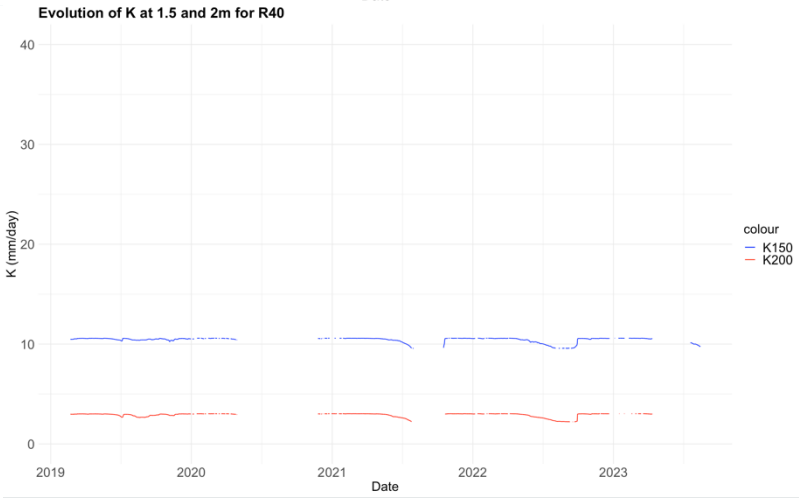

Appendix 6: Van Genuchten parameters optimized by LABROS software.

Area	n1	alpha 1	n2	alpha 2	w2	Theta r	Theta s
P – 1.5m	1.688	0.0385	1.161	0.00014	0.574	0	0.467
P – 2m	1.947	0.0411	1.080	0.00283	0.707	0	0.459
CA - 1.5m	1.122	0.00324	2.312	0.0373	0.266	0	0.473
CA – 2m	1.591	0.0929	1.03	0.0018	0.648	0	0.45
R10 – 1.5m	1.2	0.1174	1.266	0.00071	0.873	0	0.485
R10 - 2m	1.828	0.00094	1.545	0.0354	0.42	0	0.441
R40 – 1.5m	1.897	0.0362	1.359	0.00101	0.748	0.173	0.48
R40 – 2m	1.828	0.0017	1.123	0.1187	0.8	0.108	0.507

Appendix 7: Total drainage and capillary rise for R40 from 2019 to 2022

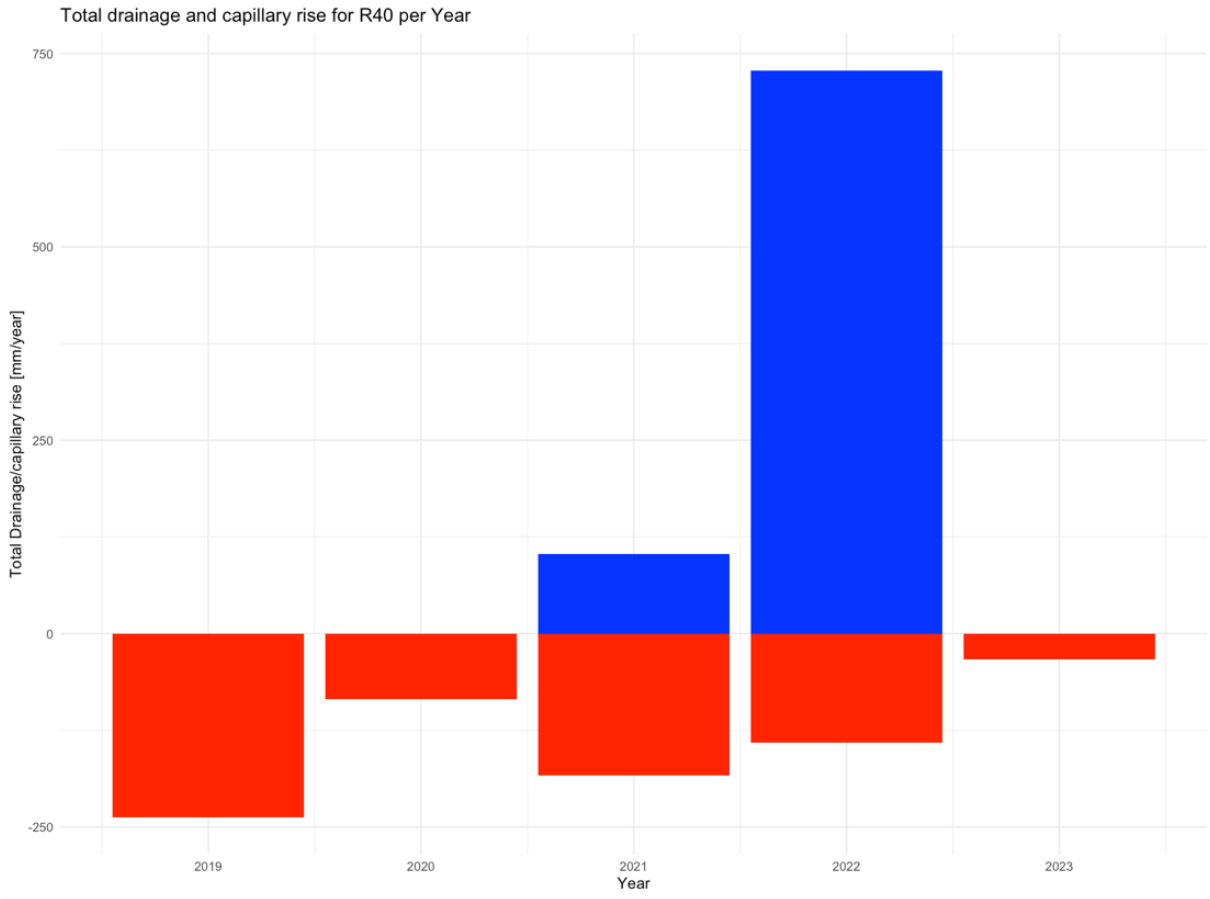

Appendix 8: Comparison of the measured conductivity for P, CA, R10 and R40 at 2m depth.

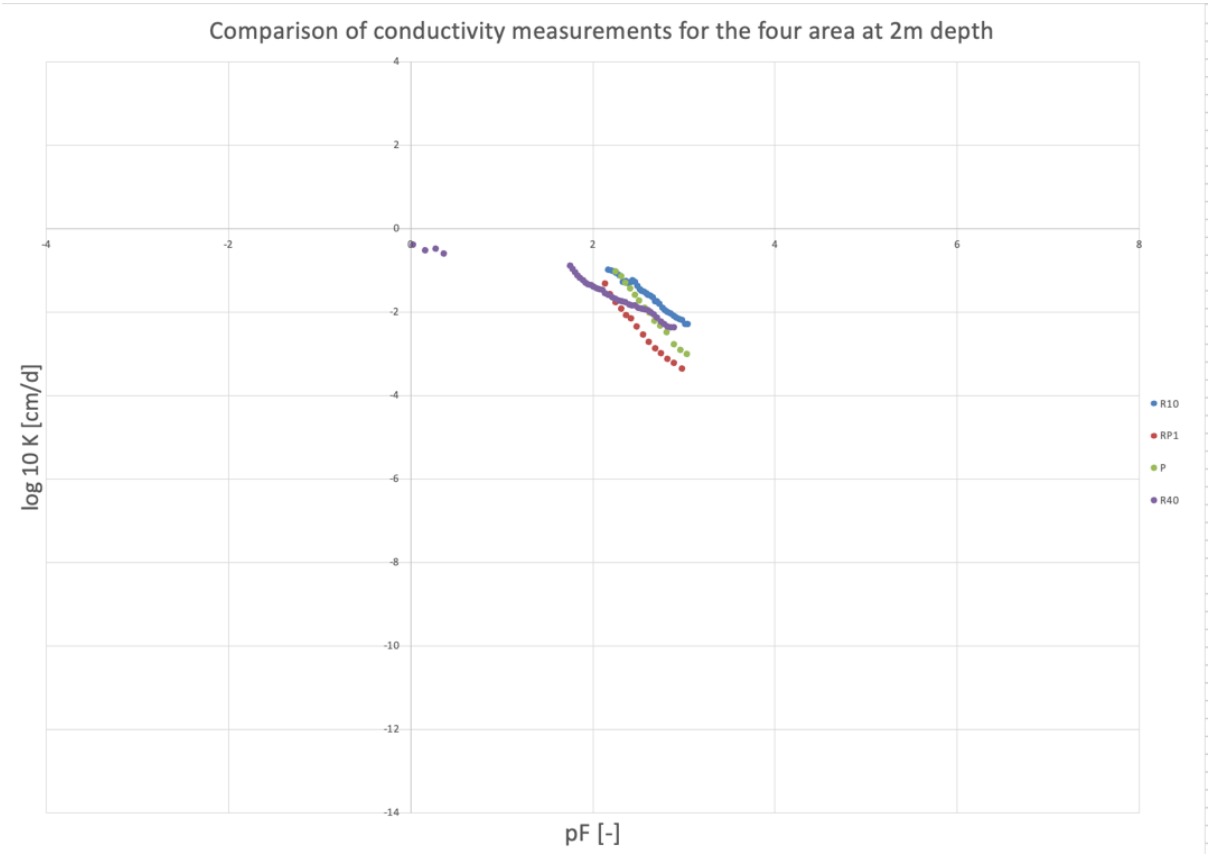

Appendix 9: Daily water balance for P, CA, R10 and R40.

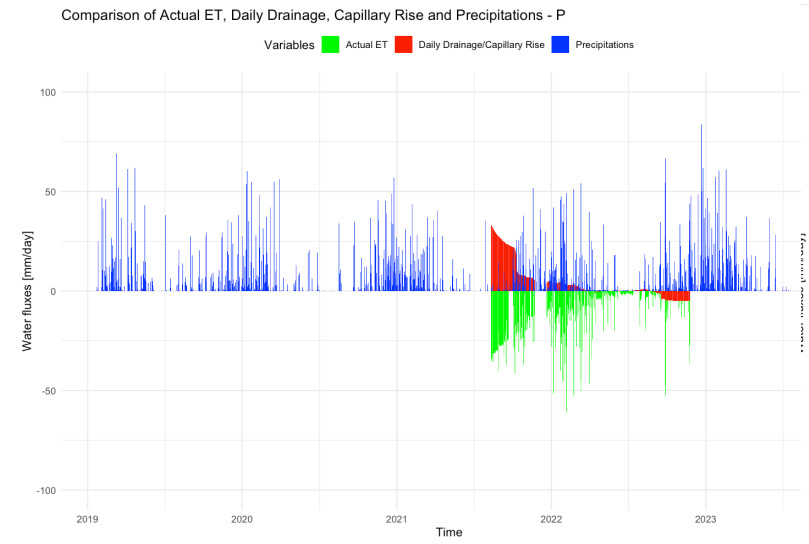

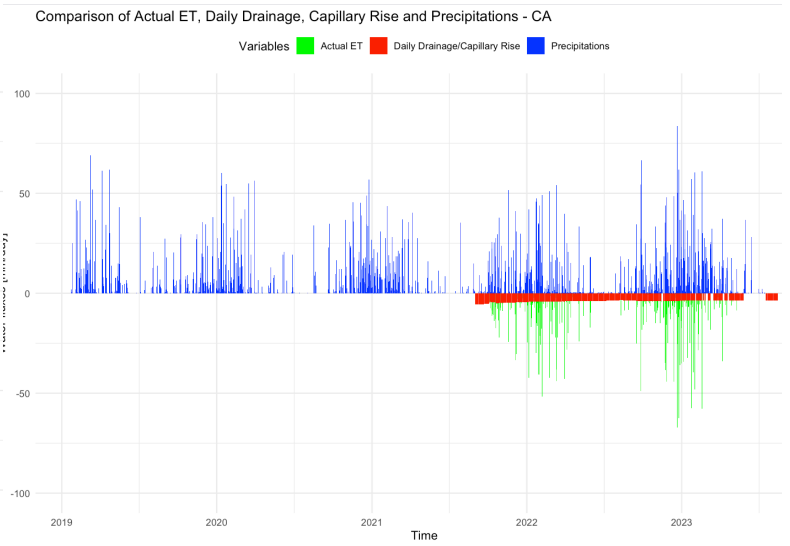

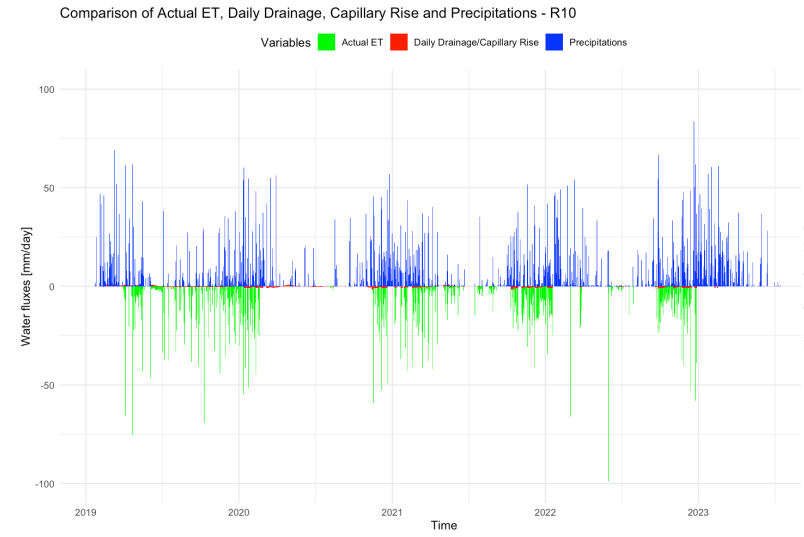

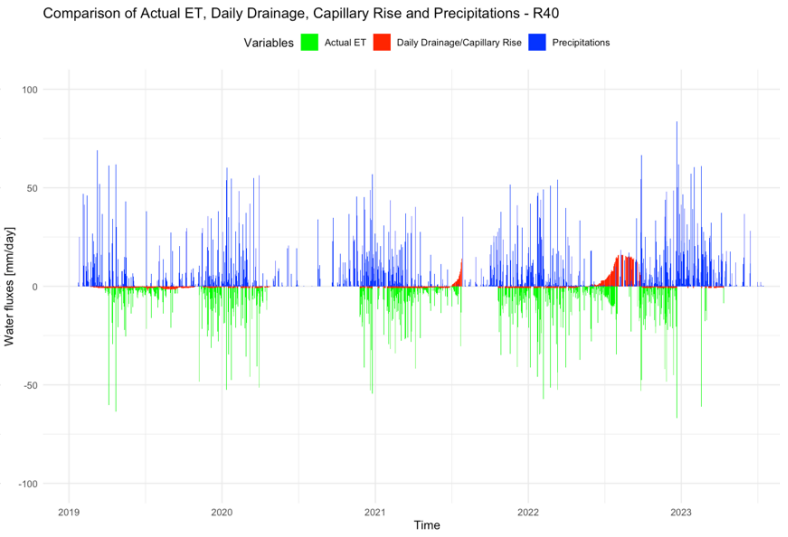

Appendix 10: Potential and Actual evapotranspiration measured by MODIS for pixel 1 (R40) and pixel 2 (R10, CA and P)

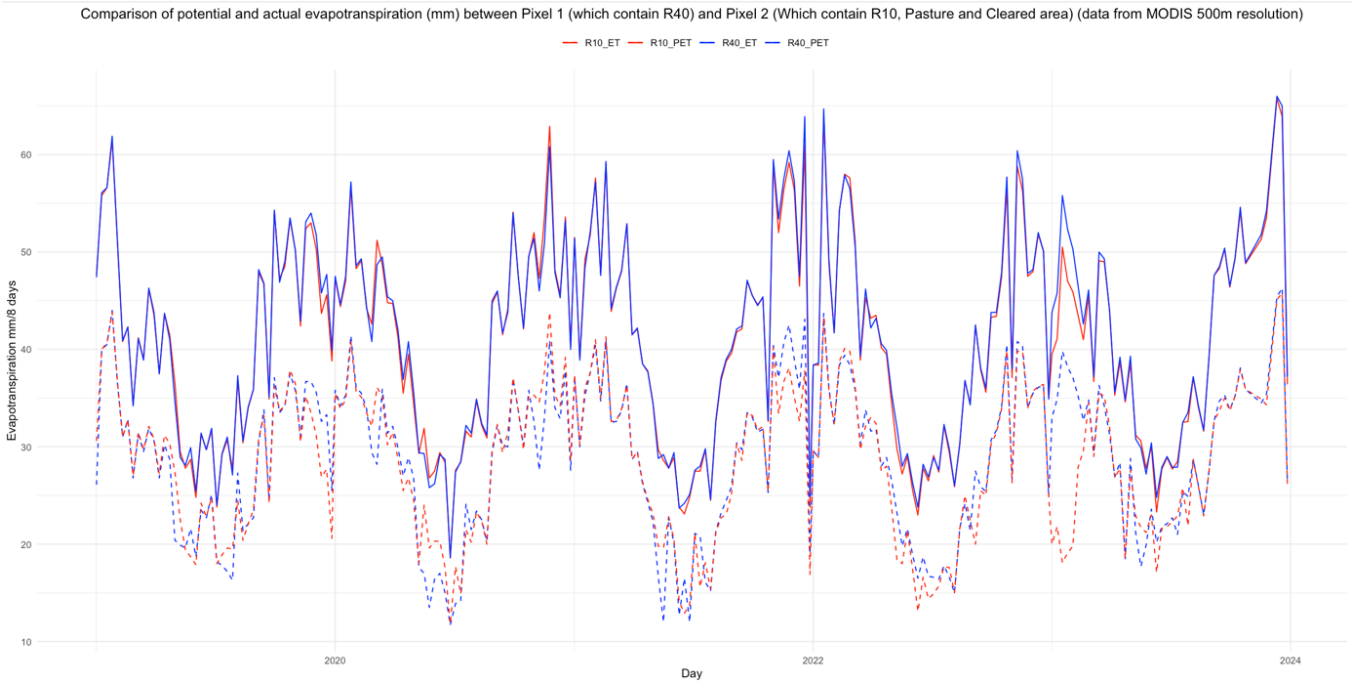

Appendix 11 : Penman Monteith Equation

$$ET_0 = \frac{0{,}408\Delta(R_n - G) + \gamma \frac{37}{T+273} u_2 (e^{\circ}(T) - e_a)}{\Delta + \gamma(1 + 0{,}34u_2)} \quad \left[\frac{mm}{h}\right]$$

With ET_0 is the reference evapotranspiration [mm/h]

R_n is the net radiation from the grass surface [MJ/m²/h]

G is the Ground heat flux density [MJ/m²/h]

Δ is the slope of the saturation vapor pressure curve [kPa/°C]

γ is the psychrometric constant [kPa/°C]

T is the air temperature [°C]

e°(T) is the saturation vapor pressure at air temperature [kPa]

e_a is the actual vapor pressure [kPa]

u_2 is the wind speed at 2m high [m/s]

Where:

- The slope of the saturation vapor pressure curve is calculated as follow:

$$\Delta = \frac{4098 e^{\circ}(T)}{(T+237{,}3)^2} \quad \text{[kPa/°C]}$$

- The saturation vapor pressure at air temperature is calculated as follow:

$$e^{\circ}(T) = 0{,}6108^{\left(\frac{17{,}27T}{T+237{,}3}\right)} \quad \text{[kPa]}$$

- The actual vapor pressure is calculated as follow:

$$e_a = e^0(T)\frac{HR}{100} \quad \text{[kPa]}$$

- The psychrometric constant is calculated as follow:

$$\gamma = 0{,}665 \times 10^{-3} P_{moy} \quad \text{[-]}$$

Where:

  - P_{moy} is the mean pressure measured [kPa]

- The net radiation from the grass surface is calculated as follow:

$$R_n = R_{ns} - R_{nl} \quad \text{[MJ/m²/day]}$$

Where:

  - $R_{ns} = (1-a)R_s$, is the net shortwave solar radiation [MJ/m²/h] with a, the albedo and is equal to 0.23 [-].
  - $R_{nl} = \sigma T^4 (0{,}34 - 0{,}14\sqrt{e_a})(1{,}35\frac{R_s}{R_{SO}} - 0{,}35)$, is the net longwave solar radiation [MJ/m²/h] with:

- σ is the Stefan-Boltzmann constant and is equal to 2.0429.10^{-10}[-].
- $R_{SO} = (0{,}75 + 2.10^{-5}z)R_a$, is the calculated clear-sky radiation [MJ/m^2/h] with:
- z the meteorological weather station altitude and is equal to 1100 [m].
- $R_a = \frac{12\times60}{\pi} G_{SO} d_r[(\omega_2 - \omega_1)\sin\varphi\sin\delta + \cos\varphi\cos\delta\,(\sin\omega_2 - \sin\omega_1)]$, is the extraterrestrial radiation [MJ/m^2/h] with:
- $d_r = 1 + 0{,}033cos\frac{2\pi}{365}J$, the Earth-Sun inverse relative distance [rad].
- $\delta = 0{,}409\sin\left(\frac{2\pi}{365}J - 1{,}39\right)$, the solar declination [rad].
- $\omega_1 = \omega - \frac{\pi\, t_1}{24}$ et $\omega_2 = \omega - \frac{\pi\, t_2}{24}$, the temporal solar angle at the start of the hour [rad] and the temporal solar angle at the end of the hour [rad].
- $\omega = \frac{\pi}{12}[(t + 0{,}06667(L_z - L_m) + S_c) - 12]$, the temporal solar angle at the midpoint of the hour [rad] with:
  - Lz: Longitude of the center of the local time zone (=45 for the study zone) [°].
  - Lm: Longitude of the measurement zone (=45.982 for the study zone) [°].
- $S_c = 0{,}1645\sin 2b - 0{,}1255\cos b - 0{,}025\sin b$, the seasonal correction for solar time [h].
- $b = \frac{2\pi(J-81)}{364}$, is the latitude [rad].

Appendix 12: Code used for Google Earth Engine to extract MODIS data.

```
////////////////////////////////////////////////////////////////////////////
// Associate time series to each fluxnet sites (like transpiration)

var start = ee.Date('2019-01-01')
var finish = ee.Date('2023-12-31')
var PML_V2 =
ee.ImageCollection("MODIS/061/MOD16A2GF").select('PET').filterDate(start,finish).filterBoun
ds(RP1)

var count = PML_V2.size();
print('size of the image collection', count)

var triplets = PML_V2.map(function(image) {
  return image.reduceRegions({
    collection: RP1.select(['id']),
    reducer: ee.Reducer.mean(),
    scale: null
  }).filter(ee.Filter.neq('mean', null))
  .map(function(f) {
      return f.set('imageId', image.id());
  });
}).flatten();


// drop .geo contents
var tripletsOut = triplets.select(['.*'], null, false);
// print(ui.Chart.image.seriesByRegion(PML_V2, Fluxnet, ee.Reducer.mean()));

// create function: Format a table of triplets into a 2D table of rowId x colId.
var format = function(table, rowId, colId) {
// Get a FeatureCollection with unique row IDs.
  var rows = table.distinct(rowId);
// Join the table to the unique IDs to get a collection in which
// each feature stores a list of all features having a common row ID.
var joined = ee.Join.saveAll('matches').apply({
  primary: rows,
    secondary: table,
    condition: ee.Filter.equals({
    leftField: rowId,
      rightField: rowId
  })
});

 return joined.map(function(row) {
    // Get the list of all features with a unique row ID.
      var values = ee.List(row.get('matches'))
```

```
    // Map a function over the list of rows to return a list of
    // column ID and value.
      .map(function(feature) {
      feature = ee.Feature(feature);
      return [feature.get(colId), feature.get('mean')];
    });
  // Return the row with its ID property and properties for
  // all matching columns IDs storing the output of the reducer.
  // The Dictionary constructor is using a list of key, value pairs.
    return row.select([rowId]).set(ee.Dictionary(values.flatten()));
 });
};

// apply formatting function to your data
var table1 = format(tripletsOut, 'id', 'imageId');

//Name for your file export
var desc1 = 'RP1_PET_MODIS_500M'
Export.table.toDrive({
collection: table1,
 description: desc1,
 fileNamePrefix: desc1,
 folder: 'RP1',

fileFormat: 'CSV'
});
```

Appendix 13: ET_0 measured through the different meteorological stations.

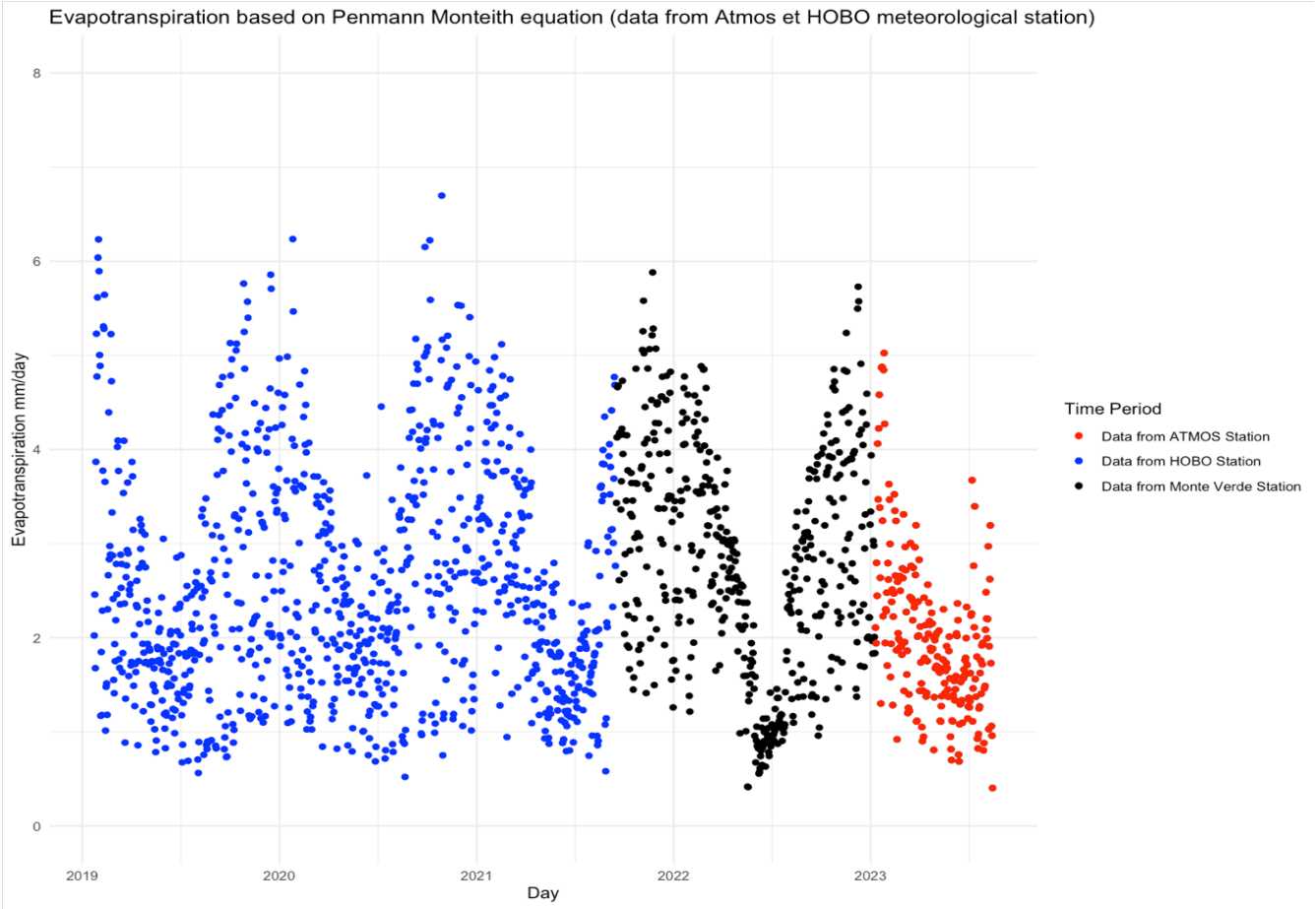

What is the impact of reforestation on evapotranspiration? How to better assess evapotranspiration in the Atlantic Brazilian Forest?
A case study in Brazil's Atlantic Forest, in São Francisco Xavier, São Paulo State

The Brazilian Atlantic Forest has been particularly affected by deforestation in recent decades. The importance of forests in terms of biodiversity and climate regulation noted has led to measures being taken globally for forest conservation and restoration and the Atlantic Forest is no exception. However, concerns have been raised by several scientists and specialists about the water consumption of these young, reforested forests and their impact on water resources in the long term. This master thesis is a continuation of the master thesis made by Basile Delvoie during 2022-2023 and aims to address the uncertainty raised regarding evapotranspiration, a significant flow of the water cycle in tropical forests.

This thesis was realized in collaboration with the INPE (Brazil) through the co-promoter of this thesis, Laura Borma. This study was conducted on four plots with a common history but different soil cover at present: A 40-year-old forest (R40), a 10-year-old reforested forest (R10), a pasture (P) and an abandoned area (CA). Various soil properties data were used in this thesis such as water content and water potential data were measured by the INPE from 2019 to 2023. Climatic data (e.g.,: precipitation) were also used.

Two methods of estimating of evapotranspiration (**SEN-ET** and **Water Balance**) were validated in this thesis, while a third MODIS proved to be inconclusive due to its low resolution of 500m^2. Although these two methods do not agree regarding the evapotranspiration of the CA and P zones, due to uncertainties in the calculation of drainage and capillary rise and to limited time and basic data from the sensors used, they both agree that a young, reforested forest (R10) has an evapotranspiration quite similar to that of an old forest (R40) over time with even a lower evapotranspiration in the dry season. During the water balance important capillary rises were even observed for the 40-year-old forest and by analyzing the total water withdrawn compared to the total water produced by the aged forest, it was observed that older forest behave as water consumer rather than producer, which could have a significant impact on water resources in the long term.

However, several avenues for improvement have been raised for future research to address the different limitations encountered in this thesis and that will allow to better understand the dynamics of water flows during reforestation.

Lola Parmentier

UNIVERSITÉ CATHOLIQUE DE LOUVAIN
Faculté des bioingénieurs
Croix du Sud, 2 bte L7.05.01, 1348 Louvain-la-Neuve, Belgique | **www.uclouvain.be/agro**